



# UNIVERSITAT<sub>DE</sub> BARCELONA

## Final Degree Project **Biomedical Engineering Degree**

### **“SPR biosensor for BSA protein detection”**

Barcelona, 06 June, 2023

Author: Carla Solà Bosch

Director/s: Mauricio Moreno Sereno &  
Ana Belén Caballero Hernández

Tutor: Mauricio Moreno Sereno

# ABSTRACT

For the last decades Surface Plasmon Resonance (SPR) biosensors have been revolutionizing the world of optical biosensing techniques making great impact in the fields of drug discovery, environmental monitoring, food safety, and medical diagnostics. In this project a grating coupled SPR biosensor is analyzed by detecting a model protein, Bovine Serum Albumin (BSA).

The main goal is to assess the sensing capability, for that, three experimental approaches are followed. First, a characterization of the biosensor's surface is performed, and the surface is visualized through images with a Surface electron microscope (SEM), which uses electrons to generate images at the nanoscale ( $10^{-9}$  m). The second block, consist of performing several experiments to detect the model protein, this will also allow to gain knowledge on the use of SPR for protein detection. The last block is to repeat the previous experiments but this time altering the surface of the biosensor to enhance a more specific binding of the protein to the surface. Changing the surface properties is widely used in biosensing and it is called functionalizing. To ensure that this functionalization is done correctly Fluorescence Microscopy, which helps to distinguish different structures on a sample, is used.

# ACKNOWLEDGEMENTS

Through the development of this project, I have been able to get a slight scope on the world of scientific research which has led me to understand that patience is key, and errors are frequent, but the path is captivating and well worth it.

This would have been utterly impossible without the guidance of my co-tutors, Mauricio Moreno, a Physicist, and Ana Belén Caballero, a Chemist, that have supported me through each step of the process. Their knowledge in different fields has provided me with a combination of the tools needed to understand a multidisciplinary project. Furthermore, their cooperation of expertise has allowed me to develop the project in two different faculties. As for the personal learnings, I have been able, for the first time, to truly experience how to manage in a chemistry laboratory with the opportunity of constant consultation with a professional Chemist, Ana Belén. Moreover, I learned the use of the SPR sensor from Mauricio who has been supervising every performed experiment becoming an extremely helpful guide for all the encountered inconveniences. At the personal level, I highly value the treatment and caring I have received from both my tutors, and I feel more than grateful and could not have imagined a better team to carry out this to-be-continued project.

However, this team would not be complete without the constant generous help of Anna Estany, a Physicist that works in the Electronic Engineering Department of the Faculty of Physics of University of Barcelona, who has accompanied me through the entire process and that deserves a big part of the credit for the research conducted.

Moreover, I am also grateful to the University of Barcelona (UB) for facilitating the necessary specific materials and equipment to build the project. I would also like to thank IBEC (Bioengineering Institute of Catalonia) for allowing us to visit their centers and learn from their SPR sensor methodology. Furtherly, thank you to the Scientific and Technological centers of UB (CCiTUB) for enabling us to use the FE-SEM microscope and specially to the laboratory technician Manel Bosch Marimon, for helping obtain images with the high-speed fluorescent microscope and answering very kindly all the doubts.

Overall, it has been a beautiful full of learning process that I wish to continue in a near future, and that has opened the door of pursuing a career in the world of nanotechnology and scientific research.

# LIST OF FIGURES

Figure 1: Working principle and components of a Biosensor [3] .....	12
Figure 2: a) Reflected light as a function of incident angle [11] b) Biomolecular interaction analysis: a Sensorgram [14] .....	14
Figure 3: Scheme of the Kretschmann configuration detection mechanism of SPR [11] .....	15
Figure 4: SPR principle on nano constructed surface. ....	15
Figure 5: Experimental SPR set-up in the development phase in the DEE [12] .....	16
Figure 6: Methods to prepare modified surface, including (a) physical adsorption (c) covalent immobilization (SAMs-based), (d) capture, and (e) polymer film deposition methods [16] .....	17
Figure 7: a) Microchip diffraction gratings structure scheme b) Real gold-coated microchip c) Composition of the gold-coated microchip .....	24
Figure 8: SEM images of diffraction gratings of periods 500 nm and 600 nm (taken by Anna Estany) .....	25
Figure 9: Spectrum of a surface sweep for one point for period (a) 500 nm and (b) 600 nm, from experiment with isopropanol/ethanol performed with CHIP41 the 24th of February. ....	26
Figure 10: Surface sweep for all the points of the diffraction grating of both periods from the sweep from experiment with isopropanol/ethanol performed with CHIP41 the 24th of February. ....	26
Figure 11: Visual representation of the surface sweep for all the points from the sweep experiment with isopropanol for both periods performed with CHIP41 the 24th of February. ....	27
Figure 12: a) resonance wavelength for both periods from experiment with isopropanol/ethanol performed with CHIP41 the 24th of February b) Histogram with average resonance wavelength for both periods from experiment with isopropanol performed with CHIP41 the 24th of February. ....	27
Figure 13: Graph of a linear regression of the average resonance wavelengths as a function of the refractive index corresponding to different substances. ....	28
Figure 14: Microfluidic structures that prompt bubble formation [46] .....	29
Figure 15: a) microfluidic design on a double-sided adhesive tape b) methacrylate lid incorporated onto the surface of the chip c) inlet and outlet syringe needles placed and sealed with super-glue onto the methacrylate lid. ....	30
Figure 16: AutoCAD microfluidics design .....	30
Figure 17: Anterior IBEC SPR biosensor set-up .....	31
Figure 18: IBEC current microfluidic design with methacrylate lid incorporated. Note that the needles are not placed correctly at the inlet and outlet. ....	31
Figure 19: Chemisorption of alkanethiols on gold surface [38] .....	32
Figure 20: a) 11- Mercaptoundecanoic acid molecule structure b) HS-PEG-OH structure .....	33
Figure 21: Schematic drawing of the EDC/NHS addition reaction for MUA activation .....	33
Figure 22: Schematic drawing of the BSA attachment reaction .....	34
Figure 23: Sensorgram of the resonance wavelength position as function of time from an experiment performed 1st of March with CHIP 34. ....	35
Figure 24: Sensorgram of the resonance wavelength position as function of time from an experiment performed 23rd of March using BSA with different concentrations. ....	36
Figure 25: Sensorgram of the resonance wavelength position as function of time from an experiment performed 14th of April using BSA with different concentrations. ....	37



Figure 26: Fluorescein excitation and emission spectrum [47] .....	39
Figure 27: Fluorescence microscopy (a) border image and (b) histogram of dry conditioned wafer for processing explanation .....	39
Figure 28: a) Fluorescence image with enhanced of the center of the dry conditioned wafer b) Fluorescence image of the corner of the dry conditioned wafer .....	40
Figure 29: a) Fluorescence image of the center of the control wafer (only MUA formed), b) Fluorescence image of the center of the control wafer with enhanced contrast 20% c) Fluorescence image with enhanced contrast of 20% of the center of the dry conditioned wafer. ....	40
Figure 30: a) Fluorescence image of the center of CHIP 33 b) Fluorescence image of the center of the CHIP 33 with enhanced contrast 20%.....	41
Figure 31: Fluorescence image of the center of the non activated wafer .....	41
Figure 32: Sensorgram of the resonance wavelength position as function of time from an experiment performed 11th of April with the condition, activation and coupling procedure of the SAM. ....	42
Figure 33: Sensorgram of the resonance wavelength position as function of time from an experiment performed 31st of May with the condition, activation and coupling procedure of the SAM.....	43
Figure 34: The Work Break Down structure of the project. ....	48
Figure 35: PERT diagram .....	51
Figure 36: GANTT diagram of February and May.....	52
Figure 37: GANTT diagram of April .....	52
Figure 38: GANTT diagram of May and June.....	52

# LIST OF TABLES

Table 1: SAMs classification based on head group [17][19][20][21].....	18
Table 2: Other potential cancer biomarkers for SPR detection [24] .....	19
Table 3: Relevant companies in SPR technologies .....	22
Table 4: Refractive index of the substances used in the experimental part.....	28
Table 5: Sweep experiments with different substances with the average DIP wavelength .....	28
Table 6: Wafers and chips used for fluorescence image acquisition. ....	39
Table 7: SWOT analysis matrix .....	44
Table 8: Economic viability layout.....	45
Table 9: WBS theoretical analysis package .....	48
Table 10: WBS biosensor set-up package.....	49
Table 11: WBS SAM formation package .....	49
Table 12: WBS experimental analysis package .....	50
Table 13: PERT description table .....	50

# TABLE OF CONTENTS

ABSTRACT.....	2
ACKNOWLEDGEMENTS .....	3
LIST OF FIGURES .....	4
LIST OF TABLES.....	6
1. INTRODUCTION .....	9
1.1 Motivation and aim of the project .....	9
1.2 Objectives .....	9
1.3 Limitations.....	10
2. BACKGROUND .....	11
2.1 Biosensors .....	11
2.1.1 Definition and components of a biosensor.....	11
2.1.2 Important concepts of biosensors.....	12
2.1.3 Classification of biosensors .....	13
2.2 Optical biosensors.....	13
2.2.1 Surface Plasmon Resonance: .....	14
2.2.1.1 The Kretschmann configuration.....	15
2.2.1.2 Grating coupling configuration .....	15
2.3. Functionalization of a gold-based biosensor .....	16
2.3.1 Ligand immobilization methods on gold biosensor surface for SPR .....	16
2.3.2 Covalent immobilization .....	17
2.4. Applications.....	18
2.4.1 General applications of SPR in biomarker detection in the biomedical field .....	18
2.4.2 Early detection of Parkinson:.....	20
3. MARKET RESEARCH .....	21
3.1 Current companies, institutions and commercial products that use SPR .....	21
3.2 Future market prospects .....	23
4.CONCEPTION ENGINEERING .....	24
4.1 Gold-coated biosensor.....	24
4.1.1 Fabrication procedure and structure .....	24
4.1.1.1 Scanning electron microscopy .....	25
4.1.2 Characterization of the biosensor.....	25

4.1.3 Microfluidics .....	29
4.2. SAM FORMATION .....	31
4.2.1 Different SAM for gold-coated surfaces.....	32
4.2.2 Conditioning (MES) and activation (EDC/NHS).....	33
4.2.3 Coupling.....	33
5. DETAIL ENGINEERING .....	34
5.1 Experiments with non-functionalized surfaces.....	34
5.1.1 Cleaning and regeneration mechanisms .....	34
5.1.2 Initial experiments .....	34
5.1.3 Sensitivity assessment using different concentrations of BSA .....	35
5.2 Experiments with functionalized surfaces .....	37
5.2.1 SAM validation .....	38
5.2.2 SPR with SAM.....	41
6. TECHNICAL VIABILITY .....	43
7. ECONOMIC VIABILITY .....	45
8. EXECUTION SCHEDULE.....	47
8.1 Work Breakdown Structure (WBS).....	47
8.2 PERT .....	50
8.3 GANTT diagram .....	51
9. LEGISLATION AND REGULATION.....	53
10. CONCLUSIONS AND FUTURE WORK.....	53
11. REFERENCES .....	55
12. ANNEXES.....	59
ANNEX 1: CHEMICAL PREPARATIONS .....	59
ANNEX 2: BIOSENSOR CHARACTERIZATION EXPERIMENTS (SWEEP) .....	62
ANNEX 3: FLOW PUMP RATE STUDY .....	89
ANNEX 4: INITIAL EXPERIMENTS .....	90
ANNEX 5: EXPERIMENTS WITH DIFFERENT CONCENTRATIONS OF BSA .....	93
ANNEX 6: EXPERIMENTS WITH SAM .....	96
ANNEX 7: FLUORESCENT MICROSCOPY RESULTS .....	98

# 1. INTRODUCTION

## 1.1 MOTIVATION AND AIM OF THE PROJECT

As a Biomedical Engineering student fascinated by the field of nanotechnology, the world of biosensing, despite having little expertise on the matter, is of great interest. The Department of Electronic Engineering (DEE) of the Faculty of Physics of the University of Barcelona (UB) is developing an optical biosensor, which is based on Surface plasmon resonance (SPR). Other students had previously developed their final degree project using this technique, the last one, Raul Engerer Guerrero, studied the early detection of Parkinson's disease in 2022 in the DEE. The opportunity to continue this research presented itself. However, since previous errors needed to be avoided, the project had to restart from the beginning, by learning the use of the biosensing technique from scratch. The main motivation behind this was not only to extensively learn about SPR biosensors for protein detection and in the most optimistic scenario be able to contribute to the early detection of Parkinson, but also to experience for the first time what conducting real scientific research implies.

This project is aimed at exploring a SPR-based optical biosensor to detect proteins. An optical instrument in the development phase in the DEE of the Faculty of Physics of UB which measures the reflectance in the grating coupled SPR sensor's gold surface is used. These sensors are manufactured at the Denmark Technique University by members of the department.

An initial introduction to biosensing techniques and SPR biosensor will be key to understand the depth and importance of the project. However, the main objective is to determine the sensing capability of the sensor, so the relevance of the study conducted relies on the experimental analysis. One of the most important parts is the experimental design of both the substances to be detected and the preparation of the gold microchip, which involves the cleaning, regeneration, and functionalization of the surface and the selection and setting of its different components. The importance of the chemical part, that is intrinsic of the project, led to the research also being developed at the Organic Chemistry Department of the Faculty of Chemistry of the UB. The experimental part also revisits constantly the results obtained and set-up used in the detection and seeks to find solutions to experimental errors with the main goal of optimizing and improving the sensing capability of the technique with the available resources. This is key to improve the experimental design and serve as guidelines to future work on the matter.

Furthermore, the ambitious objective of the project is the medium-term detection of a protein related to the early detection of Parkinson.

## 1.2 OBJECTIVES

### First part: Theoretical analysis

- a) **Biosensing techniques:** introduction to biosensors, providing a scope on their working principle, different components, classification, main aspects and including an overview on the optical biosensing techniques.

- b) **SPR technique:** prior theoretical research on the physical principle, main applications and configurations of the SPR that enables the understanding of the optical instrument still in development at the DEE.
- c) **Functionalization of the biosensor:** analysis of the different methods for biosensor functionalization, focusing on Self-assembled monolayers (SAM) which will be implemented in the experimental part.
- d) **Applications and market research:** review on the most relevant current companies and applications related to the use of the SPR in the biomedical research field and furthermore on the early detection of Parkinson disease. Understand the future perspectives of the field.

## Second part: Experimental analysis

- a) **Characterization of the biosensor:** sweep of the surface of the grating coupled SPR microchip to study its structure and test the sensitivity of the different period diffraction gratings. The SEM microscope is also used to visualize the surface of the microchips more accurately.
- b) **Set-up of the biosensor:** includes both the chemical cleaning and regeneration of the biosensor and the setting of the different components needed to perform detection with SPR. The experimental errors derived from the set-up will be analyzed and solutions will be sought like the designing of new components, such as the microfluidics and methacrylate lid, with AutoCAD.
- c) **Functionalization of the biosensor surface:** analysis of the proper methodology and requirements to create a Self-Assembled Monolayer (SAM) and its appropriate chemical functionalization. A validation analysis of the SAM will be performed by visualizing its formation on the biosensor surface through a fluorescent microscope. The chemical preparation of the substances will be done in the Organic Chemistry Department.
- d) **Analysis of the protein-sensing capability:** the overall goal of the experimental part is to determine the sensing capability of the biosensor for protein detection. To accomplish this, different experiments with biosensors with both non functionalized and functionalized surfaces will be performed. The data obtained from the SPR detection is processed and will be used to provide a deep sensing capability analysis of different gold biosensors.
- e) **Optimistic objective:** early detection of Parkinson with in vitro samples of proteins related to the diagnosis of the disease.

## 1.3 LIMITATIONS

The two main limitations of the project have been the lack of both time and previous experience. The duration of the final degree project is only a few months, and a large percentage of it is a very extensive learning process, leaving small space to new discoveries. In this project specifically, time has been an important issue since the microchips have to be prepared and regenerated frequently which is time consuming and leads to significant time gaps between experiments. Moreover, at least 24 hours are needed to functionalize the sensor's surface. Another limitation has been that a percentage of the substances used had to be bought externally to providers like Sigma Aldrich and ThermoFisher Scientific which caused delays. Additionally, the available hours to use the microscopes in CCiTUB have been very limited and had to be scheduled weeks ahead. Furthermore, the lack of experience with the use of the SPR technique and functionalization of biosensor surfaces has led to more errors and thereby more time has been spent on finding

solutions. To obtain larger results and even to be able to develop on the early detection of Parkinson, additional time would have been required.

## 2. BACKGROUND

It is convenient to first introduce basic theoretical concepts involving the scope of the project to further understand the other parts. In this section a proper definition of a biosensor and its components will be provided while also giving an overview of the main advantages and drawbacks of this sensing technique. It will also show two ways to classify them and will focus on a specific type of biosensors, the optical sensing techniques. Finally, it will extend with detail on the detection method used in the project, Surface plasmon resonance (SPR).

### 2.1 BIOSENSORS

Biosensing is a complex, growing field that consists of the detection of target analytes<sup>1</sup>. It is built on the basis of the immune system because it follows the antibody/antigen mechanics, where an analyte is detected by a biological recognition element and through this interaction quantitative or qualitative information can be obtained.

The sensing device used is called biosensor and it allows for an accurate and efficient detection and quantification of analytes. Two of the most widely used and successful biosensors are the pregnancy tests and the glucose sensors. These artificial devices can be used for various applications. Some of the fields where they are considered more important are medical monitoring and diagnostics, environmental monitoring, biomedical research and food safety and quality control. Other relevant areas of interest are industrial process control and optimization, drug discovery and development and agriculture amongst many others. [1] [2]

#### 2.1.1 DEFINITION AND COMPONENTS OF A BIOSENSOR

A biosensor is a sensing device that uses a specific biological element and a transducer to detect and quantify analytes<sup>1</sup>. A target analyte binds specifically to the biological recognition element which generates changes in the biomolecule that are converted into a measurable signal by the transduction element. The resulting signal is calibrated to a specific scale and processed by a signal processing system. This signal will be proportional to the concentration of the analyte. [3][4]

Therefore, biosensors consist of two main parts: the biological element, which may be an enzyme, antibody, antigen, living cells, or tissues, and the transducer or sensor element, which can be an electric current, electrical potential, optical, piezoelectric, or thermal element. A Schematic representation of the working principle and components of biosensors is shown in Figure 1.

---

<sup>1</sup> **analyte:** is defined as "A substance of interest that needs detection. For instance, glucose is an 'analyte' in a biosensor designed to detect glucose" [2]

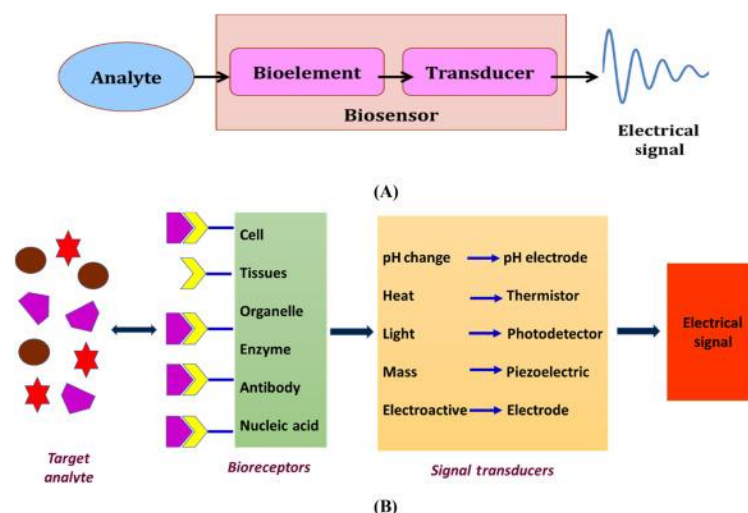


Figure 1: Working principle and components of a Biosensor [3]

## 2.1.2 IMPORTANT CONCEPTS OF BIOSENSORS

There are several parameters that are used to assess the efficiency of biosensors. One of the most important is sensitivity which defines the ability to distinguish minimal changes in concentration of the target analyte that produce a measurable signal that the biosensor can detect. Moreover, the sensing capability comprehends the sensitivity and the overall quality of the detection. Another important parameter is selectivity which is the ability to detect from a sample containing different substances, a specific analyte. It is also important to determine the reproducibility, that can be defined as the obtention of the same results when repeating the experiment under the exact same conditions. This concept is related to stability which is how sensitive is the sensor to external conditions that can interfere with the measurements [2] [5]

Biosensors are known to ensure a very high sensitivity and selectivity. Furthermore, this type of device offers many advantages over other sensing techniques. For example, the possibility to perform single-molecule detection. This reduces non-specific binding while it increases binding efficiency of the target analyte. Moreover, it can allow multiplexed detection, which is the analysis of different biomarkers simultaneously. Other positive aspects are the reduction of the requirements for sample manipulation, improvement of data quality and quantitative capabilities and the reduction of overall costs and measurement time. Many biosensors provide real-time and on-site monitoring. Furthermore, because the size of the biosensor can be in the micro or nanoscale a better signal-to-noise ratio can be obtained as well as the possibility of using smaller sample volumes, which may also reduce the overall cost.

Despite huge scientific advances on the sensing capability of biosensors have been made throughout the years, one of the major drawbacks remains to reach absolute selectivity. Moreover, a limited sensitivity and the complexity of the designing and manufacturing are also frequent problems in the field of biosensing. Other disadvantages are a low stability because they have a high surface-to-volume ratio they are more susceptible to environmental conditions, and due to the degradation of the bioelement over time. [5] [6] [2].

The future of biosensors has great potential, and it relies mainly on improvements in the increase of sensitivity, selectivity, speed of detection and multiplexing. Furthermore, if the devices are affordable, they will increasingly gain importance in the medical, environmental, and industrial field. [7]



### 2.1.3 CLASSIFICATION OF BIOSENSORS

There are several ways to classify biosensors, the most common way is based on their signal transduction mechanisms. According to this, biosensors can be categorized into four main different types. **Electrochemical biosensors** use an enzyme or other biorecognition element such as living tissues, DNA strands or cells to produce an electrical current upon the presence of the target analyte. **Thermal biosensors** measure the temperature changes to detect the substance. **Mass-sensitive biosensors** detect the changes in mass through the binding of the target analyte to a biorecognition element attached to a mass-sensitive element like a piezoelectric crystal or a magnetoelectric element. **Optical biosensors** use a fluorescent or luminescent molecule or other biorecognition element to produce a measurable change in light that indicates the presence of the target analyte. A subtype of optical biosensors, surface plasmon resonance (SPR), measures the changes in the refractive index upon binding of the target analyte to the biorecognition element immobilized on a surface to detect the presence of the analyte. [7] [1] [8]

Another well-known way to classify biosensors is by the biological element. **Whole-cell microbial biosensors** use genetically modified microorganisms, **Immunosensors** use antibodies, **DNA-aptamer based biosensors** use short DNA sequences called aptamers which bind specifically to the target analyte. **Enzyme and Protein receptor-based biosensors** use protein receptors as the sensor element. [1]

### 2.2 OPTICAL BIOSENSORS

Optical biosensors use light to detect and analyze biological molecules or interactions between them. When the light interacts with a substance, it can be absorbed, scattered, or reflected depending on the substance's characteristic properties. There are many ways to classify the different types of optical biosensors. One of the most common classifications is according to the physical principles used for the detection. One of the main methods is **Fluorescence** where the sensing element is a fluorescent molecule (fluorophore) and when the analyte binds to it, the fluorophore absorbs light at a specific wavelength and then emits it at a longer wavelength which can be detected and measured. Another widely used method and the one used in this project is **Surface plasmon resonance (SPR)** in which light is reflected off a metal surface and interacts with the electrons in the metal, creating a surface plasmon wave that is sensitive to changes in the refractive index of the surrounding medium. When using **Chemiluminescence**, light is emitted as a result of a chemical reaction. **Reflectance** is a technique in which light is reflected off a surface and the reflected light is analyzed to determine the properties of the surface, SPR uses reflectance. In **Absorbance** the quantity of absorbed light by the substance is measured. **Interference** uses the interference of light waves to measure the properties of the analyte. In **Raman scattering**, the light interacts with the vibrational modes of molecules<sup>2</sup>, causing a shift in the wavelength of the scattered light that is specific to the molecule's properties. Finally, the **Optical fiber biosensors** use optical fibers to detect changes in the refractive index of a surface caused by biomolecular interactions. [9] [10]

---

<sup>2</sup> **Vibrational modes of molecules:** refer to the different ways in which the atoms in a molecule can move relative to each other [45]

### 2.2.1 SURFACE PLASMON RESONANCE:

Surface Plasmon Resonance (SPR) biosensors are an optical label-free biosensing technique used for qualitative and quantitative binding interactions, chemical or biochemical, in real-time [11]. Label-free has the advantage that it does not require the use of fluorescent or radioactive labels, which could alter the results. The physical principle of SPR is based on the excitation of surface plasmons, which are collective oscillations of electrons at the interface between a thin layer of metal and a dielectric medium. When light is incident on the metal surface at a specific angle, it interacts with the free electrons on the metal surface generating a surface plasmon wave. This propagating electromagnetic wave at the interface causes a decrease in the reflected light intensity. Moreover, the incident angle at which this intensity drop occurs is known as the resonance angle and is sensitive to changes in the refractive index of the dielectric medium. This angle is defined as the range of angles at which the incoming light energy is absorbed by the electrons in the metal film, creating the surface plasmons. [9][10][12][13]

SPR has several applications in the study of biomolecular interactions, chemical detection, and immunoassays. It is commonly used to perform biomolecular binding interactions analysis between free analyte molecules in a solution and ligand molecules that are bound to or immobilized on the sensor surface. As the analyte molecules bind to the ligand, the refractive index and thickness of the adlayer in contact with the metal film changes, causing a shift in the SPR resonance angle (Figure 2a). This kind of study can generate different types of information. It can identify the binding between two or more interactants, such as DNA with DNA or proteins, lipids with proteins, among many others. It can also determine the affinity and specificity of these interactions and the Kinetics which study the association and dissociation rates. Moreover, it can quantify the concentration of the free analyte bound to the surface. This kind of information can be provided through a graphical representation of the biosensor's response as a function of time, called a Sensorgram (Figure 2b). It has three main phases: association, steady state, and dissociation. During association, the speed at which two or more molecules bind to each other depends on the association rate constant, the analyte concentration, and the number of free ligand sites. During steady state, the response reaches an equilibrium since the number of association events is equal to the number of dissociation events. During dissociation, the curve should follow a single exponential and the dissociation is only dependent on the dissociation rate constant. If the biosensor wants to be re-used, an extra regeneration step can be applied which consists of breaking all the remaining interactions between the analyte and ligand. [9][13][14]

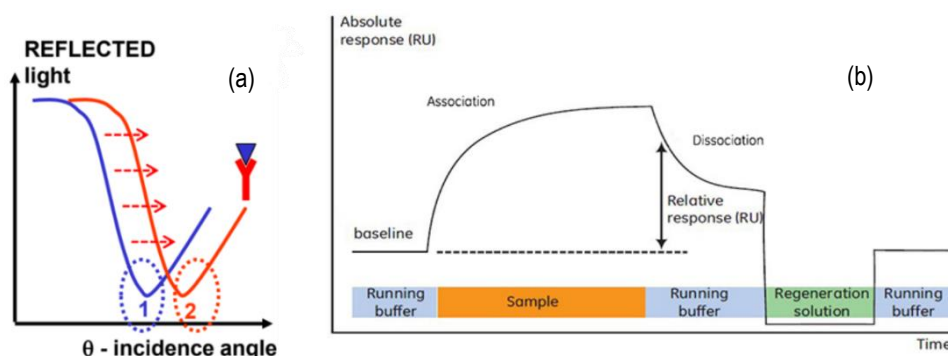


Figure 2: a) Reflected light as a function of incident angle [11] b) Biomolecular interaction analysis: a Sensorgram [14]

SPR is also used in the fields of drug discovery, environmental monitoring, food safety, and medical diagnostics, where it can be used to detect pathogens, toxins, and disease biomarkers. [13]

### 2.2.1.1 THE KRETSCHMANN CONFIGURATION

The Kretschmann configuration is the most used experimental setup in SPR. In this configuration, a thin metal film is placed on a glass substrate, and a prism is used to couple light into the metal film at the resonance angle. As previously mentioned, this angle is sensitive to changes in the refractive index of the surrounding medium and the loss of intensity in the reflected beam due to the surface plasmon resonance can be detected and measured as a drop (referred as resonance DIP) of the intensity in the SPR reflection spectrum (Figure 3). The location of this resonance DIP can then be used to extract information about the properties of the molecules or biomolecules on the sensor surface, such as their binding kinetics or concentration. In this configuration, the incident light is a monochromatic laser, and the reflected light is detected by a photodetector.[11] [12]

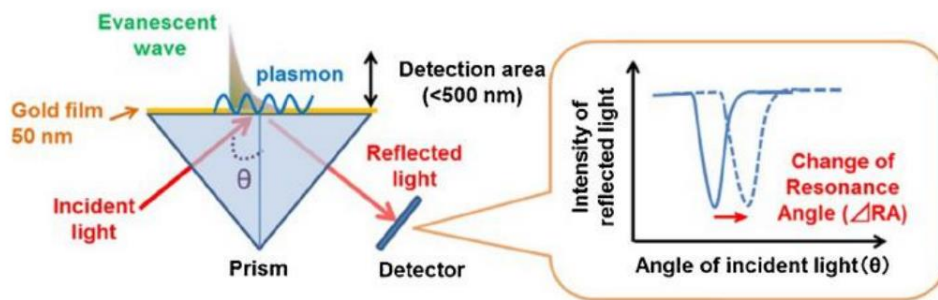


Figure 3: Scheme of the Kretschmann configuration detection mechanism of SPR [11]

### 2.2.1.2 GRATING COUPLING METHOD

Another configuration, grating coupling, uses a nano constructed surface with diffraction gratings to allow the detection through SPR. The grating consists of periodic structures on the surface, and the period of the grating determines the wavelength of resonance. When the incident light with a specific angle, that matches the interface between the gold and the dielectric layer, hits the diffraction gratings light gets diffracted into different angles which correspond to different wavelengths. By measuring the intensity of the diffracted light as a function of the wavelength, the SPR response can be detected. [15]

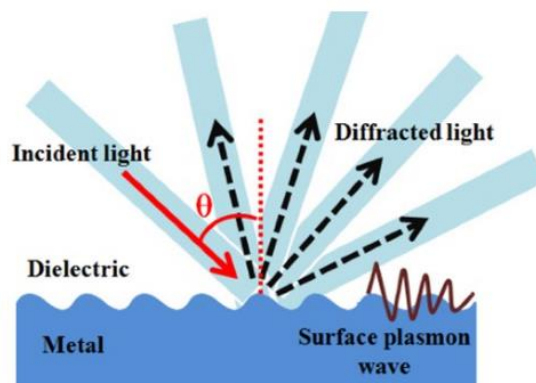


Figure 4: SPR principle on nano constructed surface.

The set-up developed in this project (Figure 5), is composed of a White light from a source (LS1 from OCEAN OPTICS) which is sent by a fiber optic cable to the SPR system. The light is collimated and divided into two beams using a beam splitter (50%-50% division). One of the beams is TM polarized whereas the other beam can be used as a reference signal. The polarized beam is

focused onto the surface of the metal coated biosensor, using a 4x OLIMPUS objective. When the polarized light reaches the surface, it interacts with the electrons in the metal of the biosensor and creates a surface plasmon resonance which causes the intensity of the reflected light to decrease at a specific angle, which is related to the refractive index of the medium placed on the sensor's surface. The reflected light then goes through a second fiber optic cable and is sent to a spectrometer (SD2000 from OCEAN OPTICS). In this configuration the angle is fixed, there is no mechanical movement of the sensor. Therefore, as opposed to the Kretschmann configuration, the spectrometer measures the intensity of the reflected light as a function of the wavelength not the angle. [14]

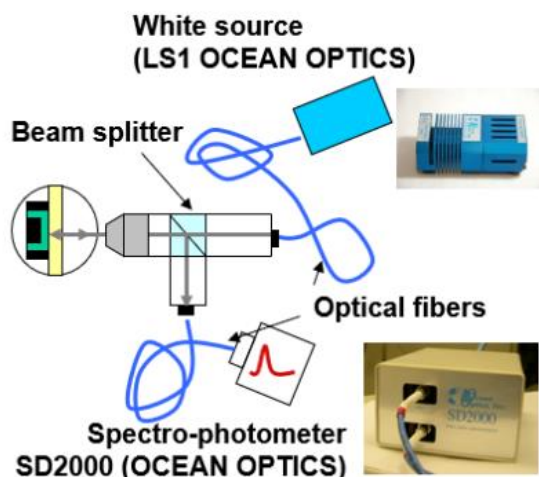


Figure 5: Experimental SPR set-up in the development phase in the DEE [12]

Overall, with this configuration, changes in the intensity of the diffracted light at different wavelengths provide information about variations in the refractive index of the surrounding medium or the presence of analytes on the surface.

## 2.3. FUNCTIONALIZATION OF A GOLD-BASED BIOSENSOR

The functionalization of biosensors refers to the treatment of the sensor's surface to enhance the binding of target analytes.

### 2.3.1 LIGAND IMMOBILIZATION METHODS ON GOLD BIOSENSOR SURFACE FOR SPR

Ligand immobilization on a biosensor's gold coated surface is generally needed to recognize and bind a target analyte. There are several methods to do so, by using **Physical adsorption**, the target ligand attaches to the biosensor's surface through hydrogen bonding, van der Waals forces, electrostatic forces, and hydrophobic interactions. This technique has some major setbacks such as disordered orientation of the attachment layer, weak binding, and heterogeneity of ligand. A second method would be **Covalent immobilization** that involves the formation of Self-assembled monolayers (SAM), which are highly organized, via chemisorption onto the gold surface of the biosensor. The **capture method** is used when the ligand is damaged as a consequence of covalent immobilization, a capture molecule that has a high affinity for the ligand contributes to ligand

immobilization. Another method would be **polymer film deposition** which consists of fabricating a polymer nanolayer on the surface of the biosensor [16].

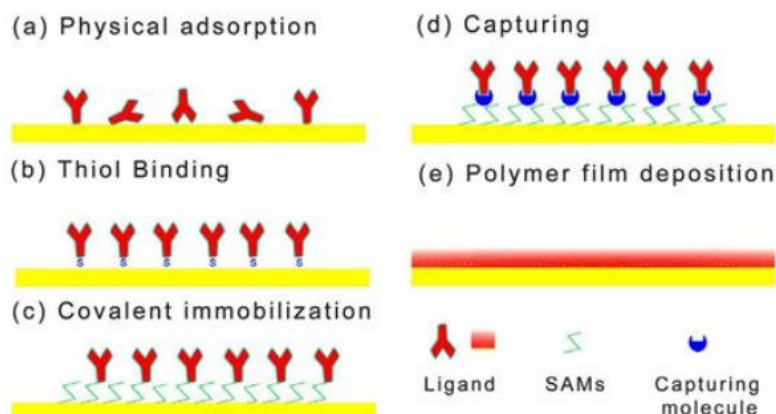


Figure 6: Methods to prepare modified surface, including (a) physical adsorption (c) covalent immobilization (SAMs-based), (d) capture, and (e) polymer film deposition methods [16]

### 2.3.2 COVALENT IMMOBILIZATION

Self-assembled monolayers (SAM) are an ordered layer of organic molecules that spontaneously form on a substrate surface, in this case the gold layer of the biosensor. The organic molecules used for SAM usually have three main components, a head group to interact with the substrate surface, an alkyl chain and a tail group that gives the functionality. The formation is typically done through a process called chemisorption, by immersing the substrate in a solution containing the SAM molecules, the head groups of the SAM form strong chemical bonds with the substrate surface. The strong bonds, typically covalent, make this layer durable and stable. Once adhered on the surface, SAM molecules start spontaneously creating an organized, well-packed layer. This is produced because of the presence of Van der Waals forces between the alkyl chains of the SAM molecules and the substrate surface. As it will be seen in the experimental part, the process of formation takes many hours. SAMs have a wide range of applications in biosensors and bioelectronics due to their ability to immobilize biomolecules like enzymes, antibodies, and nucleic acids, which can then be used for the detection of analytes in a sample, and their compatibility with metal surface substrates useful for biosensing. They are also easily tunable, since they can be designed with various functional groups to accomplish either hydrophobic or hydrophilic surfaces. As previously stated, they are durable and stable layers and this allows for long-term monitoring and to give information about biomolecular interactions, such as protein adsorption, DNA hybridization, and antigen-antibody interaction. [17] [18]

One classification method for SAMs is based on their head groups, as shown in Table 1.

Table 1: SAMs classification based on head group [17][19][20][21]

	Head group	Process of formation	Substrate surface commonly used
Alkanethiol SAMs	Alkanethiol molecules (-SH)	Chemisorption	gold or silver
Silane SAMs	Silane group	Chemisorption	Silicon dioxide, glass
Phospholipid SAMs	Phospholipid group (-PO <sub>4</sub> H <sub>2</sub> and -OH)	Chemisorption	Gold, glass, silicon dioxide
Carboxylic acid SAMs	Carboxylic acid group (-COOH)	Chemisorption	glass, silicon dioxide
Amine SAMs	Amine group (-NH <sub>2</sub> )	Chemisorption	gold, glass silicon dioxide

## 2.4. APPLICATIONS

### 2.4.1 GENERAL APPLICATIONS OF SPR IN BIOMARKER DETECTION IN THE BIOMEDICAL FIELD

There are several applications for protein detection with SPR in the biomedical field, however, this section will be focusing on three of the main areas of research: **Cancer**, **viral diagnostics**, and **neurodegenerative diseases**.

**Cancer** is the first cause of death in the world, in 2020 OMS estimated that almost ten million people lost their lives to this disease [22]. That is why it is no surprise that an important part of the research conducted by universities, research institutions and companies is the use of SPR sensors for detecting cancer biomarkers. One of the most important investigations in the field of SPR biosensing is the detection of prostate-specific antigen (PSA), a protein that is produced by the prostate gland in men, widely used for the early detection of the most common cancer for male, the prostate cancer. [23]. The early detection of this disease has a direct impact on the successfulness of the treatment and in improving the patient's outcome. To address this, the SPR biosensor is coated with antibodies specific to PSA and when a sample containing PSA is introduced to the biosensor's surface, the PSA molecules bind to the antibodies on the metal surface, causing a change in the refractive index and resonance angle which is detected by the SPR biosensor and used to quantify the amount of PSA present in the sample. Furthermore, nanoSPRs have been developed, which use noble metal nanoparticles and nanos-structures as sensing elements, for high-throughput screening of biomolecular binding interactions in a real-time. Additionally, due to their miniaturized dimensions they will be useful for a future implementation of Point of Care testing (POCT)<sup>3</sup>. SPR has great future in point of care techniques because of its non-destructive nature, which allows to analyze the evaluation of the cancer biomarker without damaging or altering the sample, which is sometimes important because the sample may be limited or hard to obtain. Furthermore, there are many other biomarkers from different cancers that could potentially be detected through SPR, some of the most important ones are seen in Table 2 [24].

<sup>3</sup> Point of Care testing (POCT): type of medical diagnostic testing that replaces centralized laboratory testing for on-site or near the patient.



**Table 2: Other potential cancer biomarkers for SPR detection [24]**

Biomarker	Biomarker Type	Sensitivity/Specificity and Predictive Value	Cancer Type	Source	Biological Concentration	Clinical Use	Conventional Technique
Alpha-fetoprotein (AFP)	Protein	Sensitivity: 65%/Specificity: 89%	Hepatocellular carcinomas	Serum	>400 ng/mL	Diagnostic and prognostic	Immunoassay
Bladder tumor antigen (BTA)	Protein	Sensitivity: 83%/Specificity: 92%	Bladder cancer	Urine	-----	Monitoring	Immunoassay
BRCA-1 and BRCA-2 mutations	Genomic	Sensitivity: 80%/Specificity: 100%	Breast cancer	Blood	----	Prognosis	DNA sequencing
Cancer antigen 19-9 (CA 19-9)	Protein	Sensitivity: 81%/Specificity: 90%	Pancreatic cancer	Serum	≤100 U/mL	Diagnostic and prognostic	ELISA
Cancer antigen 15-3 (CA 15-3)	Protein	Sensitivity: 31%/Specificity: 86%	Breast cancer	Serum	25 U/mL	Monitoring	Immunoassay
Cancer antigen 125 (CA 125)	Glycoprotein	Sensitivity: 80%/Specificity: 99.6%	Ovarian cancer	Serum	35 units/mL	Detection, diagnosis, and prognosis	Immunoassay
Carbohydrate antigen 27.29 (CA 27.29)	Protein	Sensitivity: 65%/Specificity: 100%	Breast cancer	Serum	>35 U/mL	Monitoring	Immunoassay
Carcinoembryonic antigen (CEA)	Protein	Sensitivity: 88.3%/Specificity: 46.2%	Lung cancer	Serum	8.2 ng/mL	Detection, diagnosis, and	Immunoassay

A second important area of research are **Viral diseases**, which have significant impacts on human health and can spread rapidly, causing outbreaks and pandemics. The emergence of new and more virulent strains of viruses calls for more advanced detection methods. SPR sensors is one of the main techniques for the study and detection of viral pathogens, such as the norovirus, HIV, influenza, and Zika virus. It is also used to analyze virus-host interactions and to develop antiviral drugs and vaccines. A review of applications of the SPR biosensors in this field are compiled in "Surface Plasmon Resonance: A Boon for Viral Diagnostics" [25]. Some of the most relevant applications it describes are nanoparticle-based viral detection, such as peptide-functionalized gold nanoparticles and magnetic nanoparticles for detecting norovirus, the use of aptamers-based bioreceptors, sandwich-type SPR biosensing platforms, gold nanobipyramids for ultrasensitive detection of the Influenza Virus, Fluoroimmunosensor SPR for Norovirus Detection, SPR analysis of Coronavirus Protease Inhibitors and SPR aided systems for Ebola Vaccine Design.

Another research field where biosensing with SPR could have an enormous impact are **neurodegenerative diseases**. Alzheimer's disease, Parkinson's disease, and glaucoma affect millions of people worldwide and are characterized by the progressive loss of neurons in the brain, leading to cognitive and motor impairments that can severely affect the quality of life of affected individuals. The impact of these diseases extends to their families, caregivers and to the economy, individual and global, since the cost of healthcare for these diseases is usually long-term and demands a lot of resources. Early detection and diagnosis of neurodegenerative diseases are crucial for effective treatment and to obtain better outcomes. Chip-based biosensing techniques, such as SPR sensors, offer great potential as compared to the conventional diagnostic methods like neuroimaging (PET, SPECT, MRI) which are not only expensive but also time-consuming. Moreover, SPR could achieve POCT of these diseases which would offer many advantages. To detect these diseases with SPR, specific probes such as peptides or aptamers are

immobilized on the surface of the sensor, and the biomarker of interest is flowed over the microchip. The binding of the biomarker to the immobilized probe is detected by changes in the reflected light, which are captured usually by a CCD camera, instead of a spectrometer. The resulting images are analyzed to determine the binding kinetics and affinity of the interaction. The change in refractive index of the surface is detected as a shift in the SPR angle which is proportional to the amount of biomarker present in the sample. Therefore, SPR can be used to detect neurodegenerative diseases by identifying specific probes that have high affinity and specificity to the biomarkers of interest. In the case of Alzheimer, different types of SPR biosensors that can be used are immunosensors which use antibodies to capture the biomarker, aptasensors that use aptamers, which are synthetic oligonucleotides, Waveguide SPR chips that utilize a waveguide to enhance the resolution of SPR signals and bimetallic SPR sensors which detect low concentrations of analytes using gold and silver metals. [10][26]

#### 2.4.2 EARLY DETECTION OF PARKINSON:

The optimistic objective at medium term of the DEE is to achieve the early detection of the Parkinson disease.

Parkinson's disease is a chronic neurodegenerative disorder that affects the nervous system and mainly causes motor symptoms. It can cause inability to control movements, shaking, stiffness, and problems with balance and coordination. The symptoms typically start gradually and get worse over time. The disease occurs when nerve cells in the substantia nigra which is located in the basal ganglia of the brain, a part of the brain that controls movement, become damaged or die. These cells produce an important chemical called dopamine, which helps regulate movement. When these neurons die, there is a decrease in dopamine levels, causing the movement problems associated with Parkinson's. It can also cause non-movement symptoms such as fatigue, irregular blood pressure, and memory difficulties. This is because people affected with Parkinson's also lose the nerve endings that produce norepinephrine, a chemical messenger that helps control many functions of the body. The cause of neuron death is still unknown, and scientists believe the disease is caused by a combination of genetic and environmental factors. However, the loss of dopamine is linked to the presence of Lewy bodies in the substantia nigra and other brain regions, which are deposits mainly composed of aggregated alpha-synuclein. This is a presynaptic neuronal protein that contributes to the disease's pathogenesis by forming aberrant soluble oligomeric conformations, known as protofibrils, that are thought to be toxic species that disrupt cellular homeostasis and lead to neuronal death, causing effects on various intracellular targets, including synaptic function. [27] [28] [29]

There is currently no effective treatment for Parkinson's disease, however there are different treatment options that can help relieve its symptoms. The main therapy for Parkinson's is levodopa, which helps increase dopamine levels in the brain. Other medications, such as dopamine agonists, enzyme inhibitors, amantadine, and anticholinergic drugs, may also be prescribed. For those who don't respond well to medications, deep brain stimulation may be recommended. Moreover, physical therapy and exercise can help to improve mobility and balance. Early treatment of Parkinson's disease is important because it can help slow down the progression of the disease and improve the quality of life for patients. [28] [29]

As for the diagnosis of the disease, it is typically detected through a medical history and neurological examination, and by analyzing the improvement in symptoms after medication. There are currently no blood or laboratory tests to diagnose non-genetic cases of Parkinson's. Imaging



studies to assess dopaminergic nigrostriatal projections and targeting the toxic functions of alpha-synuclein may lead to novel therapeutic strategies not only in Parkinson, but also in other neurodegenerative diseases that involve abnormal accumulation of alpha-synuclein, known as synucleinopathies, like Lewy bodies dementia or multiple system atrophy (MSA). Optical sensing techniques are also being explored in research and clinical trials. Furthermore, there are many potential biomarkers under investigation to assess the diagnosis or progression of the disease. [27] [28] [29]

SPR can be used as a mechanism to detect biomarkers related to the early detection of the disease. This has usually been done in the past by detecting alpha-synuclein. One way to do it is to fix on a gold-coated biosensor a probe called synuclein binding peptoid-7 (ASBP-7) which is able to detect the alpha-synuclein from a sample that is flowing over the biosensor's surface. The binding between ASBP-7 and alpha-synuclein is measured by changes in reflected light, allowing the detection of Parkinson's disease by analyzing the binding affinity between the two. [12]

It has also been found that other combinations of biomarkers could provide a more accurate diagnosis. A study conducted by a team of researchers from various institutions in Spain aimed to evaluate whether certain proteins and cytokines found in cerebrospinal fluid (CSF) and plasma could be used as diagnostic markers for Parkinson's disease or to determine the severity. The researchers collected CSF samples from 51 patients with Parkinson's disease and 40 healthy controls, and plasma samples from 51 patients and 26 additional controls. They measured the levels of various proteins and cytokines in the samples using enzyme-linked immunosorbent assay (ELISA) kits and Luminex technology. The study found through statistical methods that the P-Tau/a-synuclein ratio in the CSF showed a sensitivity of 97.1% which is a more accurate diagnostic marker for Parkinson's disease than any of the proteins studied on their own. [27]

## 3. MARKET RESEARCH





The market sector concerned by this project is the use of SPR biosensors in the biomedical research field.


### 3.1 CURRENT COMPANIES, INSTITUTIONS AND COMMERCIAL PRODUCTS THAT USE SPR

In this section a summary of the main instruments currently available and suppliers of SPR biosensors is gathered. This information is extracted from the web "SPR pages" [16] which provides a highly detailed analysis of the technique.

There are many companies that have a great impact on SPR technologies, however due to the limited extension of the project, only a summary of five of the most relevant is provided in Table 3.

Table 3: Relevant companies in SPR technologies

SPR SUPPLIER	DESCRIPTION	SERVICES OR INSTRUMENTS
<p>Biacore:</p> 	<p>Pioneer company born in Sweden in 1984 that provides instruments and sensor chips that use SPR technology. It is now a part of Cyvita since 2020. [30]</p>	<p>Biacore AB instruments use a wedge-shaped prism as a light source and a diode array detector to measure the reflected light intensity at multiple angles. This design avoids any moving parts in the optical interface, leading to a more stable and reproducible instrument for analyzing biomolecular interactions.</p>
<p>Biosensor Tools LLC:</p> 	<p>World leader company in label-free analysis with sites in the US and now the EU. They provide everything biosensor related from assay development and screening to kinetics and biosimilar analysis.</p>	<p>They offer contract services utilizing instruments from <b>Biacore</b>, BioRad, <b>Bruker</b>, <b>Carterra</b>, ForteBio &amp; <b>Nicoya</b>.</p>
<p>Bruker:</p> 	<p>They specialize in SPR technology and have made significant breakthroughs in microfluidics, sensor design, and SPR detection.</p>	<p>Their instruments include the Sierra SPR-32 and Sierra SPR-24 Pro, which offer high throughput analysis (simultaneously inject 8 samples with a total of 32 individual addressable sensor spots) and high sensitivity detection. They also provide related supplies and software for their SPR systems.</p>
<p>Nicoya:</p> 	<p>Founded in 2012 by a graduate student while doing master's research at the University of Waterloo. Centered on drug discovery research. Created The first ever Digital Microfluidics powered SPR system.</p>	<p>Offers the world's first SPR instrument, Nicoya Alto, to integrate digital microfluidics, artificial intelligence, and nanotechnology. They use Digital Microfluidics which is a technology that allows precise control and manipulation of small volumes of fluids in the microliter to nanoliter range using electrical fields without the need of pumps, valves or tubes. The use of single disposable microwell plates (Alto cartridges) that integrate fluidics and SPR sensors enables eliminating the need for cleaning and maintenance and reducing contamination.[31]</p>
<p>Carterra:</p>	<p>Carterra is a company founded in the US in 2005 that provides innovative technologies to accelerate</p>	<p>Their high-throughput LSA instrument is used for monoclonal antibody screening and characterization which combines microfluidics technology with real-time</p>

	the discovery of novel therapeutic candidates.	array SPR and industry-leading data analysis software. This enables all antibodies to be screened early in the discovery process, helping to identify unique epitopes <sup>4</sup> and potential novel therapeutic candidates. They enhance IP coverage (useful for preventing other companies from taking advantage of their inventions).
---	--	--

Moreover, based on proximity, an important institution, which uses SPR biosensors for research purposes and has even tried to investigate the early detection of Parkinson, is the Biomedical Institute of Bioengineering of Catalonia (**IBEC**). During this project, a visit to their centers has been made to learn their methodology since the SPR set-up, mechanisms and objectives are very similar to the ones of this project.

### 3.2 FUTURE MARKET PROSPECTS

The future of SPR is promising as it is potentially one of the most powerful techniques to study biomolecular interactions and it serves for several purposes in many fields. However, new technological advancements must be made for the technique to progressively gain relevance. According to a well-known market research and consulting firm called Future Market Insights (FMI), the SPR market will double in size in 10 years, from 910,4 million in 2022 to 1807,7 million in 2032. The average growing rate per year (CAGR) will be approximately 7,1 %. This incredible upgrade will be mainly due to the increased demand in real-time, label-free measurements of biomolecules, the implementation of point of care testing (POCT), the incorporations of microfluidics and nanotechnology into SPR and the rising use in fields of scientific research including drug development and medical imaging and diagnosis. This growth of SPR is limited by existing problems its solution is still in discovery phases. These are primarily the lack of sensitivity, studied deeply in this project, the cost of incorporating microfluidics, the difficulty to accomplish Point of care testing, the implementation of high-throughput screening and to industrially produce a large number of durable metal nanostructures on a substrate. [32]

One of the most important future advancements is the implementation of **POCT systems** in SPR biosensors. These systems are characterized for being fast, portable, and easy to use, allowing for a rapid diagnosis and treatment decision. Recent advances in miniaturizing SPR technology have made it possible to develop portable systems for the screening of biomolecular binding interactions in a real-time, label-free manner. Moreover, the next generations of SPR biosensors should all incorporate **high-throughput analysis** which refers to the simultaneous detection of multiple substances to obtain a profile of concentrations for the molecular diagnosis of diseases such as certain types of cancers or degenerative diseases. They should also be able to **measure complex samples** such as serum, urine, saliva, and even tissues, with adequate specificity. Another target is the obtention of **ultra-sensitive biosensors** to reach the detection of extremely nanoscopic concentrations of biomarkers ( $10^{-9}$  mol/L). This can be achieved by nanoSPR, by coating with noble metal (gold or silver) nanoparticles or nanoconstructs, with different unique optical properties and functionalized with antibodies with different specificities, arranged in an array format. The use of an

<sup>4</sup> **Epitope**: is the part of an antigen recognized by the immune system of the host

array format enables the simultaneous analysis of multiple analytes, which increases the throughput of the screening process. [23] [33]

Despite the challenges that need to be tackled, with continued research and development, it is likely that effective solutions will be found, and SPR biosensors will become even more prevalent and essential in a wide range of applications, including scientific research and medical diagnosis.

## 4.CONCEPTION ENGINEERING

This part contemplates the resources and requirements necessary to carry out the experimental analysis, described in the section of detailed engineering. The gold-coated SPR biosensor, SPR detection set-up and microfluidics had already been given so there has been no space for alternatives. However, the biosensor has different periods of diffraction gratings and therefore a sweep of the surface with SPR will be useful to study which period has a better sensitivity to perform the experiments. Moreover, other alternatives for the microfluidics can be analyzed or designed for future improvements. The selection of the SAM to functionalize the gold layer of the sensor and the substances to be detected are the main decisions needed to be made.

### 4.1 GOLD-COATED BIOSENSOR

#### 4.1.1 FABRICATION PROCEDURE AND STRUCTURE

The gold-coated microchips used in this project have been fabricated at the Nanotech Department of the Technical University of Denmark (DTU). The microchips are squares of 15 mm x 15 mm. The process of fabrication begins by depositing the dielectric layer of the microchip on a silicone substrate. To do so, through thermal oxidation, a 500 nm thick thermal layer of  $\text{SiO}_2$  is deposited and on top through Low-Pressure Chemical Vapor Deposition (LPCVD) a 100 nm layer of  $\text{Si}_3\text{N}_4$ . In the next step, a photoresist layer is spin-coated on top of the  $\text{Si}_3\text{N}_4$  layer, and a 20 nm thick layer of aluminum is thermally evaporated on top of the photoresist layer. Then, this aluminum layer is removed by immersion in a strong alkaline solution, TMAH in this case, and the photoresist is developed using an appropriate developer (chemical solution). Then, the  $\text{Si}_3\text{N}_4$  layer is etched using CHF<sub>3</sub> chemistry in a Reactive Ion Etching system to create the desired subwavelength diffraction gratings, which have periods ranging from 500 nm to 600 nm in 25nm steps and each have a square area of 0.5mmx0.5mm (Figure 7a shows the gratings). Finally, the remaining photoresist is stripped off and through electron-beam evaporation an adhesion layer of 3 nm of Titanium is deposited on top of the  $\text{Si}_3\text{N}_4$  layer, and on top a layer of gold with thicknesses ranging from 40 to 60 nm by the same procedure. The resulting gold-coated microchip is shown in Figure 7b and its composition in Figure 7c. [11][15].

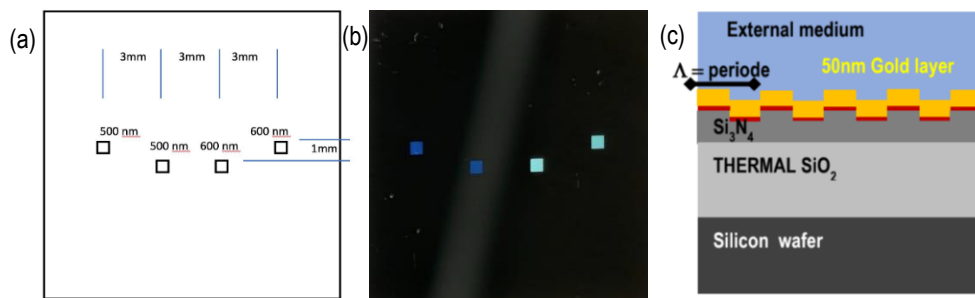


Figure 7: a) Microchip diffraction gratings structure scheme b) Real gold-coated microchip c) Composition of the gold-coated microchip

#### 4.1.1.1 SCANNING ELECTRON MICROSCOPY

To see with greater detail the diffraction gratings, microscopic images of the two diffraction gratings have been obtained. The microscope used is a Field Emission Scanning Electron Microscope (FE-SEM) from the brand Jeol 7100 found at the Scientific and Technological Centers of UB (CCiTUB).

FE-SEM is an advanced imaging technique that provides topographical and chemical composition information at high magnifications. It produces clearer and less distorted images with spatial resolution down to 1 and 0.5 nm, which is three to six times better than traditional SEM. It allows examination of smaller contamination spots and produces high-quality, low-voltage images with minimal sample charge suppressing the need for conducting coatings on insulating materials. It works by using a field-emission cathode found in the electron gun of the microscope. This cathode generates narrower beams of electrons at different energy levels, allowing for better precision and detail in imaging. Therefore, it achieves improved spatial resolution and minimized sample damage, making it a useful tool for the characterization of materials. [43]

The images generated by FE-SEM are gathered in Figure 8. It can be clearly seen that in the 500 nm period the grooves are separated at smaller distances.

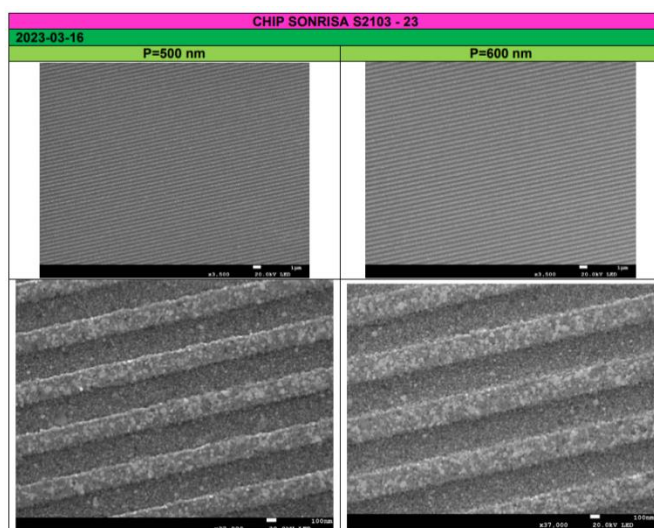


Figure 8: SEM images of diffraction gratings of periods 500 nm and 600 nm (taken by Anna Estany)

#### 4.1.2 CHARACTERIZATION OF THE BIOSENSOR

A sweep of the surface of the sensor is useful prior to the experimental part to analyze the detection mechanisms of SPR, the structure of the surface and to study the sensitivity of the two periods of the diffraction gratings. The main goal is to assess the sensitivity, which in simple terms means to quantify how much nm the wavelength shifts in each period to detect the different refraction indexes. Higher sensitivity means that for smaller changes in refractive index, larger changes of wavelength. To do so, several sweep experiments have been conducted with different substances that have different refractive indexes as a medium.

The experiments consist of placing the cleaned microchip, the cleaning mechanisms will be explained later, on the SPR machine. Then, the sensor is immersed in the different substances and on top a methacrylate lid or quartz cover, or another option is to flow the liquids through a microfluidics set-up. Once it is prepared, the SPR machine performs a sweep of the surface of the

sensor. For each point of the surface, a resonance DIP, its profundity depends on fabrication parameters among other factors, appears at a specific wavelength, called resonance wavelength. The wavelength detects changes as a function of the refractive index of the substance. In Figure 9, two spectrum of the measurement of one point for each period is shown. The spectrum on the left corresponds to the 500nm period which shows a resonance DIP at wavelength 715 nm and on the right the period 600 nm with a resonance DIP at 849nm. The other DIPs of less magnitude belong to the optical interference between silicon oxide and silicon nitride layers.

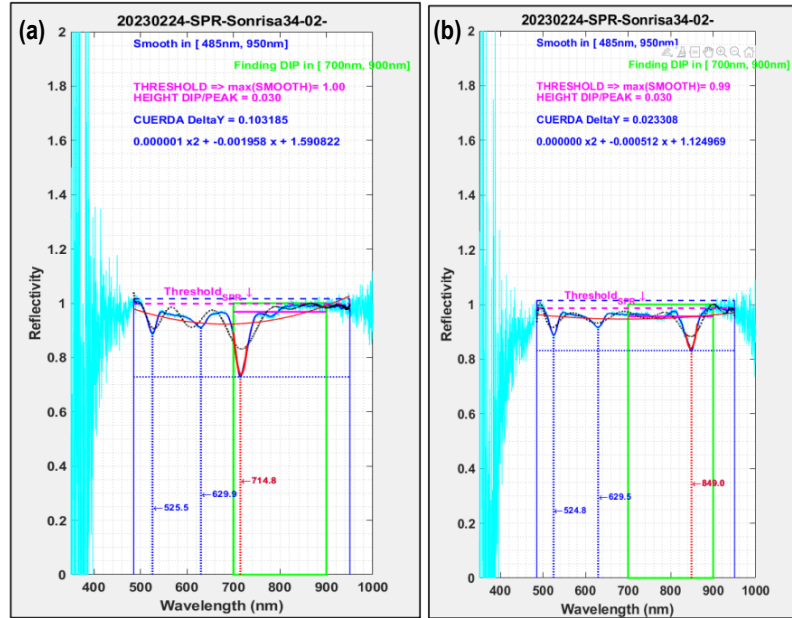


Figure 9: Spectrum of a surface sweep for one point for period (a) 500 nm and (b) 600 nm, from experiment with isopropanol/ethanol performed with CHIP41 the 24th of February.

If the sweep is done for all the points of the surface of the sensor, the motor's path is not able to scan all four sensitive areas. Therefore, only one diffraction gratings of each period will be included in the sweep. In Figure 10, measurements for all the points for the two diffraction gratings are shown, being P1 the one of 500 nm and P2, 600 nm.

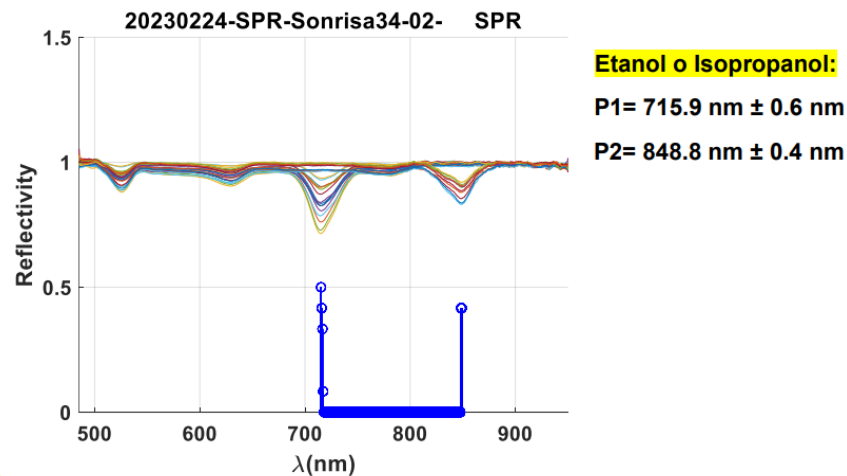


Figure 10: Surface sweep for all the points of the diffraction grating of both periods from the sweep from experiment with isopropanol/ethanol performed with CHIP41 the 24th of February.



Furthermore, in Figure 11, a visual representation of the sweep of the surface shows the positioning of the diffraction gratings and shows on the left, the wavelength of the resonance DIP, known as resonance wavelength (nm), of each point, and on the right the depth or magnitude.

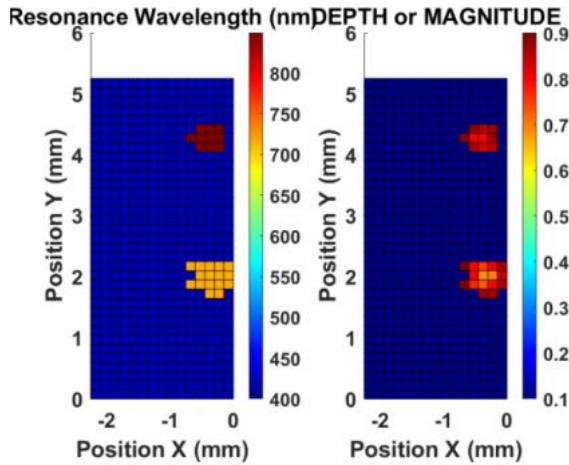


Figure 11: Visual representation of the surface sweep for all the points from the sweep experiment with isopropanol for both periods performed with CHIP41 the 24th of February.

The resonance wavelength for each point of the sweep from the diffraction gratings are represented in Figure 12a, where the top measurements that are around wavelengths 850 nm correspond to the period of 600 nm and the ones around 720 nm are from period 500 nm. From this, on Figure 12b, a histogram with the computed average of the resonances wavelengths of each period is generated.

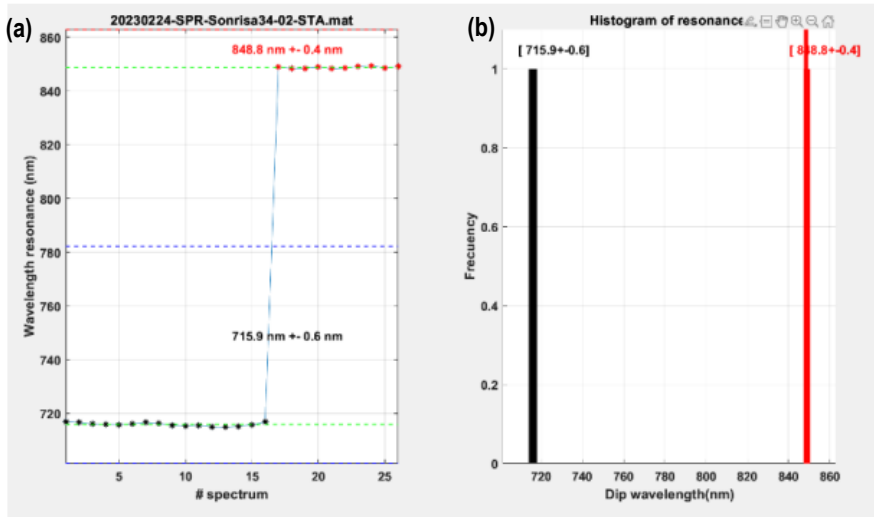


Figure 12: a) resonance wavelength for both periods from experiment with isopropanol/ethanol performed with CHIP41 the 24th of February b) Histogram with average resonance wavelength for both periods from experiment with isopropanol performed with CHIP41 the 24th of February.

This average value is the one that is going to be used to compute the sensitivity. Now, this procedure must be performed with several substances with different refractive index. The substances used are shown in Table 4, and the different experimental results are gathered at Table 5, where the highlighted in red are discarded.

Table 4: Refractive index of the substances used in the experimental part.

Substance	Refractive Index
Water	1.33
Isopropanol	1.3772
Ethanol	1.361
Glycerol 10% in water	1.34346
Glycerol 25 % in water	1.3621
Glycerol 40% in water	1.38084
Glycerol 60 % in water	1.40576
Glycerol 86-69 % in water	1.4556

Table 5: Sweep experiments with different substances with the average DIP wavelength

#			REF	CHIP	DIPS FIJOS		P1 (500nm)	P2 (600nm)	P1 (500nm)	P2 (600nm)	P1 (500nm)	P2 (600nm)
					FP1	FP2	WATER		ETHANOL		GLYCEROL	
2	Metacrilato	Sweep	EtOH	41	526	630			715.9±0.6	848.8±0.4		
3	Fluidica	Sweep	EtOH	41	527	631			701.6±0.7	829.5±0.6		
4	Fluidica	Sweep	EtOH	41						831.6±0.9		
5	Fluidica	Sweep	EtOH	41			703.4±0.5	830.5±0.3				
6							DESCARTADA					
10	Metacrilato	Sweep	Water MilliQ	12	532	634	707.5±1.3	832.5±1.0				
11	Metacrilato	Sweep	EtOH	12	530	634			717.6±1.9	-		
12	Cuarzo	Sweep	EtOH	12	529	632			716.5±0.7	831.4±0.4		
13	Cuarzo	Sweep	EtOH	12					720.6±1.1	851.0±0.9		
14							DESCARTADA					
15	Cuarzo	Sweep	GLY (86-89%)	12	529	634					760.2±3.7	902.8±0.7
16	Cuarzo	Sweep	GLY (86-89%)	12							754.8±2.6	-
17	Cuarzo	Sweep	GLY (86-89%)	12							755.1±5.4	907.7±1.1
18	Cuarzo	Sweep	GLY (86-89%) (10% in Water)	12							710.2±1.4	846.6±3.0
19	Cuarzo	Sweep	GLY (86-89%) (10% in Water)	12							708.6±2.4	844.4±0.6
21	Cuarzo	Sweep	Water MilliQ	12			701.5±3.5	-				
22	Cuarzo	Sweep	Water MilliQ	12			-	835.5±7.2				
23	Cuarzo	Sweep	GLY (86-89%) (10% in Water)	12							707.8±1.1	-
27	Cuarzo	Sweep	GLY (86-89%) (10% in Water)	12							-	847.7±2.3
28	Cuarzo	Sweep	GLY (86-89%) (40% in Water)	12	529	634					730.7±0.7	863.8±0.9
29	Cuarzo	Sweep	GLY (86-89%) (60% in Water)	12							741.5±0.6	874.3±0.9
30	Cuarzo	Sweep	GLY (86-89%) (25% in Water)	12	527	635					722.4±1.8	855.9±0.6

The results for all the sweep experiments are gathered with great detailed at Annex 2 by the name “Biosensor characterization experiments (sweep)”.

Finally, a linear regression is done to determine the slope, which is the resonance wavelength (nm) divided by the Refractive index Unit (RIU). This is the sensitivity for each period. The points used to create this graph of the linear regression (Figure 13) are the computed average resonance wavelength corresponding to different substances with different refractive index.

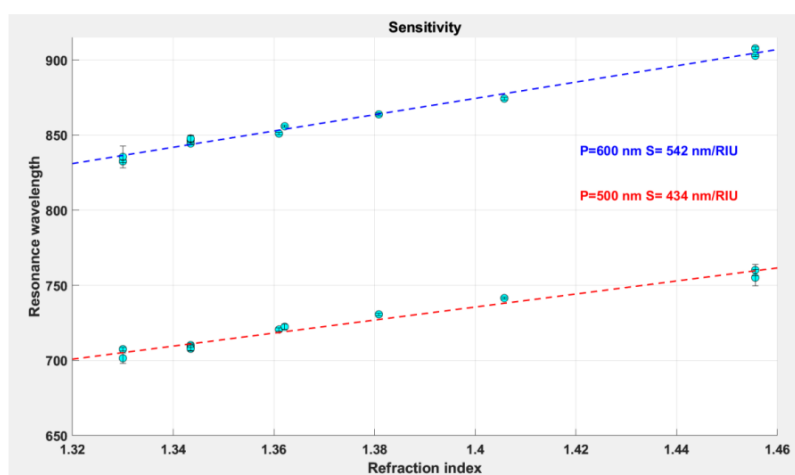


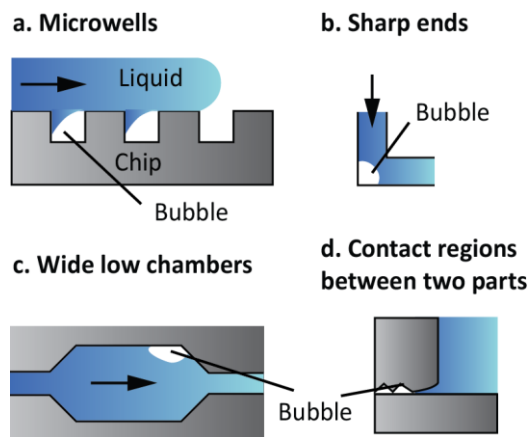
Figure 13: Graph of a linear regression of the average resonance wavelengths as a function of the refractive index corresponding to different substances.



It is shown in Figure 13, that the sensitivity for the period of 600 nm is 542 nm/RIU which is larger than the 500 nm period that is 434 nm/RIU. This means that for a unit of RIU, the 600 nm period can move 542 nm, therefore, smaller changes can be better detected because it has a wider range of detection. However, due to fabrication parameter reasons, it is seen experimentally that the resonance DIP is deeper in the period of 500 nm, which leads to less recording of noise which could imply more accurate results. The profundity of the DIP determines the reflected light, the 600 nm, has a DIP with less than 0.8 reflectivity, which is less deep than the 500 nm that has approximately 0.7 reflectivity. In an ideal scenario, the more the electrons on the gold surface absorb light the less reflectivity there would be, hence, a deeper DIP would be best. Despite this, DIP profundity is not related to sensitivity, only to noise recording.

#### 4.1.3 MICROFLUIDICS

One of the major concerns of the microfluidic design is to avoid the formation of air bubbles that obstruct the detection. There are certain designs that affect wetting properties and the formation of bubbles. Dead ends, microwells, and sharp corners are structures where wetting is difficult, and air can get trapped. Moreover, wide low chambers, which are microscale channels or chambers with larger width-to-height ratios, may also form this air agglomerations because the liquid inside may flow at different speeds on each side. [46]



**Figure 14: Microfluidic structures that prompt bubble formation [46]**

Furthermore, other factors that affect the flowing through the microfluidics are the properties of the surface, the flow rate, the pressure, and the temperature. This can be easily controlled to avoid the formation of air bubbles by setting a high pressure, constant temperature, and a high flow rate so the experiments are performed with the minimum time needed.

To avoid the formation of air bubbles the microfluidic design must be analyzed. Three different microfluidic designs will be investigated, first the design of the DEE of the physics faculty, then a new design done by AutoCAD and finally designs of IBEC.

##### **a) Microfluidic design of the DEE of the Faculty of Physics of UB**

The microfluidics design by the DEE is a single microfluidics pool with an hexagon shape, larger in the vertical axis, that covers the 4 diffraction sites. The design is printed on a double-sided adhesive tape and cropped with a cutting plotter, as seen in Figure 15a. To integrate it to the microchip, the cover of the tape is removed, and the sticky part is pasted to the methacrylate lid which has two holes of 0.4 mm radius corresponding to the inlet and the outlet that must be placed inside the

hexagon. The other side of the tape, integrated in the methacrylate lid, is pasted onto the surface of the chip (Figure 15b). Finally in the inlet and outlet, syringe needles are placed, and super-glue is put to close any gap and avoid leakage when flowing substances (Figure 15c). Super-glue has a slow drying, up to 24 hours, which is also time consuming between experiments.

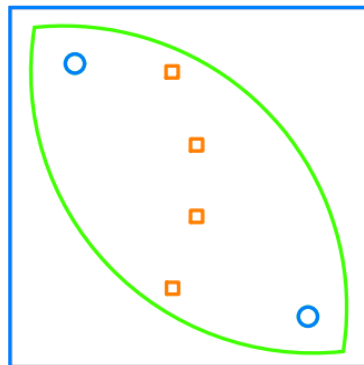


**Figure 15:** a) microfluidic design on a double-sided adhesive tape b) methacrylate lid incorporated onto the surface of the chip c) inlet and outlet syringe needles placed and sealed with super-glue onto the methacrylate lid.

This design has two major problems, first, the inlet and outlet are placed very near the diffraction gratings and so the two periods closer to the boundaries of the chip are hard to analyze and more so if super-glue is added. Secondly, this microfluidic design prompts the formation of air bubbles because of its large width-to-height ratio and the edgy corners of the hexagon. On the contrary, the diffraction gratings are in the nanometer scale, so they are not considered to produce the air formation associated with microwells. [46]

#### b) AutoCAD design

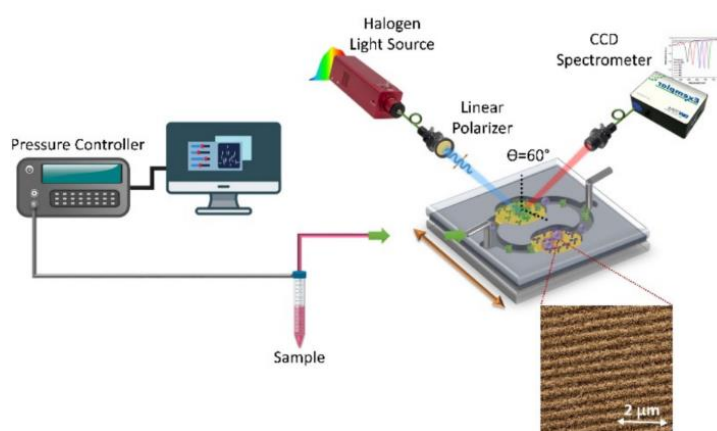
To solve a few of the current microfluidic design problems, a new design is proposed. For the new design the main objective is that the inlet and outlet are as far as possible from the diffraction gratings. Moreover, for flow reasons straight lines and edgy corners are inappropriate, so an almost perfectly ellipse shape is adopted. The design is done with the program AutoCAD 2024, and a multilayer strategy consisting of three layers has been performed. The orange layer is the microchip, the green is the double-sided adhesive tape, and the blue the methacrylate lid, they are set in that order. Figure 16 shows the design, and in the program layers can be filtered so they can be seen and printed individually.



**Figure 16:** AutoCAD microfluidics design

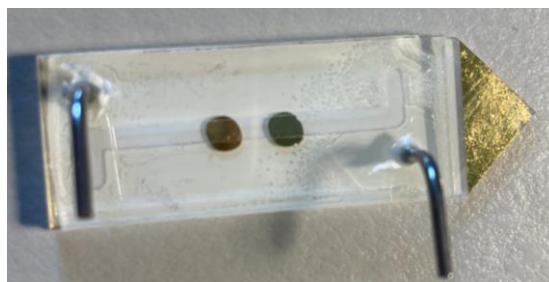
#### c) IBEC designs

The IBEC is studying how to optimize the microfluidics integrated in their microchips. In a visit to their centers the 29th of March, the institute had been studying a label-free nanostructured plasmonic biosensor based on Blu-ray discs with integrated microfluidics. In the visit, a real-time demonstration of the set-up and simple liquid detections were performed and the reasons behind their microfluidic design were explained. IBEC had previously been using a patterned microfluidics consisting of a channel that splits in parallel into two microchannels which each contain a circular pool, that avoids sharp edges, to allow duplicated biodetection (seen in Figure 17). It had been manufactured using a simple and inexpensive double-sided adhesive tape obtained with a cutting plotter. The microchannel had been designed to promote laminar flow and to increase the mass transfer near the sensor surface. Moreover, A PDMS 2 mm layer had been added as a cover, which increased the pressure inside the chip to force the air bubbles to dissolve. [36]



**Figure 17: Anterior IBEC SPR biosensor set-up**

However, nowadays a new design is being fabricated (shown in Figure 18). This is because now the sensor is placed in series instead of parallel. Moreover, in the previous design there were defects produced by the edges and the presence of two wide low chambers that did not allow the two sensing areas to be bathed equally. This has been replaced by a single thin microchannel design. Furthermore, the inlet and outlet are not near the diffraction gratings.



**Figure 18: IBEC current microfluidic design with methacrylate lid incorporated. Note that the needles are not placed correctly at the inlet and outlet.**

## 4.2. SAM FORMATION

The creation of the SAM in the gold surface of the biosensor is done by immersion in an ethanolic solution of organic molecules. There are two main molecules, polyethylene glycol and alkanethiols that can be used to provide an effective functionalization.

#### 4.2.1 DIFFERENT SAM FOR GOLD-COATED SURFACES

Thiolate monolayers on gold surfaces are the most extensively adopted SAMs on SPR sensors. This is because thiolates are compounds that contain -SH groups and can form strong covalent bonds with gold atoms through chemisorption (Figure 19). [37].

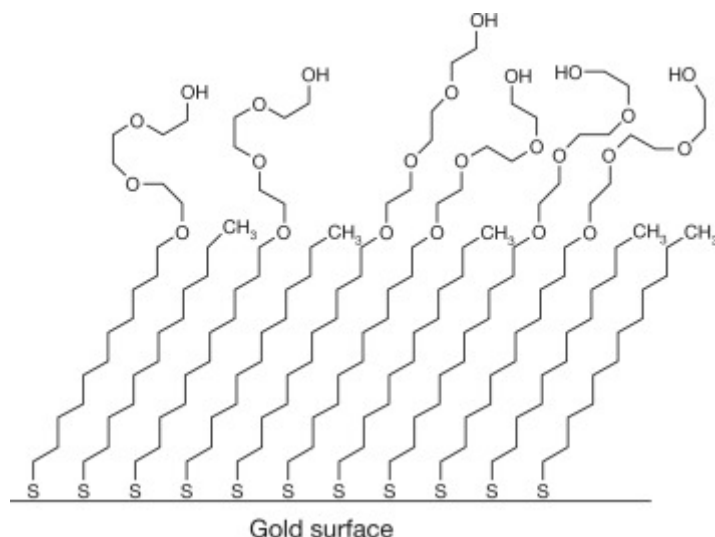
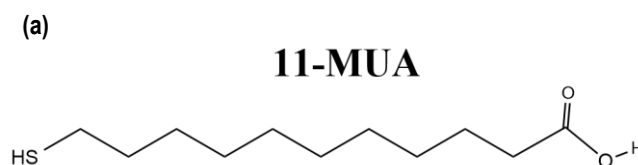


Figure 19: Chemisorption of alkanethiols on gold surface [38]

Moreover, long alkane thiols (over 6 methylene groups) form well-ordered, closely packed monolayers on gold. One of the most used compounds is 11- Mercaptoundecanoic acid (Figure 20a). The thiol group (-SH) forms covalent bonds with the gold surface whereas the carboxylic group (-COOH) is the active functional group used for immobilization of ligands to the surface of the biosensor. The acid end group can be modified by other functionalized groups for specific applications. [39]

On the other hand, thiol-PEG (Figure 20b) are also widely used molecules to form SAM on gold surfaces. The molecules have a thiol functional group at one end and a PEG polymer chain at the other end. The PEG chain provides a hydrophilic, non-fouling surface. The head groups can be terminated with -OH or -COOH. If terminated with -OH, the resulting SAM is used for preventing non-specific adsorption of proteins and other biomolecules to surfaces. If terminated with -COOH, the SAM can have additional functionality. [40]



(b)

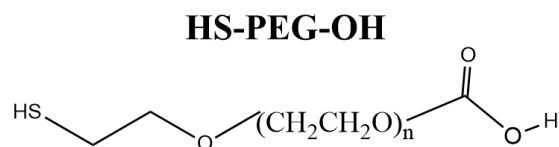


Figure 20: a) 11- Mercaptoundecanoic acid molecule structure b) HS-PEG-OH structure

#### 4.2.2 CONDITIONING (MES) AND ACTIVATION (EDC/NHS)

Before the activation of the SAM, MES monohydrate (2-Morpholinoethanesulfonic acid) which is a buffering agent with a pH ranging from 5.5 to 7, is added to hydrate the SAM of the microchip, this is known as the conditioning phase. Afterwards, the functional head group of the formed SAM, in this case the carboxylic group, are activated so they can perform a better immobilization of biomolecules. The first step is the addition of EDC (1-(3-Dimethylaminopropyl)-3-ethylcarbodiimide Hydrochloride) which is a Coupling Agent for Peptides Synthesis. The carboxylic acid group of the SAM reacts with the carbodiimide group ( $-N=C=N-$ ) of EDC creating an intermediate compound. The second step consists of introducing NHS (N- Hydroxysuccinimide) which displaces EDC. This is because the NHS ester group reacts with the carboxylic acid groups of the SAM resulting in the formation of amide bonds ( $-CO-NH-$ ), creating a reactive intermediate. The activation reactions are shown schematically in Figure 21.

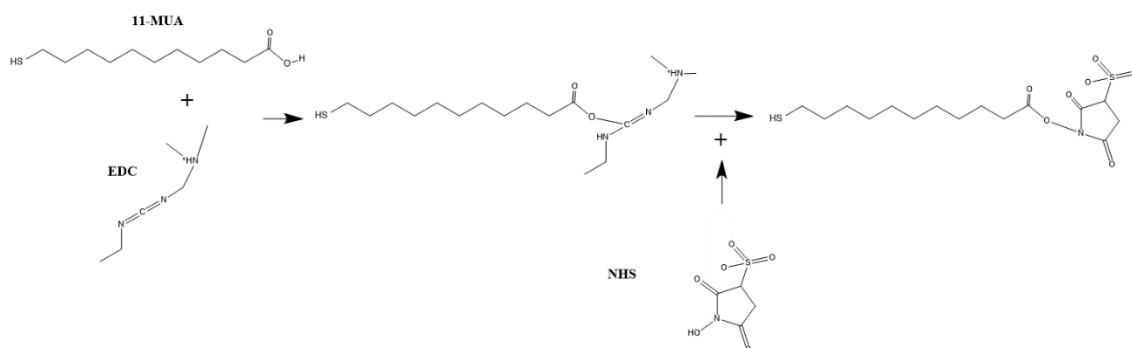


Figure 21: Schematic drawing of the EDC/NHS addition reaction for MUA activation

#### 4.2.3 COUPLING

The model protein used in this project is Bovine Serum Albumin (BSA). The coupling of this protein to the activated surface is done because the primary amines ( $-NH_2$ ) present on the surface of BSA react with the NHS ester group of the reactive intermediate forming stable amide bonds ( $-CO-NH-$ ). By doing this, a functionalized biosensor with BSA as antibody and with NHS-activated carboxyl groups is obtained. The coupling procedure is shown in Figure 22.

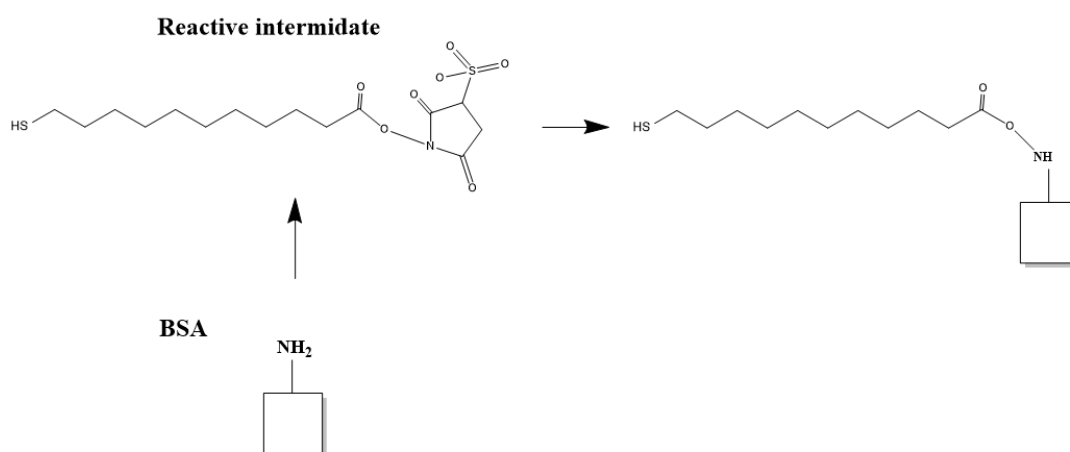


Figure 22: Schematic drawing of the BSA attachment reaction

Finally, ethanolamine is added to block those carboxyl groups that have not reacted.

## 5. DETAIL ENGINEERING

### 5.1 EXPERIMENTS WITH NON-FUNCTIONALIZED SURFACES

#### 5.1.1 CLEANING AND REGENERATION MECHANISMS

The sensor surface is very delicate since the diffraction gratings must not be damaged. For this reason, the cleaning and regeneration mechanisms must be accurate for the type of surface. In this project the protocol for cleaning and regenerating has been agreed upon with the Department of Organic Chemistry at the Faculty of Chemistry of UB. To clean the gold-coated biosensors, Acetone is poured into a beaker to completely cover the sensor. The beaker is then placed in an ultrasonic bath for 10 minutes. The biosensors are dried using a nitrogen stream, and the same procedure is repeated with isopropanol. As for the regeneration, the procedure is the one used in experiments prior to this project in the DEE, and it is done with HCL of 1M.

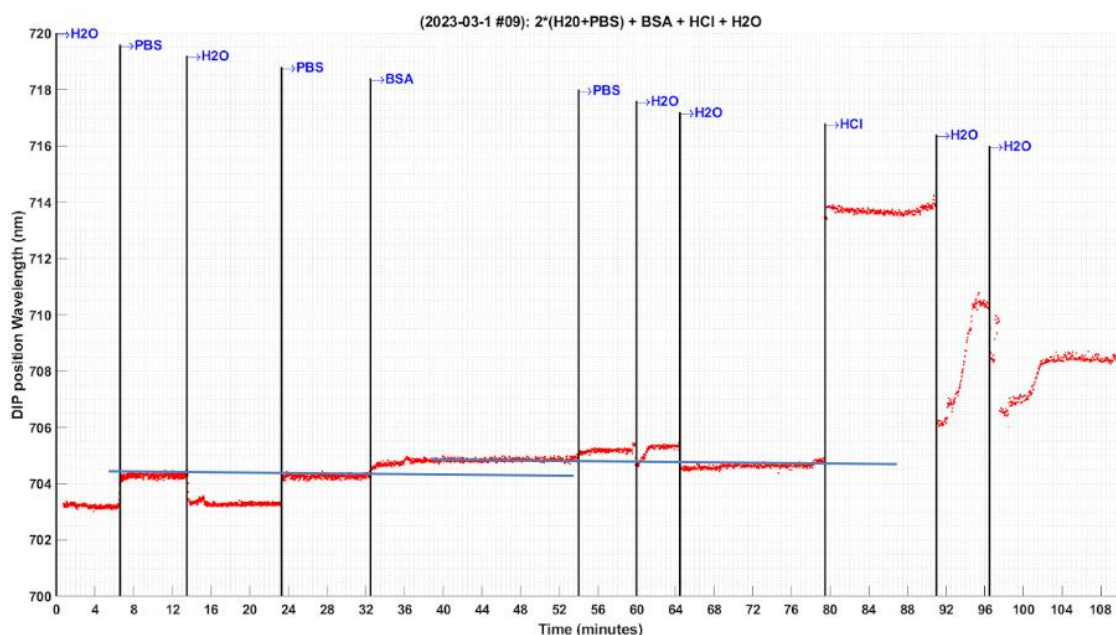
#### 5.1.2 INITIAL EXPERIMENTS

Several experiments are performed without the functionalized surface. The experiments are done with the 500 nm period diffraction grating. The only reason behind this is the fact that reproducibility is needed to compare results and the first experiments started to be performed with this period. If the period is switched, the wavelength range would be importantly altered. The sensorgrams obtained and processed represent the resonance wavelength as a function of time for a specific point in the diffraction grating. This is done to visualize the kinetics of substance adhesion, saturation, and dissociation. The substances used in the first's experiments have very similar refractive indexes to analyze how SPR responds to very small index changes. The substances are introduced in the microchip through the microfluidics set-up and with the help of a flow pump, whose rate can be varied. The setting of a relatively high flow rate is important to avoid the formation of air bubbles, see Annex 3 (flow pump rate study), to see an experimental analysis with different flow



rates. For all the experiments, the best flow rate is seen to be 0.1 ml/min. The microfluidics design used is from the DEE since it is the one available for the project.

The results of an experiment performed the 1st of March show that the resonance wavelength changes when detecting substances with similar refractive index (Figure 23). Initially, Milli Q water, with refractive index 1.33 is added and the resonance wavelength detected by SPR is 703.25 nm. Then PBS is flowed over the chip, it has a refractive index 1.339, and the resonance wavelength changes to 704.25 nm. In sensitivity terms, this means that for a very small variation of refractive index, 0.009, the resonance wavelength moves 1 nm. As for the sensing capability, also, visually the difference is easily detected, and signals are clear after processing. Then BSA of 1 mg/ml is added which has a refractive index very similar to PBS since it is diluted in it. When BSA is introduced, there is an increase in the refractive index and a certain adhesion kinetic slower than for the previous substances is appreciated. Then PBS is flowed over again, and the resonance wavelength increases instead of decreasing. This may demonstrate that BSA has attached to the surface. When water is introduced, an important initial decrease is detected followed by an increase of resonance wavelength. It is then reintroduced for a second consecutive time and highly noticeable decrease is observed; however, it does not return to the initial value at the beginning of the experiment, the reason is thought to be the presence of BSA onto the surface. As mentioned, HCl is used to regenerate the chips, when it is flowed over the refractive index of the substance provokes a strong increase. Then when water is introduced, it would be expected that the initial resonance wavelength values are recovered. However, a strange dynamic with values above the initial ones is detected, being the cause unknown.

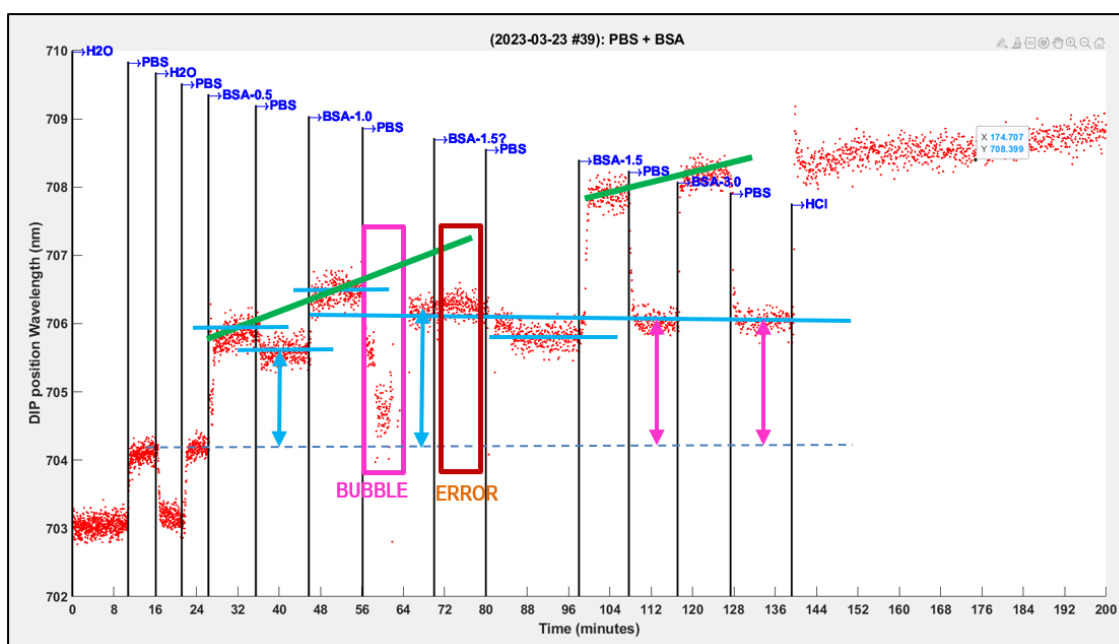


**Figure 23: Sensorgram of the resonance wavelength position as function of time from an experiment performed 1st of March with CHIP 34.**

### 5.1.3 SENSITIVITY ASSESSMENT USING DIFFERENT CONCENTRATIONS OF BSA

To further study the kinetics and sensing capability, small concentration shifts of the same substance can be studied. To do so, different concentrations of BSA are prepared. In a first experiment on the 23rd of March, four different concentrations, 0.5, 1, 1.5 and 3 mg/ml are

introduced, in increasing order, along with PBS between each, the results are gathered in Figure 24. From PBS to BSA 0.5 mg/ml the shift in resonance wavelength is very noticeable, 2nm, this is because the refractive index changes a lot which is contradictory to the results seen in Figure 23 where the change from PBS to BSA 1 mg/ml was half more subtle, 1nm. It is inconsistent that with half the concentration, the resonance wavelength displacement is double. The reason behind this may be an inaccurate concentration preparation or unknown causes. When PBS is introduced after the first concentration of BSA, the resonance wavelength decreases again but with a higher value than the initial for PBS, a little more than 1 nm. This, as in the initial experiments, may be because the BSA has adhered to the surface of the sensor. A second concentration is flowed over, and the increase is higher than with the lower concentration. This is expected to be due to the increase in concentration, which could mean that it is sensitive enough to detect this size of changes. The presence of a bubble causes difficulties in reading the signal of PBS but once it is stabilized, it is seen that the resonance wavelength is higher than the previous value of PBS but lower than the BSA signal. An error is produced when inducing the next concentration, so minutes 72 to 96 are neglected. With the third and four concentrations, the same happens, each time the resonance wavelength of BSA is higher the higher the concentration is; however, the values of PBS remain the same as with the second concentration. This leads to think saturation has been reached since the cleaning value with PBS does not shift in the last cycles. Finally, it is seen that the increase between the different substances is mainly bulk which may be because of the flow pump rate of infusion.

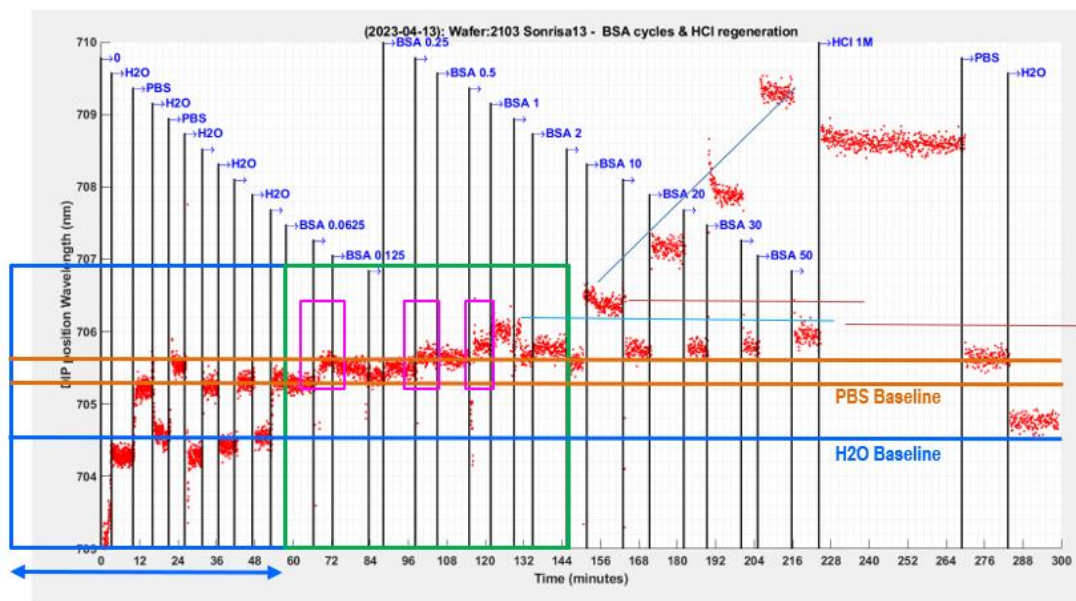


**Figure 24: Sensorgram of the resonance wavelength position as function of time from an experiment performed 23rd of March using BSA with different concentrations.**

The inconsistency in the resonance wavelength of BSA concentrations between the first experiments needs to be further investigated. A second experiment from the 14th of April using ten different concentrations prepared through dilution ranging from 0.0625 mg/ml to a maximum of 50 mg/ml is analyzed. First, several cycles of water/PBS are performed, however they are not reproducible, especially the water value varies considerably every time. The signal for the BSA of 0.0625 mg/ml cannot be differentiated from the previous PBS, however, when PBS is reintroduced the signal increases which leads to think that BSA did in fact adhere to the surface. It is not until a



concentration of BSA of 0.5 mg/ml that the signal is visually increased from the PBS baseline. The cleaning signal with PBS after this concentration is higher than the initial value which reaffirms that BSA may have adhered. For 1.5 and 2 mg/ml results are neglected since the results are incorrect possibly due to an inaccurate preparation of the concentrations. For the remaining concentrations each time they are flown over the resonance wavelength increases more than the previous lower BSA concentration, which means that SPR is able to detect these changes of concentration. The higher the concentration is, the more nm it moves and the easier it is to differentiate them. However, PBS baseline values vary very little in comparison which leads to think that the chip has reached its saturation of BSA.



**Figure 25: Sensorgram of the resonance wavelength position as function of time from an experiment performed 14th of April using BSA with different concentrations.**

These results lead to think that in the experiment of the 23rd of March, the concentrations, instead of being, 0.5, 1, 1.5 and 3 mg/ml, where in fact a factor of 10 bigger, 5, 10, 15 and 30 mg/ml respectively. Moreover, the threshold concentration where the SPR has a sensitivity able to distinguish between different concentrations of BSA is 0.5 mg/ml, as seen in the experiment from the 24<sup>th</sup> of March. However, it is not until concentrations of 1 mg/ml, where there is a good sensing capability, the signal can be clearly distinguished and the kinetics observed, as seen in the experiment from the 1<sup>st</sup> of March. For concentrations 5 mg/ml or higher, the sensing capability is very good. Saturation of BSA is determined by the shift in the baseline of the cleaning with PBS, it is estimated to occur approximately at a concentration of 10 mg/ml.

## 5.2 EXPERIMENTS WITH FUNCTIONALIZED SURFACES

The protocol for the functionalization of the surface has been established with the department of organic chemistry at the Chemistry Faculty of UB. It is agreed upon that the substance used for the formation of the SAM is MUA since it is noticeably cheaper and provides practically the same benefits as thiol-PEG. Experiments with the functionalized surface are divided in two blocks, the observation through fluorescent microscopy of the attachment of the SAM to the sensor by coupling fluorescent coated molecules to the surface, and the detection with SPR of different concentrations of BSA. The second block will allow to determine the consequences of functionalization in protein

detection by comparing it to the results of the previous experiments with non-functionalized surfaces.

### 5.2.1 SAM VALIDATION

It is important to study if the SAM has formed on the surface of the biosensor. For that, gold wafers and microchips are functionalized and then coated with BSA FITC, which is Bovine Serum Albumin coated with a fluorescent protein called fluorescein, through immersion. Then it is visualized with a fluorescent microscope from the Biology Faculty of UB included in the CCiTUB. The protocols followed for the preparation of all the substances of the project is included at Annex 1.

The protocol to functionalize the surface is the following, and it is identical for the gold wafers and microchips.

1. Clean the gold wafers.
2. Immerse the wafers with MUA 3mM at 4°C in darkness for 22 hours.
3. Clean the wafers with Ethanol, rinse several times with a pipette.
4. Then there are two procedures to conserve the wafers before the activation phase. The first one, is to immerse them in ethanol and the second to dry the surface with a nitrogen stream and leave them dry. Both must be in the fridge at 4 °C protected from the light by covering them with parafilm.
5. Before activation of the SAM, MES pH 5,7 and 25mM is added to condition/hydrate the surface of the wafer that was in dry conditions. For the one in Ethanol, also dry with a stream of nitrogen.
6. EDC 0.2 mol/L and NHS 0.05 mol/L dissolved together in 2 ml of MES and immersed the gold microchip into this solution for 20 minutes.
7. Rinse with MES with the help of a pipette.
8. The chip is immersed in the 2ml of BSA FITC 50 µg/ml at room temperature for two hours.
9. Two rinses with PBS with a pipette
10. It is then changed to Ethanolamine 50µg/ml for 15 minutes.
11. Two rinses with PBS with a pipette
12. It is left immersed in PBS 1x until usage or being analyzed with the fluorescent microscope.

The wafers and microchips are then analyzed with a high-speed fluorescent microscope LEICA Thunder of the advanced optical microscopy department at the biology faculty of UB (included in the CCiTUB). Widefield Fluorescent Microscopy uses fluorescent molecules, fluorophores, to label specific cellular structures. These fluorophores absorb light at a specific wavelength (excitation) and emit it at a higher wavelength (emission). The sample is illuminated with the excitation wavelength, and only the emitted wavelength is allowed to pass through a filter. The structures coated with fluorophores are detected because they emit light. Widefield microscopy illuminates the entire specimen, which is suitable for thin samples with low autofluorescence. [44]

In the case of this project, the fluorescent molecule used is fluorescein and therefore the microscope is set with the excitation wavelength ranging from 462 to 496 nm and the emission ranging from 506 to 532 nm. The microscope has an LED light source with 8 lines for fluorescent illumination, in this case, the LED excites at wavelength 475 nm. The emission filter used is specific for FITC, and it has a center wavelength of 535 with a bandwidth of 70 (range 500 to 570 nm). Moreover, it uses an objective of 20x to collect the emitted fluorescence and determine the

magnification and field of view. To visualize this, a spectrum is generated with the tool Fluorescence SpectraViewer from ThermoFisher Scientific [47] (Figure 26).

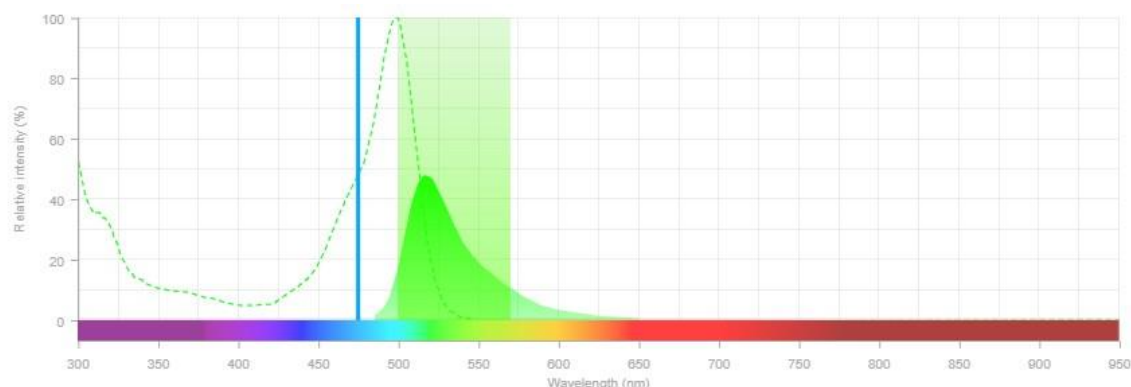


Figure 26: Fluorescein excitation and emission spectrum [47]

The images are then analyzed and processed with ImageJ to set a homogenous pixel intensity range (set from 0 to 10.000) that enables comparison, and to compute the mode of each image computed for quantification. This maximum intensity value is chosen because the border images have intensity values that reach 10.000. Therefore, if the maximum value was set lower, important information would be lost. In figure 27a, a histogram of a border image, with a homogenous pixel intensity range, is shown. Note that even though it seems there are no values near 10.000 if the cursor is placed in that area, there are several counts of intensity values. For example, there are 8969 pixels that have an intensity value of 9882,812. Moreover, the mode indicates the most repeated intensity value, and it is useful to quantitatively compare images. All the results and an explanation of the processing are gathered at Annex 7.

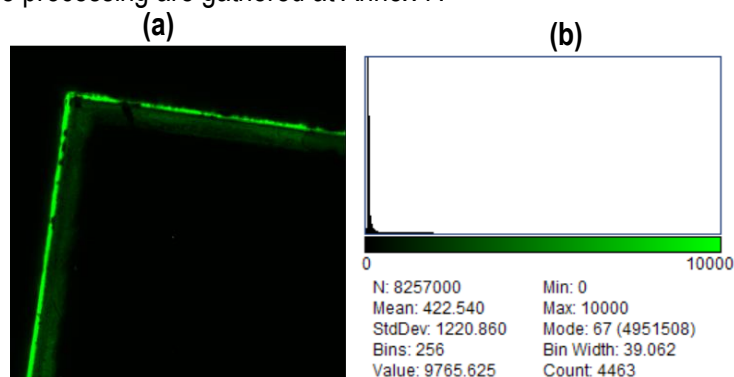


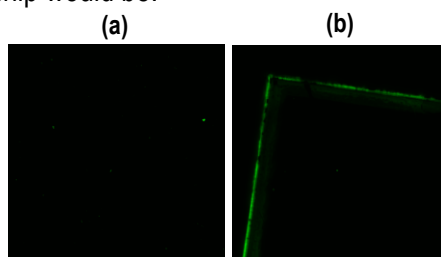
Figure 27: Fluorescence microscopy (a) border image and (b) histogram of dry conditioned wafer for processing explanation

The wafers and chips used for fluorescence image acquisition are gathered in Table 6.

Table 6: Wafers and chips used for fluorescence image acquisition.

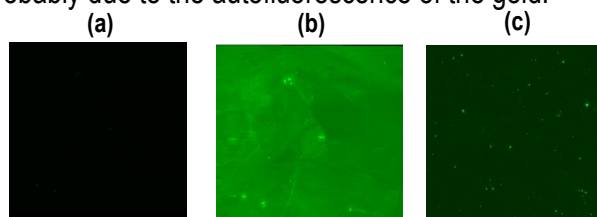
Wafer/Chip	Description
Dry conditioned wafer gold surface	Functionalized gold wafer that was conserved in dry conditions before the activation and coupling with BSA FITC.
Ethanol conditioned wafer gold surface	Functionalized gold wafer that was conserved in Ethanol before the activation and coupling with BSA FITC.
CHIP 33	Functionalized with all the steps by microfluidics.
Control wafer	Only Mua formed
Non-activated wafer	MUA and BSA FITC coated but without the activation step.

The first images obtained show that the fluorescence is much brighter in the corners of the wafers than in the center, as seen in Figure 28. The reason behind this is unknown but it is not given importance since the relevance relies on the fluorescence distribution at the center where the diffraction gratings of the microchip would be.



**Figure 28: a) Fluorescence image with enhanced of the center of the dry conditioned wafer b) Fluorescence image of the corner of the dry conditioned wafer**

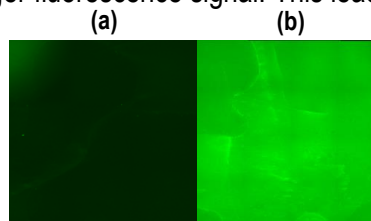
In Figure 26a, it is seen that there are a few spread fluorescent signal particles and the mode is 66 so the image has little signal. These appreciated particles could be the signal from the coated fluorescein or due to the properties of gold which can exhibit autofluorescence. Gold surfaces can reflect the excitation light from the microscope and generate noise which can interfere with the fluorescent signal from the BSA FITC. To determine the origin of this fluorescence, a control image of the center must be obtained, which consist of a gold wafer with only MUA and not activated (EDC/NHS step) or coupled with any fluorescent molecule. The control image is not obtained the same day so they may be some acquisition differences (Figure 29a). It is seen that the image is completely black and therefore with a mode of 0, which could mean that the few spread particles were in fact fluorescein signal. To visualize the images with greater detail, the contrast is enhanced by 20%, this is not useful for comparison since pixel intensity values are altered and not set to the same scale. However, it allows to know if there is hidden fluorescence inside the images. Figure 29c shows the enhanced contrast of 20% of the center of the dry conditioned wafer where it is seen the presence of more particles of fluorescence that were hidden, this may be noise due to the autofluorescence of the gold since they are not detected without the contrast. Moreover, when the contrast is enhanced in the control wafer (Figure 29b), fluorescent particles appear. The control wafer is not coated with fluorescence which sustains the hypothesis that this is not signal from the fluorescein, and it is probably due to the autofluorescence of the gold.



**Figure 29: a) Fluorescence image of the center of the control wafer (only MUA formed), b) Fluorescence image of the center of the control wafer with enhanced contrast 20% c) Fluorescence image with enhanced contrast of 20% of the center of the dry conditioned wafer.**

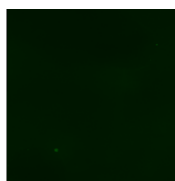
To further investigate, CHIP 33 is functionalized, activation and coupling with BSA FITC included, by microfluidics and is examined few hours later the same day as the control wafer. Images from the center of the chip (Figure 30a) show a higher level of fluorescence not only visually but also the mode is 1363 as compared to the control, which is zero or to the dry conditioned wafer, 66. This may lead to think that since the CHIP 33 is functionalized the same day it is analyzed, it has a

higher level of fluorescein. Moreover, the image is more homogenous and when contrast is enhanced no particles are appreciated (Figure 30b), the noise may have been covered by the presence of this apparent stronger fluorescence signal. This leads to think that the SAM did form.



**Figure 30: a) Fluorescence image of the center of CHIP 33 b) Fluorescence image of the center of the CHIP 33 with enhanced contrast 20%**

Furthermore, the type of binding of the fluorescence added with the SAM is also studied. To know if the fluorescent molecules are bind to the SAM by physical adsorption or by covalent bonding, a wafer without the activation step (EDC/NHS) is used. If the fluorescence in this wafer is lower than CHIP 33 which is functionalized with the activation step, it means that in the chip, the fluorescence has bound covalently, however, if it is the same, the binding is probably by Physical adsorption and the SAM is less effective. This is because the activation step is necessary to allow the covalent bonding, and if it is missing the fluorescence coated will not be forming this type of bonds. Figure 29 shows that the center of the non-activated wafer has a lower fluorescence than CHIP 33 with a mode of 901 which is also lower. This could indicate that the part of BSA FITC is binding covalently in CHIP 33. More results would be needed to affirm this hypothesis.



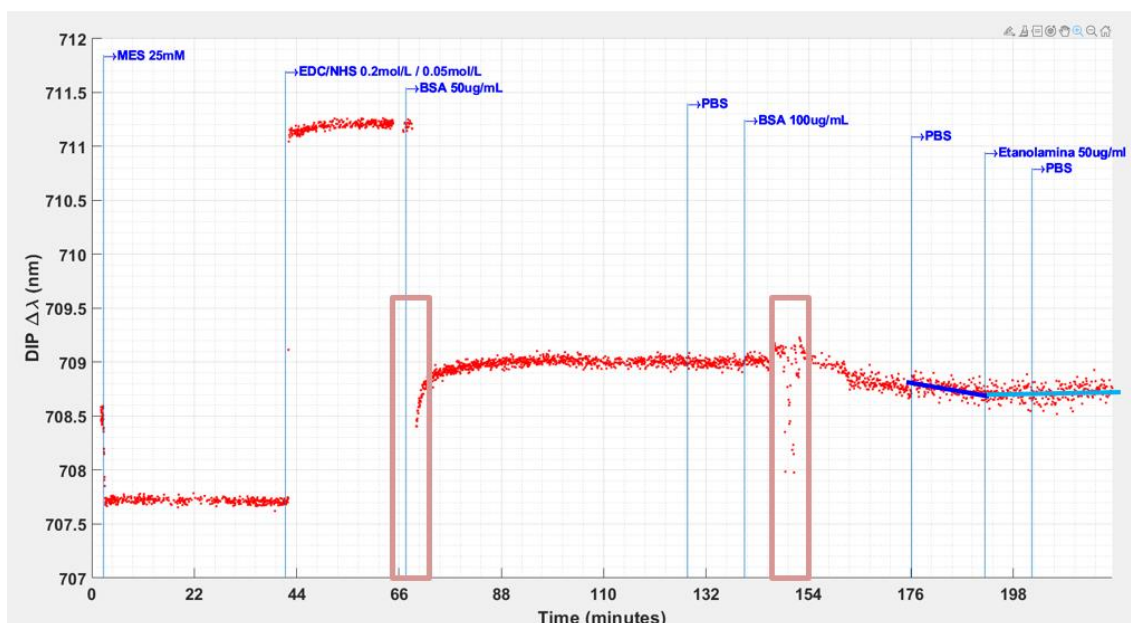
**Figure 31: Fluorescence image of the center of the non activated wafer**

Overall, more results would be needed to affirm if BSA FITC is truly coupling to the SAM, and so the SAM has formed, and if the bonding is covalent or by physical adsorption.

### 5.2.2 SPR WITH SAM

For the experiments with the functionalized surface, the SAM is created following the same protocol as with the gold-wafers (found at section 6.1 SAM validation). The first experiment conducted aimed to analyze the condition, activation and coupling steps with microfluidics with the flow pump at rate 2.5 rpm (0.1ml/min). To do so, the timings and substance infusion order are followed exactly as the immersion procedure. For the coupling step, two different concentrations of BSA are used, 50 and 100  $\mu\text{g/ml}$ . This way, it aims to visualize changes in wavelength due to changes in concentration at the microscale. This is not possible without the functionalized surface since concentrations lower than 0.5 mg/ml were not detected. Moreover, the kinetics of adhesion of the different substances are analyzed, especially of BSA since the saturation concentration is sought. The results for the first experiment performed, are seen in Figure 32, and show the resonance wavelength as a function of time.

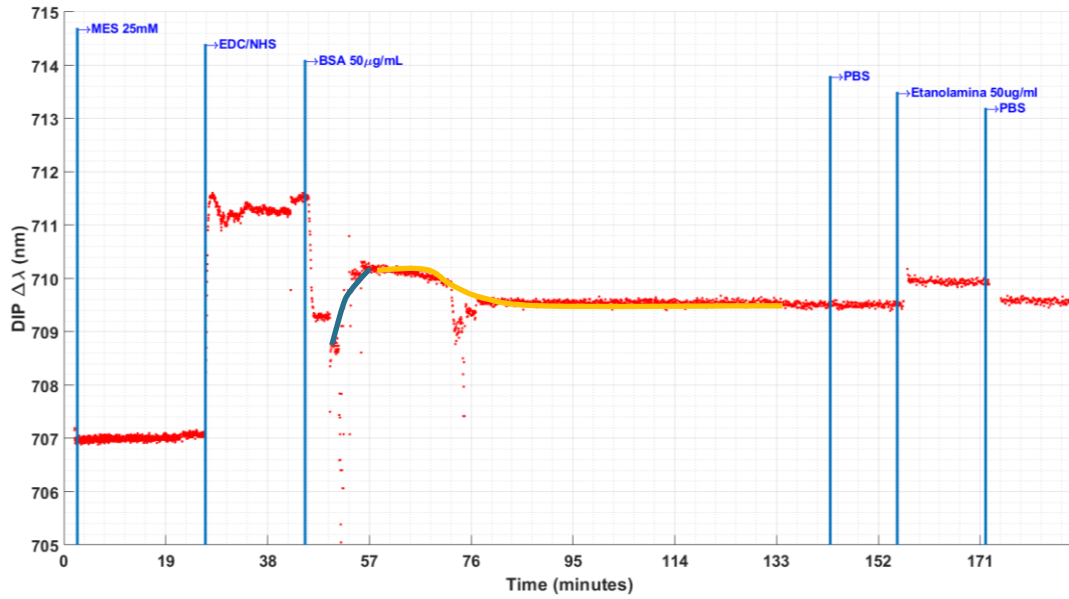




**Figure 32: Sensorgram of the resonance wavelength position as function of time from an experiment performed 11th of April with the condition, activation and coupling procedure of the SAM.**

From these results it is observed that in the activation phase the EDC/NHS mixture shows a very high refractive index, inducing a shift of 3 nm with respect to the MES signal. The first concentration of BSA is flowed over and the resonance wavelength is lowered. In the infusion, a dynamic behavior is observed but not from the beginning because of an air bubble. After a few minutes, the concentration is saturated at wavelength 709 approximately. At 110 minutes, a slight decrease is observed which could be a consequence of a small detaching of BSA. When PBS is introduced, no difference is appreciated even though the refractive index should be different, this could be because the surface is already filled with BSA. The addition kinetics of the 100  $\mu\text{g}/\text{mL}$  concentration is masked through the presence of a bubble. The air may be the reason why the signal decreases with this concentration. The second cleaning with PBS does slightly lower the resonance wavelength. Finally, Ethanolamine causes a small change due to the difference in refractive index.

In another experiment (Figure 33), the activation phase has an initial dynamic behavior and the shift from the MES baseline is larger, 5nm. Moreover, in the kinetics of addition of BSA 50  $\mu\text{g}/\text{mL}$  the wavelength increases almost 2 nm to reach saturation whereas in the previous experiment 0.5 nm. This is because in this experiment the dynamic behavior could be observed from beginning to end. After a few minutes, an important decrease of almost 1 nm is observed, this is prompted by the formation of a bubble, and it is unable to return to the initial value. As in the previous experiment, the detachment of BSA could also be another cause for this decrease.



**Figure 33: Sensorgram of the resonance wavelength position as function of time from an experiment performed 31st of May with the condition, activation and coupling procedure of the SAM.**

It can be concluded that the SAM is formed and activated on the surface because the sensing capability is increased to the point that the kinetics of a concentration of 50  $\mu$ g/ml can be observed. However, there seems to be no decrease in the signal when adding PBS, but this could be because the formation of the SAM makes the saturation concentration be very small, and with a concentration of 50 and 100  $\mu$ g/ml the surface is already filled. Another reason could be that the sensing capability is not good enough to sense changes of this magnitude. Concentration differences are also extremely hard to appreciate. Overall, the formation of bubbles has damaged the results and to reach further conclusions more experiments would need to be performed.

## 6. TECHNICAL VIABILITY

To evaluate the internal and external factors a SWOT matrix that comprehends the Strengths, Weaknesses, Opportunities, and Threats of the SPR biosensor for protein detection of this project, is generated (Table 7).



Table 7: SWOT analysis matrix

SWOT ANALYSIS		
INTERNAL	<b>Strengths</b> <ul style="list-style-type: none"> <li>• Good sensing capability for BSA concentrations from 1 mg/ml and very good for 5 mg/ml or higher.</li> <li>• The SAM formed can detect BSA adhesion kinetics for concentrations of 50 µg/ml and higher.</li> <li>• Fluorescence microscopy images suggest that the SAM has formed.</li> <li>• Easy to use Software.</li> <li>• Developed in the University of Barcelona</li> </ul>	<b>Weakness</b> <ul style="list-style-type: none"> <li>• Air bubble formation</li> <li>• Problems of leakage</li> <li>• The preparation of the microchip, regeneration and functionalization are time-consuming.</li> <li>• No high throughput (multiplexing)</li> <li>• Lack of more experimental results to sustain conclusions reached, more time is needed.</li> <li>• No automatized detection</li> <li>• Difficult reproducibility</li> <li>• No private investment</li> </ul>
	<b>Opportunities</b> <ul style="list-style-type: none"> <li>• SPR market will double in size in 10 years.</li> <li>• Future Research on the early detection of Parkinson disease and other biological biomarkers</li> <li>• Improvement of the sensing capability by varying fabrication parameters of the microchips</li> <li>• Development of an ultra-sensitive biosensor</li> <li>• UB partnership</li> <li>• Public research funds</li> </ul>	<b>Threats</b> <ul style="list-style-type: none"> <li>• Rise of POCT systems</li> <li>• Competitor companies that dominate the market and have great resources such as Biosensor Tools LLC</li> <li>• High throughput systems like Bruker</li> <li>• Digital microfluidics (implemented by Nicoya company) that enables eliminating the need for cleaning and maintenance and reduces contamination.</li> <li>• Designs that enhance easy reproducibility like the Biacore models</li> </ul>

## 7. ECONOMIC VIABILITY

The project is developed under the University of Barcelona therefore all the materials and machines have not been bought specifically for this project; the few added resources needed during the development of the project were covered by a research grant. This included only two substances which had to be purchased from outside providers such as Thermo Fisher Scientific and Sigma Aldrich and meant a total of 362,8 € as seen in Table 8. It also included the cost per hour to use the microscopes from the CCI-TUB and the technician which cost a total of 76,72 €. Therefore, the total cost of the project covered by the grant is 439, 52 €.

However, for future reproducibility and to study the economic viability of the project it is interesting to analyze the total approximate cost if the study had to be built without any initial resources. To do so, a list of all the materials and machines used is confectioned and the prices are extracted from Fisher Scientific Company [42] which is a leading scientific supply company subsidiary to the multinational Thermo Fisher Scientific, and from the DEE. The economic study is gathered at Table 8, where it is divided in 4 blocks: outside provider purchase, Organic chemistry department, DEE and microscopes. The working personnel, infrastructures, electricity, nitrogen supply costs, among others, are neglected.

Table 8: Economic viability layout

ITEM	QUANTITY or CAPACITY	UNITS	PRICE (€)
Outside provider purchase			
<b>Bovine Serum Albumin (BSA), FITC conjugate – Thermo Fisher Scientific</b>	5 mg	1	272 €
<b>11- Mercaptoundecanoic acid (MUA) – Sigma Aldrich</b>	5 g	1	90,80 €
<b>SUBTOTAL</b>			<b>362,8 €</b>
Organic chemistry department faculty of Chemistry UB			
<b>Phosphate-buffered saline</b>	98.90 g	1	34, 80 €
<b>2-(N-morpholino)ethanesulfonic acid (MES)</b>	25 g	1	25,60 €
<b>1-etil-3-(3-dimethylaminopropyl) carbodiimide (EDC)</b>	10 g	1	133 €
<b>N-Hydroxysuccinimide (NHS)</b>	25 g	1	35,80 €
<b>Ethanolamine 99%</b>	250 ml	1	24,70 €
<b>Hydrochloric Acid 37%</b>	5 L	1	44,70 €

<b>Glycerol 86-89%</b>	1 L	1	115,86 €
<b>Ethanol absolute</b>	2,5 L	1	80,45 €
<b>Isopropanol</b>	1 L	1	82, 90 €
<b>Millipore Milli-Q Synthesis</b>	-	1	3.151,08 €
<b>Disposable transfer pipettes</b>	3 ml	500	32, 40 €
<b>Analytical scale (resolution of 0.0001 g)</b>	-	1	705 €
<b>Microanalytical scale</b>	-	1	5025 €
<b>Glass vials</b>	100 ml	24	99,55 €
<b>Beakers</b>	10 ml	10	49,65€
<b>Centrifuge tubes</b>	2 ml	500	33,60 €
<b>Glassware drying oven</b>	-	1	2367,60 €
<b>Acetone</b>	5 L	1	55,80 €
<b>Nitric acid (HNO<sub>3</sub>) for Agua Regia <sup>5</sup></b>	1L	1	70,45
<b>Mechanical micropipette</b>	10-1000 µL	1	277 €
<b>Mechanical Micropipette</b>	1-100 µL	1	277 €
<b>Pipette tips for micropipette</b>	10 µL	960	98.25€
<b>Pipette tips for micropipette</b>	1000 µL	1000	95.05€
<b>Graduated cylinder</b>	10 ml	1	5,35 €
<b>Stainless steel spatula</b>	-	5	31,25 €
<b>Safety goggles</b>	-	1	21,65 €
<b>Nitrile gloves</b>	-	100	31,30 €
<b>Cotton lab coat</b>	-	1	22,25 €
<b>SUBTOTAL</b>			<b>12.661,39 €</b>
<b>DEE department Faculty of Physics of UB</b>			
<b>SPR set-up</b>	-	1	12000 €
<b>Gold-coated microchips</b>	-	12	1200 €
<b>Ultrasonic bath</b>	-	1	917 €
<b>Methacrylate lid</b>	-	30	15 €
<b>Double-sided adhesive tape sheet</b>	-	1	19,06 €
<b>Cutting plotter brand Silhouette (IBEC)</b>	-	1	199 €
<b>Syringe pump</b>	-	1	66,40 €
<b>Flow pump gilson mini pulse 3</b>	-	1	2145,00 €

<sup>5</sup> Agua Regia is a mixture of nitric acid (HNO<sub>3</sub>) and concentrated hydrochloric acid (HCl) in a specific ratio.

<b>Needles</b>	10 ml	6	171,00 €
<b>SUBTOTAL</b>			<b>16732 €</b>
<b>Microscopes</b>			
<b>SEM Microscope cost per hour</b>	-	1	38,36 €
<b>Fluorescent Microscope cost per hour</b>	-	1	38,36 €
<b>SUBTOTAL</b>			<b>76,72 €</b>
<b>ESTIMATED TOTAL</b>			<b>29833,37 €</b>

The total estimated cost of the project without the collaboration of the UB would be 29.833,37 €. Whereas the total amount invested during the course for this project is 439,52 €, and is covered by a research grant. Therefore, if the project was developed without any partnership or grant form of payment, it would have a total cost of approximately 30.000 €. This highlights the importance of partnerships and grants to conduct scientific research.

## 8. EXECUTION SCHEDULE

A project of this extension demands good planning to achieve the goals on time. A few considerations must be taken into account for the understanding of the organizational process that took place by using three main management tools: WBS, PERT and GANTT.

- The tools are used once the project is already chosen on the 14th of February 2023 and so the process and tasks before are not considered. Furthermore, the organization is only for the written document and does not include the oral presentation.
- There is no specific task for the writing of the project because the writing of the different sections is intrinsic in each of the tasks. This is chosen since it is found that the structure is seen more clearly the less packages and tasks there are, and it is very important to use these tools to provide a general scope of the project. Consequently, the time duration estimated for each task is increased since it comprises the writing.
- These are the initial objectives and time schedule, some of the task durations have varied and the optimistic objective of the early detection of Parkinson could not be performed.
- The duration of the project is approximately 4 months. It started on the 14<sup>th</sup> of February with the first official meeting with the tutor and it ended on the 6<sup>th</sup> of June with the online delivery of the project.

### 8.1 WORK BREAKDOWN STRUCTURE (WBS)

The first important step of the organization is to define the tasks that will be executed and obtain a global scope of the project. To do that, the Work Breakdown Structure (WBS) project management tool is used.

The project is divided into four main packages which are each decomposed into smaller tasks, also known as deliverables. This gives a visual representation of the development of the project. The structure is presented in Figure 34.

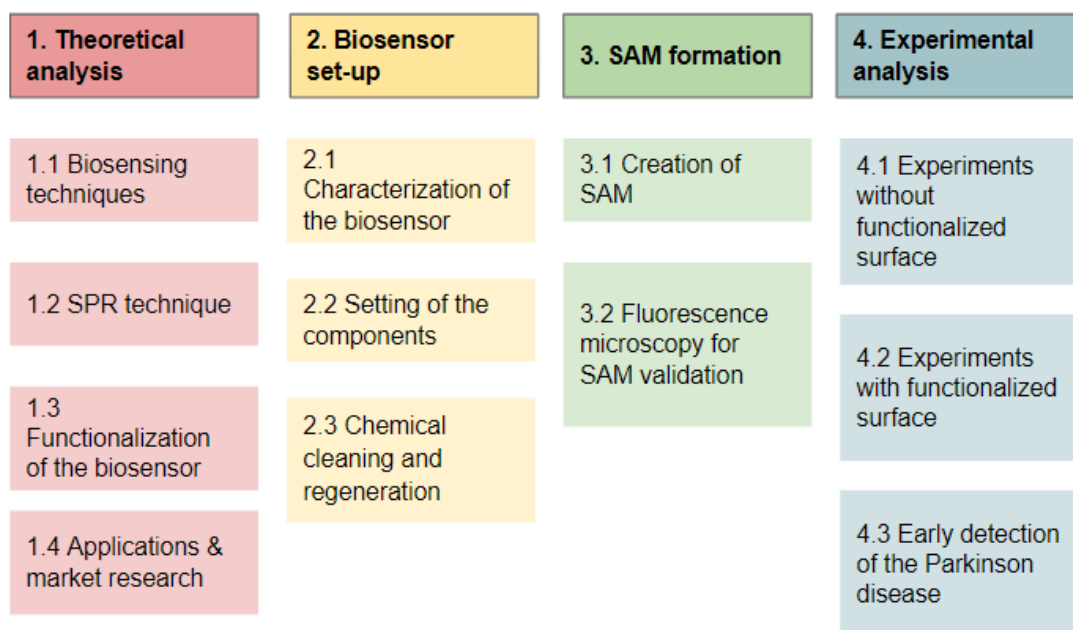


Figure 34: The Work Break Down structure of the project.

#### a) Theoretical analysis

This package is based on literature research, and it is necessary to understand the entirety and depth of the project.

Table 9: WBS theoretical analysis package

Deliverable Number	Name	Description
1.1	Biosensing techniques	Introduction to biosensing techniques, including biosensors and optical biosensing techniques, their working principles, components, classification, and main aspects
1.2	SPR technique	Description of the SPR technique including its physical principle, main applications, and configurations
1.3	Functionalization of the biosensor	Analysis of the different methods for biosensor functionalization, with a focus on SAMs.
1.4	Applications and Market research	Review of the most important companies in the field and the main applications related to the use of SPR for biosensing in biomedical research and in the early detection of Parkinson's disease. It includes an analysis on the future perspectives of SPR.

## b) Biosensor set-up

This package is necessary for the experimental analysis.

Table 10: WBS biosensor set-up package

Deliverable Number	Name	Description
2.1	Characterization of the biosensor	Description of the structure and composition of the biosensor used. Includes a tracking of its surface of the SPR sensor. It is useful to study the sensitivity of the different diffraction gratings periods.
2.2	Setting of the components	Incorporation of the microfluidics and the methacrylate lid into the biosensor's surface and the deposition of the microchip in the SPR detection set-up. It also requires the microfluidics to be connected to a system to flow the substances over the sensor. Comprehends the design of new components to fix repetitive errors.
2.3	Chemical cleaning and regeneration	Generation of cleaning and regeneration protocols for the use of the biosensor. This part will be agreed on with the Organic chemistry department at the faculty of chemistry of the UB.

## c) SAM formation

Table 11: WBS SAM formation package

Deliverable Number	Name	Description
3.1	Creation of SAM	A protocol for the formation of the SAM in the biosensor surface will be established with the department of Organic Chemistry of UB. The needed substances that are not available in the laboratory in the Faculty of Chemistry must be bought from outside providers such as Sigma Aldrich and ThermoFisher Scientific. Finally, the SAM will be created on the required biosensors.
3.2	Fluorescence microscopy for SAM validation	Before the experimental analysis with the functionalized surfaces, the SAM will be immersed with a protein coated with a fluorescent marker to validate the success of the formation.

## d) Experimental analysis

This is the backbone of the project, through the experimental analysis the sensing capability of the SPR technique on a gold coated biosensor can be assessed.

**Table 12: WBS experimental analysis package**

Deliverable Number	Name	Description
<b>4.1</b>	Experiments without functionalized surface	To learn the use of SPR and obtain first results of the sensing capability without wasting time and expensive substances needed for the creation of the SAM, several experiments will be conducted with a free surface using the set-up previously established.
<b>4.2</b>	Experiments with functionalized surface	Experiments with the functionalized surface will be performed and an analysis of the effectiveness of the SAM will be conducted.
<b>4.3</b>	Early detection of the Parkinson disease	Establishment of the protocol and experiments for the early detection of Parkinson disease.

## 8.2 PERT

To coordinate the different tasks that must be done to finish the project without delay, a PERT diagram is created. This diagram visually represents the tasks to be performed, their time duration and the relationship between them. This information is gathered in Table 13, and the diagram is shown in Figure 35.

**Table 13: PERT description table**

Deliverable Number	Description of the deliverable	PERT task name	Origin	Duration (days)
<b>1.1</b>	Biosensing techniques	<b>A</b>	-	<b>3 days</b>
<b>1.2</b>	SPR technique	<b>B</b>	<b>A</b>	<b>4 days</b>
<b>1.3</b>	Functionalization of the biosensor	<b>C</b>	-	<b>3 days</b>
<b>1.4</b>	Applications and Market research	<b>D</b>	<b>A, B</b>	<b>7 days</b>
<b>2.1</b>	Characterization of the biosensor	<b>E</b>	-	<b>5 days</b>
<b>2.2</b>	Setting of the components	<b>F</b>	-	<b>32 days</b>
<b>2.3</b>	Chemical cleaning and regeneration	<b>G</b>	<b>F</b>	<b>1 day</b>
<b>3.1</b>	Creation of SAM	<b>H</b>	<b>F, G</b>	<b>14 days</b>



3.2	Fluorescence microscopy for SAM validation	I	H	4 days
4.1	Experiments without functionalized surface	J	F, G	30 days
4.2	Experiments with functionalized surface	K	J, H, I	30 days
4.3	Early detection of the Parkinson disease	L	J, K	10 days

Moreover, to do the diagram the minimum (early) and maximum (late) time in which each task can be finished is computed. With this the critical path will be determined, which is the path composed of the tasks that, if finished later than scheduled, will modify the final timing of the project.

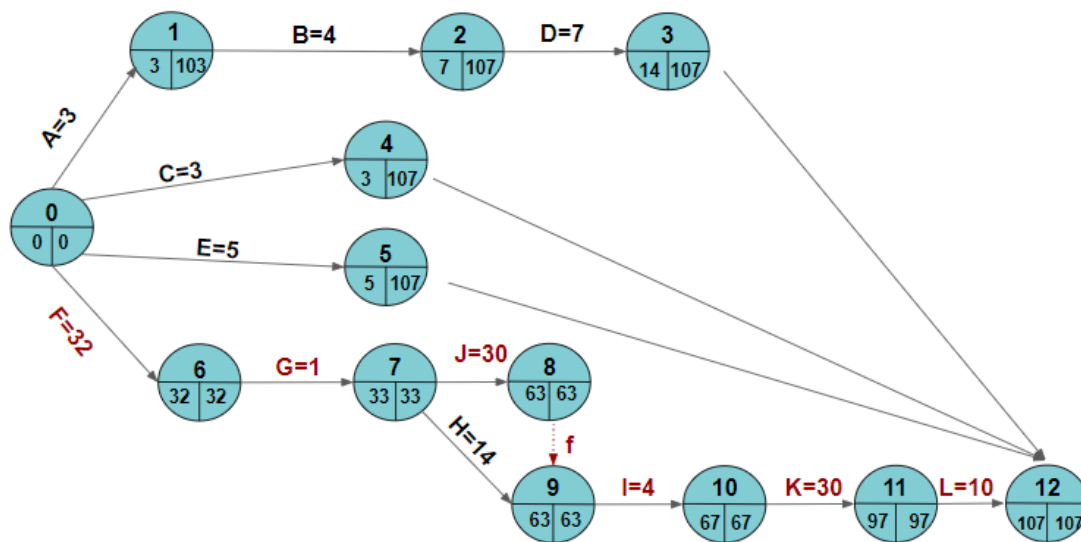


Figure 35: PERT diagram

It is seen that the project's critical path is composed of tasks F, G, J, I, K and L which are highlighted in red. These correspond to the experimental tasks, therefore, if there are any delays or unpredicted problems on the experimental analysis, the project will have to be re-organized to finish on time.

### 8.3 GANTT DIAGRAM

To visualize the time layout more specifically during the four months of the project, a GANTT diagram is generated with Excel. As shown in the PERT diagram, most tasks must wait, for other tasks to be completed, to begin. Despite a few tasks could be done simultaneously, in the GANTT, since the timing enabled it and the writing is included, they are all scheduled individually, except the 10<sup>th</sup> of April where two tasks coincide.

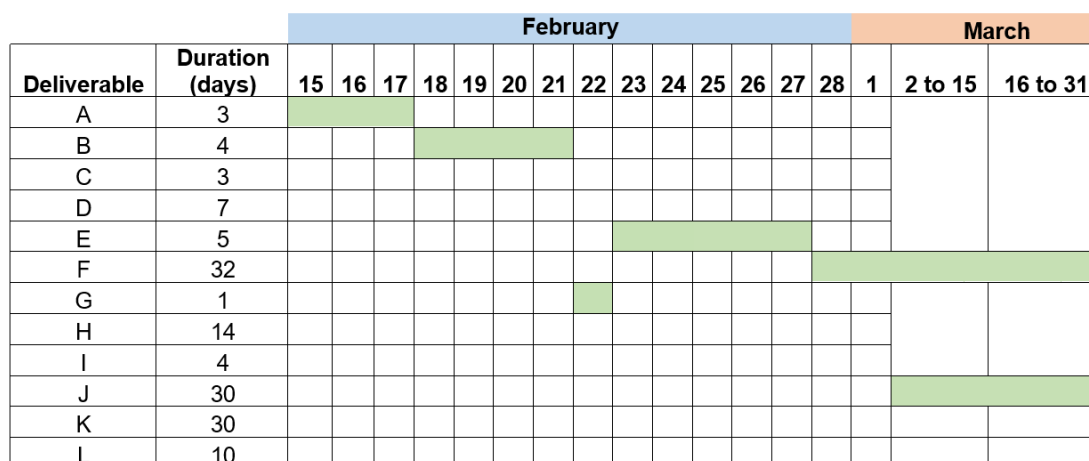


Figure 36: GANTT diagram of February and May

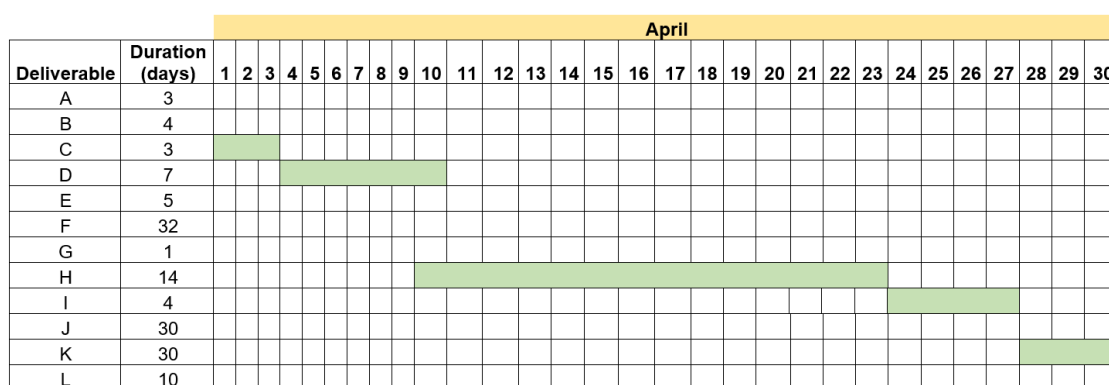


Figure 37: GANTT diagram of April



Figure 38: GANTT diagram of May and June

As seen in Figure 38, it was estimated that the last task of the project, which was set to be the early detection of the Parkinson disease, would finish the 6<sup>th</sup> of June. However, as already mentioned this task was not performed mainly because of the lack of time attributed to the task and secondly because the previous task which were the experiments with functionalized surface, finished out of schedule, the 31<sup>st</sup> of May. Another task that did not follow the established order is the Fluorescence microscopy for SAM validation. This was because the Department of Biology didn't have available dates until the 16<sup>th</sup> of May. Also, another visit was decided after incomplete information was obtained in the first one, and the sooner it could be scheduled was the 31<sup>st</sup> of May. Due to this initial delay on the SAM validation, the order was inverted and the task of experiments with functionalized surface was done before. Moreover, the first experiment with functionalized surface

was performed the 11<sup>th</sup> of April and to have the available substances and protocol set, the SAM formation task was changed to the first 10 days of April. On the contrary, the experiments without the functionalized surface were developed mainly during March, as previously scheduled. The characterization of the biosensor began on time but took much longer than the expected 5 days, it initiated the 23<sup>rd</sup> of February as planned but it ended the 15<sup>th</sup> of March. The rest of the tasks were all performed according to the GANTT diagram.

In conclusion, due to several inconvenience, the SAM formation and other experimental analysis tasks did not follow the established schedule, as opposed to the theoretical analysis which does not depend on external factors and could be developed on time. Nonetheless, the project was able to be finished by the 6<sup>th</sup> of June.

## 9. LEGISLATION AND REGULATION

The whole Project has been carried out in Barcelona, and therefore it is governed by Spanish Law.

The project research has been done by using a SPR completely manufactured by the Electronic Engineering Department of the Faculty of Physics of the University of Barcelona.

Only samples of animal origin have been processed (BSA). In case human biological samples - from Parkinson patients- are analyzed in the future, this may arise ethical issues and will be subject to specific regulations (regarding express consent of the persons concerned, protection of personal data, etc.), in particular those contained in Spanish Law 14/2007, of July 3, of Biomedical Research.

## 10. CONCLUSIONS AND FUTURE WORK

The development of this project has allowed to explore with great detail the use of SPR sensors for the detection of a model protein, BSA. Despite the obtention of important results on the sensing capability, the research must be continued to be more consistent. The lack of time and previous knowledge have been the major drawbacks to reach initial optimistic goals. However, the research conducted in the project is fundamental to continue the exploration of the SPR sensor of the DEE. Moreover, the experimental testing has uncovered challenges that require effective solutions, and further analysis has revealed paths to seek answers.

From the biosensor characterization, a comparison of the diffraction gratings has been generated. It can be concluded that the sensitivity is larger for the period of 600 nm than the 500 nm period. However, for fabrication parameter reasons, the DIP profundity of the period of 500 nm leads to less recording of noise. In the future, it is highly possible that the fabrication parameters of the biosensors can be varied to increase the sensing capability.

For the experiments with the microfluidics, two major problems in the design have been detected. The inlet and outlet position mask two of the diffraction gratings. Secondly, and the most problematic, the design prompts the formation of air bubbles because of its large width-to-height ratio and the edgy corners of the hexagon. The design by AutoCAD could potentially solve this problems or other designs inspired in current IBEC proposals could be implemented.

Furthermore, in the first experiments with the non-functionalized surface, it has been found that for a very small variation of refractive index, 0.009, the resonance wavelength moves 1 nm when switching from Milli Q water (refractive index of 1,33) to PBS (refractive index of 1,339). This added to the fact that the difference is easily detected visually, and signals are clear after processing, can imply a good sensing capability. As for protein detection, several experiments have suggested that BSA is attaching to the surface since the PBS baseline increases when added to clean. Moreover, the sensor has been able to distinguish between small shifts in concentration of BSA. The threshold concentration that SPR has enough sensitivity to distinguish is 0.5 mg/ml. However, it is not until concentrations of 1 mg/ml where there is a good sensing capability, and the adhesion kinetics can be observed. For concentrations 5 mg/ml or higher, the sensing capability is very good. Also, saturation is thought to be reached at approximately 10 mg/ml.

Experimental results with the functionalized surface have suggested that the SAM has formed. On one hand, fluorescent microscopy images have shown the control image is completely black with a mode of 0, as opposed to the dry conditioned wafer, where fluorescent spread particles appeared, that had a mode of 66, and, more importantly, the chip, that visually seemed more fluorescent, had a mode of 1363. When image contrast has been increased signal from autofluorescence of the gold seems to have been unveiled. Other results have slightly suggested that the SAM is bound covalently. The SAM validation is one of the major lines of work that needs to be continued in the project since it is extremely important to determine if the functionalization has been done correctly. On the other hand, the adhesion kinetics of a concentration of 50  $\mu\text{g/ml}$  have been observed, which has also suggested the formation of the SAM. However, the difference in concentration between 50  $\mu\text{g/ml}$  and 100  $\mu\text{g/ml}$  has not been detected which could imply saturation of the surface or that the sensing capability is not good enough for changes of this magnitude.

Overall, results with SPR have been damaged by the constant formation of bubbles. To fix this in future experiments, a bubble trap, which is a device designed to capture and remove gas bubbles from a fluidic system, could be bought and integrated. This is the system IBEC is currently using as a solution. Other future lines of work for the DEE are to detect, at medium-term, relevant biological biomarkers and to continue research on the early detection of Parkinson. As seen in the market research analysis, the SPR market will double in size in 10 years, so to continue this research would be a highly recommended decision. In personal terms, I hope to re-take this investigation in a near future in the DEE.

# 11. REFERENCES

- [1] Alhadrami, H.A., Biosensors: Classifications, medical applications, and future prospective. *Biotechnology and Applied Biochemistry*, Volume 65, Issue 3 (2018)
- [2] Bhalla N, Jolly P, Formisano N, Estrela P. Introduction to biosensors. *Essays Biochem.* (2016 June 30);60(1):1-8. doi: 10.1042/EBC20150001. PMID: 27365030; PMCID: PMC4986445.
- [3] M. Farré, L. Kantiani, D. Barceló, Chapter 7 - Microfluidic Devices: Biosensors, Editor(s): Yolanda Picó, *Chemical Analysis of Food: Techniques and Applications*, Academic Press (2012) Pages 177-217, ISBN 9780123848628, <https://doi.org/10.1016/B978-0-12-384862-8.00007-8>.
- [4] Rohini Karunakaran, Merve Keskin, Chapter 11 - Biosensors: components, mechanisms, and applications, Editor(s): Chukwuebuka Egbuna, Kingsley C. Patrick-Iwuanyanwu, Muhammad Ajmal Shah, Jonathan C. Ifemeje, Azhar Rasul, *Analytical Techniques in Biosciences*, Academic Press (2022) Pages 179-190, ISBN 9780128226544, <https://doi.org/10.1016/B978-0-12-822654-4.00011-7>
- [5] Saraju P. Mohanty, *Biosensors: A Survey Report*, ResearchGate (2002). Visited February 2023.
- [6] Shengbo Sang, Wendong Zhang and Yuan Zhao, *Review on the Design Art of Biosensors* (2013), IntechOpen. doi: 10.5772/52257.
- [7] Mehrotra P. Biosensors and their applications - A review. *J Oral Biol Craniofac (Res.* 2016 May-Aug);6(2):153-9. doi: 10.1016/j.jobocr.2015.12.002. Epub (January 2016). PMID: 27195214; PMCID: PMC4862100.
- [8] Types of Biosensors | Working principle of Biosensor types - RF Wireless World. Visited February 2023.
- [9] Sabine Szunerits, Atef Shalabney, Rabah Boukherroub et Ibrahim Abdulhalim, *Dielectric coated plasmonic interfaces: their interest for sensitive sensing of analyte-ligand interactions*, ResearchGate (2008). Visited February 2023.
- [10] Song, C.; Que, S.; Heimer, L.; Que, L. On-Chip Detection of the Biomarkers for Neurodegenerative Diseases: Technologies and Prospects. *Micromachines* (2020), 11, 629. <https://doi.org/10.3390/mi11070629>
- [11] 30\_NanoPhotonics\_SPR\_Introduction\_Instruments\_2023, Universitat de Barcelona.
- [12] Biosensing Instrument. (2023). Biosensing. Visited March 2023
- [13] Arnoud. SPRpages (2023). Visited March 2023.
- [14] Anna Moberg, surface plasmon resonance, Cytiva (2023). Visited March 2023.
- [15] Víctor Parra-Monreal, Winnie Svendsen, María A. Ortega-Machuca, Albert Romano-Rodríguez, Javier Ramón-Azcón et Mauricio Moreno-Sereno, *Detection of cytokines in skeletal*

muscle tissue using optical SPR sensing platform. Universitat politècnica de Catalunya. (January 2020).

[16] Peng Zhang, You-Peng Chen, Jin-Song Guo, Chapter Five - SPR for water pollutant detection and water process analysis, Editor(s): You-Peng Chen, Teng-Fei Ma, Comprehensive Analytical Chemistry, Elsevier, Volume 95 (2021) Pages 145-183, ISSN 0166-526X, ISBN 9780323853095 <<https://doi.org/10.1016/bs.coac.2021.06.001>>

[17] Nirmalya K Chaki, K Vijayamohanan, Self-assembled monolayers as a tunable platform for biosensor applications, Biosensors and Bioelectronics, Volume 17, Issues 1–2 (2002) Pages 1-12, ISSN 0956-5663. [https://doi.org/10.1016/S0956-5663\(01\)00277-9](https://doi.org/10.1016/S0956-5663(01)00277-9).

[18] Anna Bergström, SPR Sensor Surfaces based on Self-Assembled Monolayers, Master thesis in the department of Physics, Chemistry and Biology Linköping University (2009)

[19] Toworfe GK, Bhattacharyya S, Composto RJ, Adams CS, Shapiro IM, Ducheyne P. Effect of functional end groups of silane self-assembled monolayer surfaces on apatite formation, fibronectin adsorption and osteoblast cell function. J Tissue Eng Regen Med. (January 2009);3(1):26-36. doi: 10.1002/term.131. PMID: 19012271; PMCID: PMC2610238.

[20] Chung YC, Chiu YH, Wu YW, Tao YT. Self-assembled biomimetic monolayers using phospholipid-containing disulfides. Biomaterials. 2005 May;26(15):2313-24. doi: 10.1016/j.biomaterials.2004.06.043. PMID: 15585234.

[21] Keiko Tawa, Kenichi Morigaki, Substrate-Supported Phospholipid Membranes Studied by Surface Plasmon Resonance and Surface Plasmon Fluorescence Spectroscopy, Biophysical Journal, Volume 89, Issue 4, (2005) Pages 2750-2758, ISSN 0006-3495, <https://doi.org/10.1529/biophysj.105.065482>.

[22] Cáncer, OMS (2022). Visited March of 2023.

[23] Healy DA, Hayes CJ, Leonard P, McKenna L, O'Kennedy R. Biosensor developments: application to prostate-specific antigen detection. Trends Biotechnol. (March 2007) ;25(3):125-31. doi: 10.1016/j.tibtech.2007.01.004. Epub 2007 Jan 24. PMID: 17257699.

[24] Das, S.; Devireddy, R.; Gartia, M.R. Surface Plasmon Resonance (SPR) Sensor for Cancer Biomarker Detection. Biosensors (2023), 13, 396. <https://doi.org/10.3390/bios13030396>

[25] Pranveer Singh, Surface Plasmon Resonance: A Boon for Viral Diagnostics, Reference Module in Life Sciences, Elsevier, (2017), ISBN 9780128096338. <https://doi.org/10.1016/B978-0-12-809633-8.12245-9>.

[26] Aysa Reza bakhsh, Reza Rahbarghazi, Farzaneh Fathi, Surface plasmon resonance biosensors for detection of Alzheimer's biomarkers; an effective step in early and accurate diagnosis, Biosensors and Bioelectronics, Volume 167, (2020), 112511, ISSN 0956-5663, <https://doi.org/10.1016/j.bios.2020.112511>.

[27] Delgado-Alvarado M, Gago B, Gorostidi A, Jiménez-Urbietá H, Dacosta-Aguayo R, Navalpotro-Gómez I, Ruiz-Martínez J, Bergareche A, Martí-Massó JF, Martínez-Lage P, Izaguirre A, Rodríguez-Oroz MC. Tau/ $\alpha$ -synuclein ratio and inflammatory proteins in Parkinson's disease:

An exploratory study. *Mov Disord.* (July 2017) ;32(7):1066-1073. doi: 10.1002/mds.27001. Epub 2017 May 26. PMID: 28548309.

[28] Parkinson's Disease: Causes, Symptoms, and Treatments, National Institute on Aging (2022). Visited March of 2023.

[29] Stefanis L.  $\alpha$ -Synuclein in Parkinson's disease. *Cold Spring Harb Perspect Med.* 2012 Feb;2(2):a009399. doi: 10.1101/cshperspect.a009399. PMID: 22355802; PMCID: PMC3281589.

[30] Biacore. Wikipedia (2021). Visited March of 2023.

[31] Westburg Life Sciences, Alto, the first digital, high-throughput, benchtop SPR system to accelerate drug discovery, YouTube (2020). Visited March of 2023.

[32] Surface Plasmon Resonance Market, Future Market insights (2022). Visited April of 2023.

[33] JUAN TREVIÑO CASTRILLO, Codirigida por Prof. Laura M. Lechuga y Dr. José Miguel Rodríguez Frade, DESARROLLO DE UN BIOSENSOR DE RESONANCIA DE PLASMÓN SUPERFICIAL PARA LA DETERMINACIÓN DE HORMONAS PITUITARIAS EN MUESTRAS BIOLÓGICAS, Tesis doctoral. Consejo superior de científicas (May 2009).

[36] Lopez-Muñoz GA, Ortega MA, Ferret-Miñana A, De Chiara F, Ramón-Azcón J. Direct and Label-Free Monitoring of Albumin in 2D Fatty Liver Disease Model Using Plasmonic Nanogratings. *Nanomaterials* (Basel). (December 2020 )15;10(12):2520. doi: 10.3390/nano10122520. PMID: 33334062; PMCID: PMC7765559.

[37] C Vericat, M E Vela, G A Benitez et J A Martin Gago, Surface characterization of sulfur and alkanethiol self-assembled monolayers on Au(111), *Journal of Physics: Condensed Matter*, (November 2006) DOI 10.1088/0953-8984/18/48/R01

[38] J.S. Rudra, S.H. Kelly, J.H. Collier, 2.4 Self-Assembling Biomaterials, Editor(s): Paul Ducheyne, *Comprehensive Biomaterials II*, Elsevier, (2017), Pages 67-89, ISBN 9780081006924, <https://doi.org/10.1016/B978-0-12-803581-8.10210-3>.

[39] Johanna Stettner ,Paul Frank et Thomas Griesser, Institute of Solid State Physics, A Study on the Formation and Thermal Stability of 11-MUA SAMs on Au(111)/Mica and on Polycrystalline Gold Foils, Graz University of Technology, Petersgasse 16, A- 8010 Graz, Austria, and Institute for Chemistry and Technology of Materials, Graz University of Technology, Stremayrgasse 16, A-8010 Graz, Austria Received (August 2008). <https://pubs.acs.org/doi/10.1021/la802534q>

[40] Rundqvist J, Hoh JH, Haviland DB. Substrate effects in poly(ethylene glycol) self-assembled monolayers on granular and flame-annealed gold. *J Colloid Interface Sci.* (September 2006) 1;301(1):337-41. doi: 10.1016/j.jcis.2006.05.012. Epub 2006 May 6. PMID: 16765974.

[41] MES monohydrate (Synonyms: 2-Morpholinoethanesulphonic acid monohydrate). *MedChemExpress* (2016). Visited May of 2023.

[42] Lab Equipment and Lab Supplies. Fisher Scientific. May of 2023.



[43] Field Emission Scanning Electron Microscopy (FESEM) . PhotoMetrics. (2018). Visited April of 2023

[44] Widefield Fluorescence Microscopy | Principle & Applications | ibidi cells in focus (2023). Visited May of 2023.

[45] Wikipedia contributors. (2023). Molecular vibration. Wikipedia. Visited March of 2023.

[46] Bubbles in Microfluidics: How They Form and How to Avoid Them. The MicroFluidic Circle (2019). Visited March of 2023

[47] Fluorescence SpectraViewer (2023). ThermoFisher. Visited June of 2023.

# 12.ANNEXES

## ANNEX 1: CHEMICAL PREPARATIONS

A highly important step of this project is the use of chemical substances which have been prepared at the Organic chemistry department. The different procedures, substances and concentrations are detailed on this annex.

### 1. BOVINE SERUM ALBUMIN (BSA)

#### 1.1 PREPARATION OF DIFFERENT CONCENTRATION OF BSA THROUGH DILUTION

On two centrifuge tubes of size 2 ml, 2 mg of BSA and 1 ml of PBS is added, which is a concentration of 2mg/ml. Then on 5 centrifuge tubes, labeled according to the mg of BSA that it will be added, with 1 ml of PBS on each are also prepared. From one of the 2 mg/ ml concentration tubes, 1 ml will be pipetted and added to one of the tubes with 1 ml of PBS. From this second tube, that will have a concentration of 1 mg/ml, 1 ml of the solution contained will be pipetted and added to another one of the tubes with 1 ml of PBS, which will now have a concentration of 0.5 mg/ ml. This procedure will be repeated 3 more times to obtain concentrations of 0.25, 0.125 and 0.0625 mg/ml.

Therefore, for the experimental analysis 6 concentrations have been obtained through dilution: 2, 1, 0.5, 0.25, 0.125, 0.0625 mg/ml.

#### 1.2 PREPARATION OF THE BSA FITC:

Density of BSA FITC: 50  $\mu$ g/ml diluted in PBS. The micrograms are measured with a microanalytical balance. If 2 ml of the solution need to be prepared, the amount of BSA that needs to be added:

$$2\text{ml PBS} \cdot \frac{50 \cdot 10^{-6} \text{BSA FITC}}{\text{ml PBS}} = 0,0001 \text{ g BSA FITC}$$

For the microfluidics 15 ml are prepared:

$$15 \text{ ml PBS} \cdot \frac{50 \cdot 10^{-6} \text{BSA FITC}}{\text{ml PBS}} = 0,00075 \text{ g BSA FITC}$$

To compute other concentrations prepared the BSA concentration is replaced by the new value.

### 2. CHLORIDE ACID (HCL) 1M

To prepare this compound HCl is mixed with distilled water. It is important to know before preparing the solution, that the density of HCL is 1,18g/ml, the molar mass is 36,5 g/mol and has a purity of 37%. With this information, if 100 ml of HCl 1M must be obtained, the following calculations must be done:

$$\frac{1,18g\ HCl}{ml\ HCl} \cdot \frac{1\ mol\ HCl}{36,5\ g\ HCl} \cdot \frac{37}{100} \cdot \frac{1000\ ml}{1L} = 11,96 \frac{mol}{L} HCl$$

$$100\ ml\ H_2O \cdot \frac{1\ mol\ HCl}{L\ H_2O} \cdot \frac{L\ HCl}{11,96\ mol} = 8,33\ ml$$

This indicates that 8,33 ml of HCl must be mixed with 100 ml of H<sub>2</sub>O to obtain HCl 1M. The quantities are measured with a test tube under the laboratory hood.

### 3. PHOSPHATE-BUFFERED SALINE (PBS) 1X

To prepare this compound PBS 1X is mixed with distilled water. It is important to know that to prepare PBS 1X the relationship is for 494,5 g of PBS there must be 50 L of water. To compute how many grams of PBS will be needed to obtain 100 ml of the compound:

$$100\ ml\ H_2O \cdot \frac{494,5\ g\ PBS}{50\ L\ H_2O} \cdot \frac{L}{1000\ ml} = 0,991\ g\ PBS$$

Therefore, 100 ml of distilled water will be mixed with 0,991 g PBS, the weighting will be done with a balance and the mixture in a beaker.

### 4. MERCAPTOUNDECANOIC ACID (MUA) 3 mM

The preparation of MUA 3mM consists of mixing 11- Mercaptoundecanoic acid with a molar mass of 218,36 g/mol and Ethanol absolute. To do this, several steps must be performed.

1. Two vials, a test tube, and the spatula are washed, first with aqua regia, and then rinsed with Milli-Q water, and finally with Acetone.



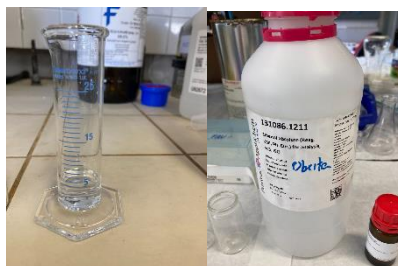
2. The vials, test tube, and spatula are dried in a glassware drying oven for 5/10 minutes.



3. The MUA is measured inside the vials on the balance until 0.0042 grams of MUA is reached.



4. Under the hood, 5 ml of Ethanol absolute is measured with the test tube and then that amount is added to each vial that contains the MUA.



## 5. 2-(N-MORPHOLINO)ETHANESULFONIC ACID (MES)

MES, which has a molecular weight of 213,2 g, is diluted in Milli- Q water with a concentration of 25 mM.

Therefore if 100 ml of MES are needed the amount of MES in grams will be:

$$100 \text{ ml H}_2\text{O} \cdot \frac{1 \text{ L H}_2\text{O}}{1000 \text{ ml H}_2\text{O}} \cdot \frac{25 \cdot 10^{-3} \text{ mol MES}}{1 \text{ L H}_2\text{O}} \cdot \frac{213,2 \text{ g MES}}{1 \text{ mol MES}} = 0,533 \text{ g MES}$$

## 6. 1-ETHYL-3-(3-DIMETHYLAMINOPROPYL)CARBODIIMIDE (EDC)/ N-HYDROXYSUCCINIMIDE (NHS)

EDC 0.2 mol/L (FW= 191,7) and NHS 0.05 mol/L dissolved together in 2 ml of MES

$$2 \text{ ml MES} \cdot \frac{1 \text{ L}}{1000 \text{ ml}} \cdot \frac{0,2 \text{ mol EDC}}{1 \text{ L MES}} \cdot \frac{191,7 \text{ g EDC}}{1 \text{ mol EDC}} = 0,07668 \text{ g EDC}$$

$$2 \text{ ml MES} \cdot \frac{1 \text{ L}}{1000 \text{ ml}} \cdot \frac{0,05 \text{ mol NHS}}{1 \text{ L MES}} \cdot \frac{115,09 \text{ g NHS}}{1 \text{ mol NHS}} = 0,07668 \text{ g NHS}$$

## 7. ETHANOLAMINE

Ethanolamine, which has a density of 1,012 g/mL is diluted in PBS. The concentration is 50  $\mu\text{g/ml}$  and 50 ml of the solution must be prepared:

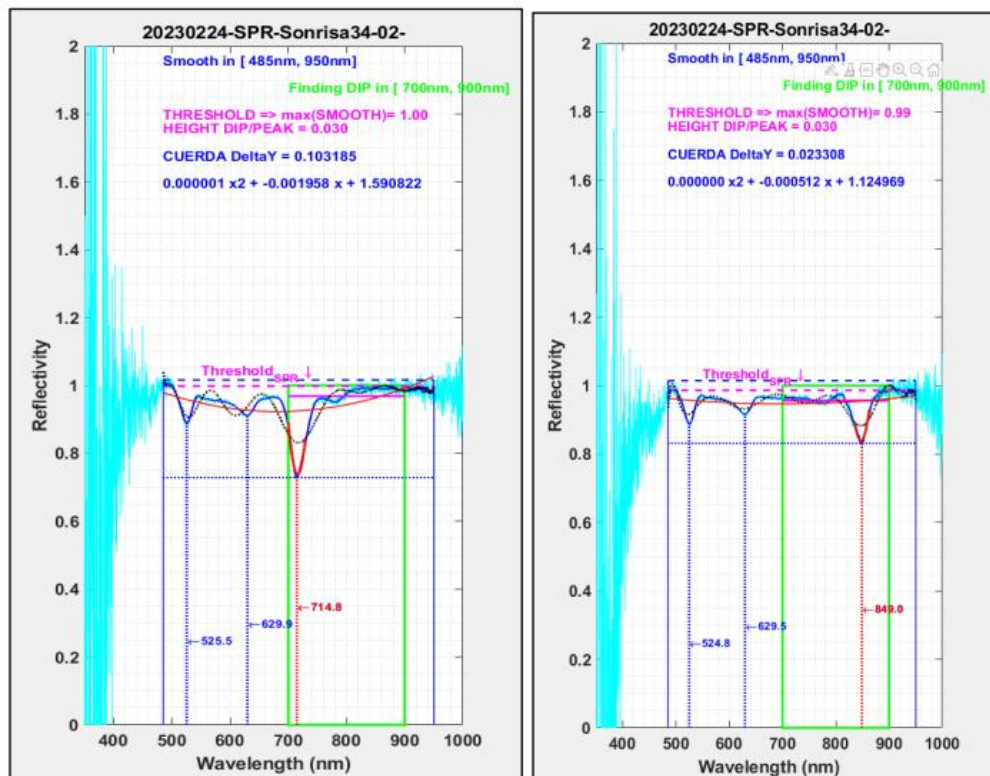
$$50 \text{ ml PBS} \cdot \frac{50 \cdot 10^{-3} \text{ g Eth}}{1 \text{ ml PBS}} \cdot \frac{1 \text{ ml Eth}}{1,012 \text{ g Eth}} = 0,00247 \text{ ml Eth}$$

## ANNEX 2: BIOSENSOR CHARACTERIZATION EXPERIMENTS (SWEEP)

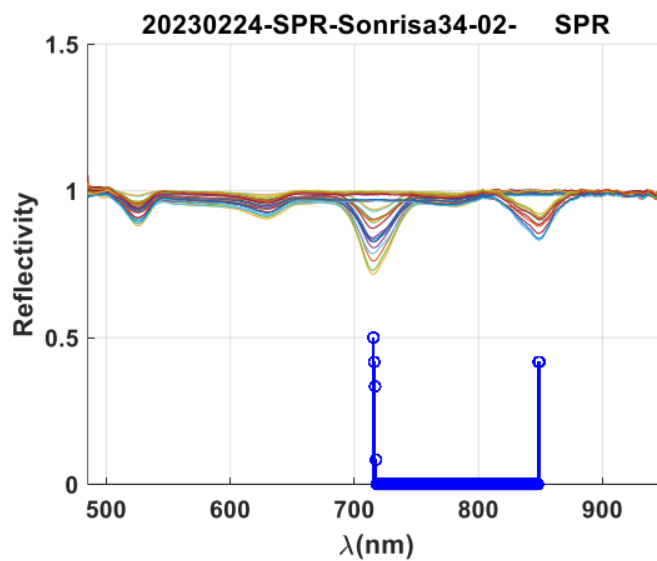
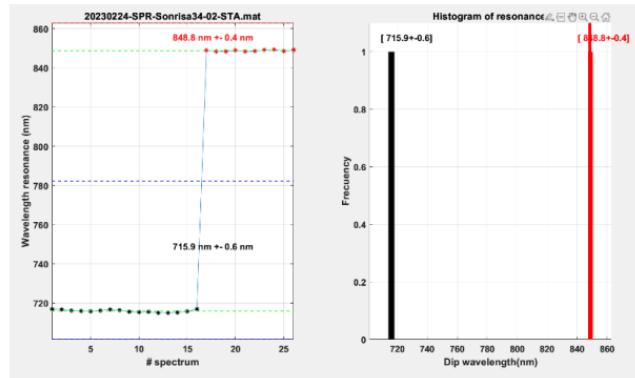
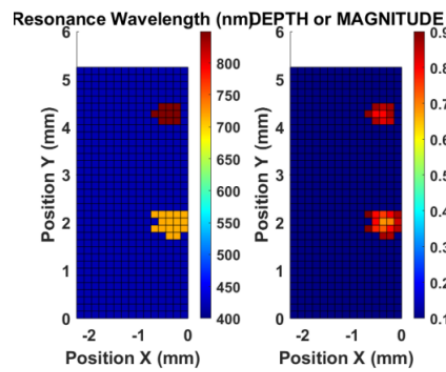
### A) EXPERIMENT FROM THE 24TH OF FEBRUARY WITH METHACRYLATE COVER AND ETHANOL OR ISOPROPANOL

The upper part measurements seem to not be performed.

20230224_SPR_Sonrisa34_02_SPEC OBLEA S2103: RIE 24" = 30nm + Ti=3nm + Gold=40nm	Friday 24-02-2023	ISOPROPANOL / ETANOL (??) Methacrylate COVER
POLARIZATION = 0°		
[X <sub>REF</sub> , Y <sub>REF</sub> ] = [0mm, 0mm] [X <sub>0</sub> , Y <sub>0</sub> ] = [1mm, 1mm]		
Δx=0.15mm	NX=15	Lx= 3mm
Δy=0.2mm	NY=30	Ly= 6mm
DARK & REF in FLAT GOLD WITH POLARIZATION = 0°		
<ul style="list-style-type: none"> <li>- El recorrido de los motores no puede escanear las cuatro zonas sensibles. Generalmente TOTAL &lt;9mm</li> <li>- Intentamos medir los dos periodos P1=500nm y P2=600nm</li> </ul>		



La gráfica de la izquierda corresponde a la reflectividad de una red de oro con periodo P1=500nm ( $\lambda_{RES}=715nm$ ). La de la derecha corresponde a P2=600nm,  $\lambda_{RES}=849nm$



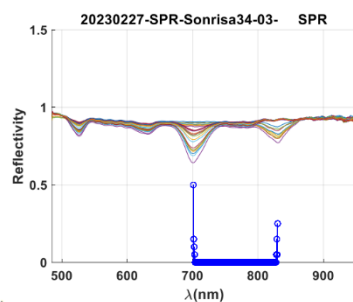
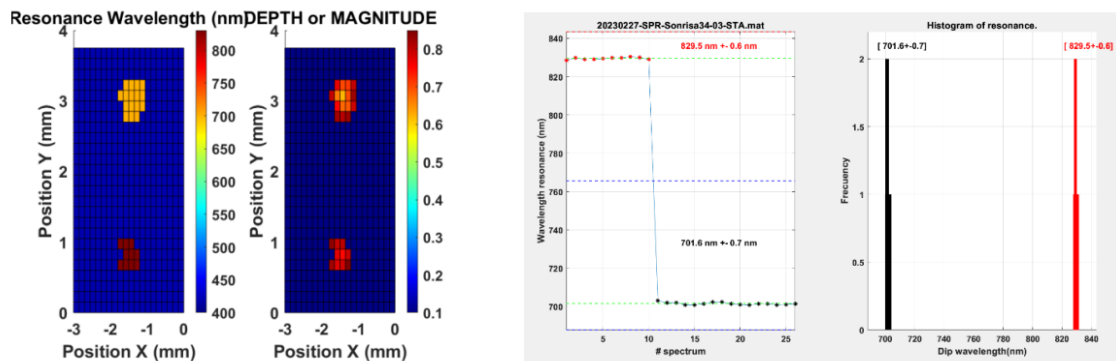
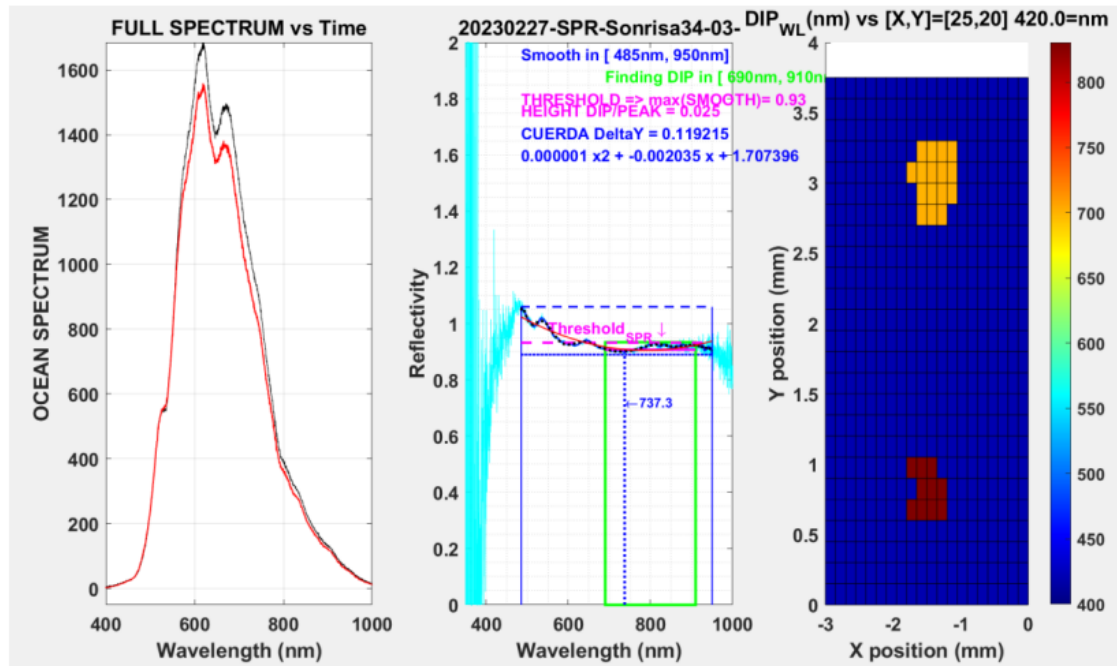
**Etanol o Isopropanol:**

**P1= 715.9 nm ± 0.6 nm**

**P2= 848.8 nm ± 0.4 nm**

## B) EXPERIMENT FROM THE 27TH OF FEBRUARY WITH MICROFLUIDICS AND ETHANOL

20230227_SPR_Sonrisa34_03_SPEC	Monday	Ethanol
OBLEA S2103: RIE 24" = 30nm + Ti=3nm + Gold=40nm	27-02-2023	FLUIDICA
POLARIZATION = 0°		
[X <sub>REF</sub> ,Y <sub>REF</sub> ]=[0mm,0mm]		
[X <sub>0</sub> ,Y <sub>0</sub> ]=[1mm,1mm]		
Δx=0.15mm	NX=15	Lx= 3mm
Δy=0.2mm	NY=30	Ly= 6mm
DARK & REF in FLAT GOLD WITH POLARIZATION = 0°		
-		



**Ethanol:**

**P1= 701.6 nm ± 0.7 nm**

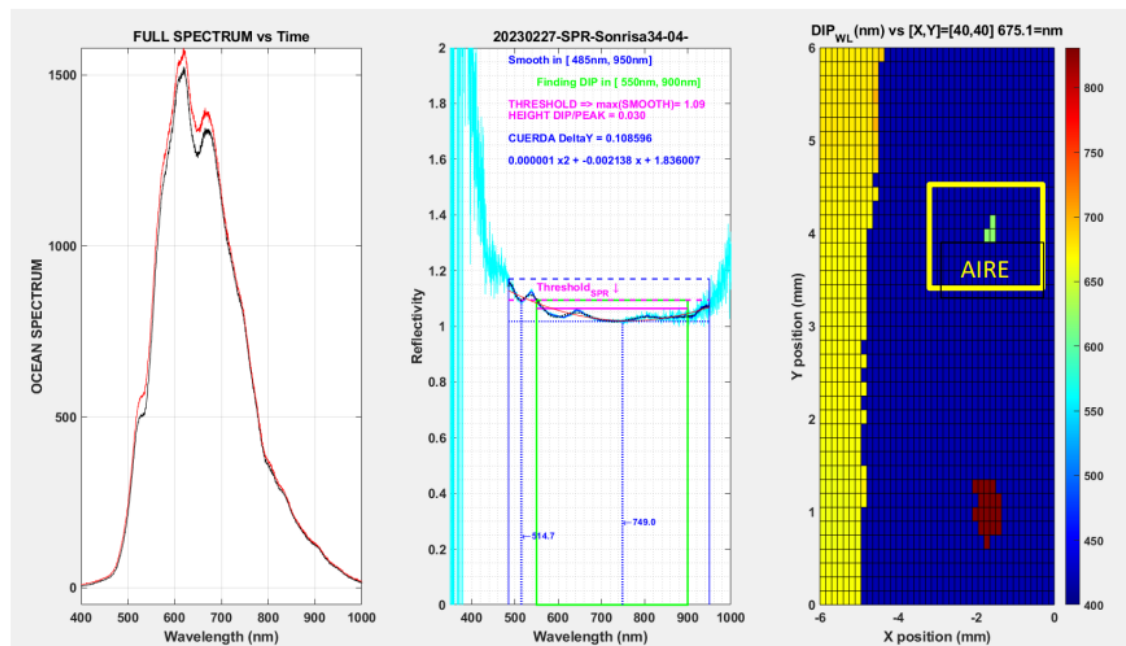
**P2= 829.5 nm ± 0.6 nm**

### C) EXPERIMENT FROM THE 27TH OF FEBRUARY WITH MICROFLUIDICS AND ETHANOL

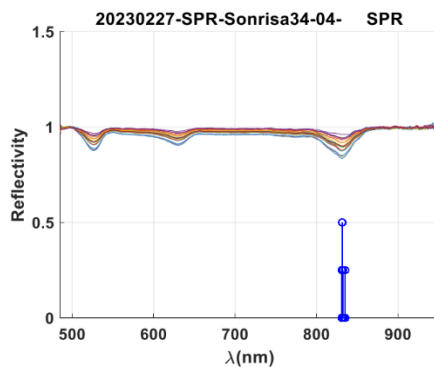
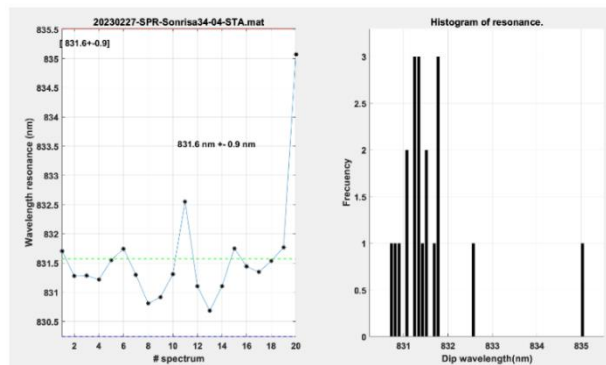
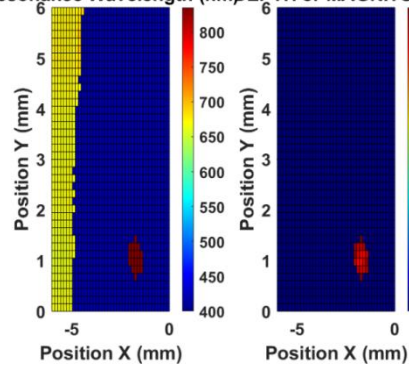
In the upper period, 500 nm, Ethanol has evaporated and therefore the substance being detected is air.



20230227_SPR_Sonrisa34_04_SPEC OBLEA S2103: RIE 24" = 30nm + Ti=3nm + Gold=40nm	Monday 27-02-2023	Ethanol FLUIDICA
POLARIZATION = 0°		
[X <sub>REF</sub> , Y <sub>REF</sub> ] = [0mm, 0mm] [X <sub>0</sub> , Y <sub>0</sub> ] = [1mm, 1mm]		
Δx=0.15mm	NX=40	Lx= 6mm
Δy=0.15mm	NY=40	Ly= 6mm
DARK & REF in FLAT GOLD WITH POLARIZATION = 0°		
<ul style="list-style-type: none"> <li>- La referencia se toma con ETANOL. Lambda t0= 830nm.</li> <li>- MUCHA RESOLUCIÓN TIEMPO DE MEDIDA 3 HORAS</li> <li>- SE HA EVAPORADO EL ETANOL EN LA RED SUPERIOR DE P1=500NM</li> </ul>		



Resonance Wavelength (nm)DEPTH or MAGNITUDE

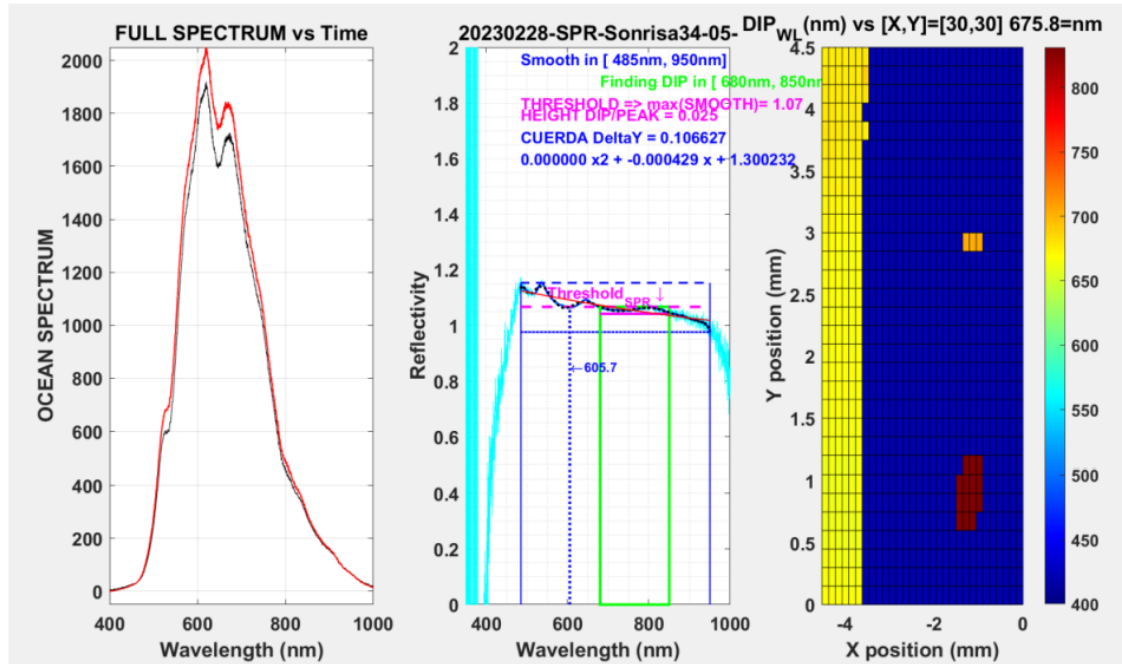


**ETANOL:**

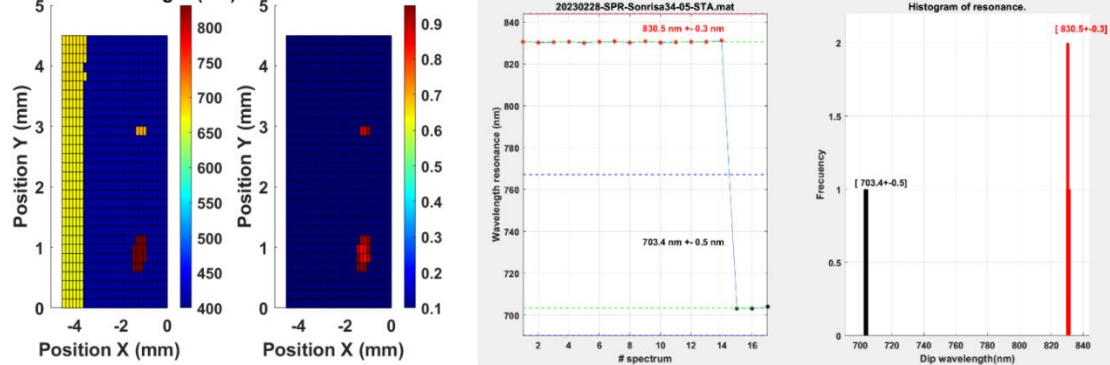
**P2= 831.6 nm ± 0.9 nm**

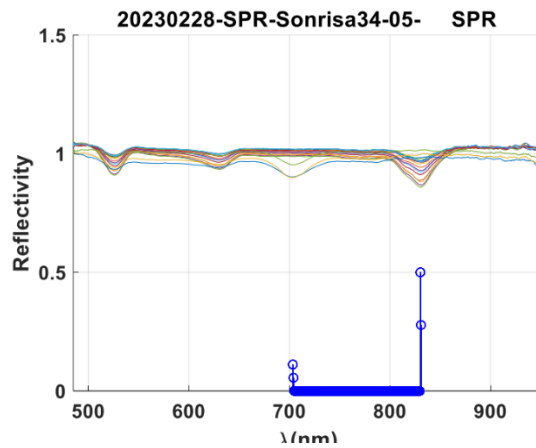
# D) EXPERIMENT FROM THE 28TH OF FEBRUARY WITH MICROFLUIDICS AND WATER MILLI Q

20230228_SPR_Sonrisa34_05_SPEC OBLEA S2103: RIE 24" = 30nm + Ti=3nm + Gold=40nm	Wednesday 28-02-2023	WATER. Fluidics
POLARIZATION = 0°		
[X <sub>REF</sub> , Y <sub>REF</sub> ] = [0mm, 0mm] [X <sub>0</sub> , Y <sub>0</sub> ] = [1mm, 1mm]		
DARK & REF in FLAT GOLD WITH POLARIZATION = 0°		
<ul style="list-style-type: none"> <li>- Intentamos medir los dos periodos P1=500nm y P2=600nm</li> <li>- TENEMOS DUDAS EN EL RESULTADO. EVAPORACIÓN</li> <li>- Para P2=600nm en H2O tenemos 830nm</li> </ul>		



Resonance Wavelength (nm)DEPTH or MAGNITUDE





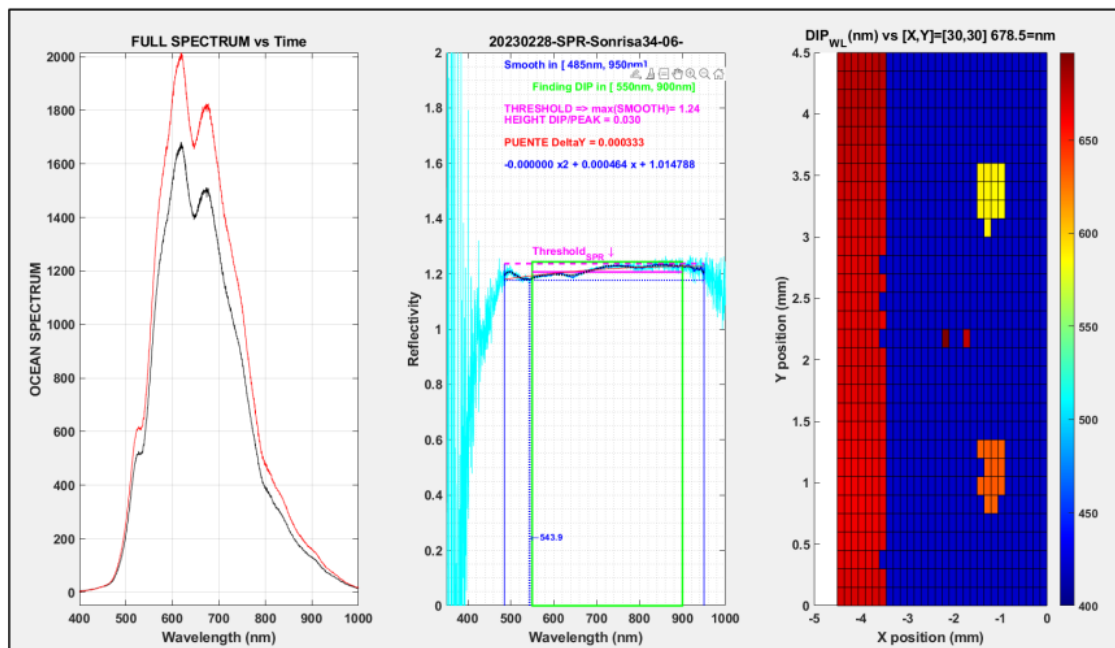
**WATER:**

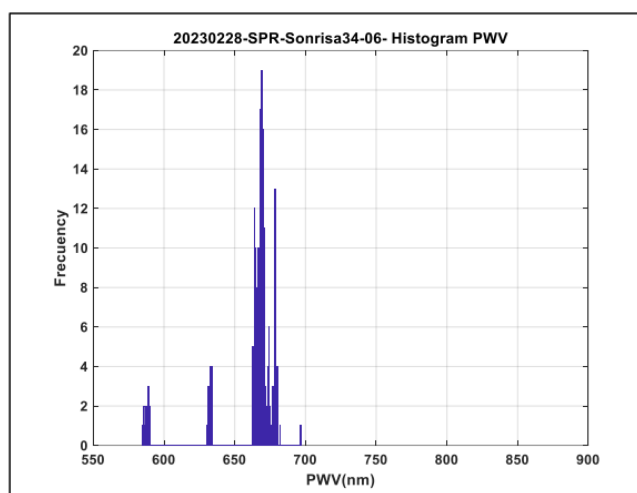
**P1= 703.4 nm ± 0.5 nm**

**P2= 830.5 nm ± 0.3 nm**

E) EXPERIMENT FROM THE 28TH OF FEBRUARY WITH MICROFLUIDICS AND ISOPROPANOL

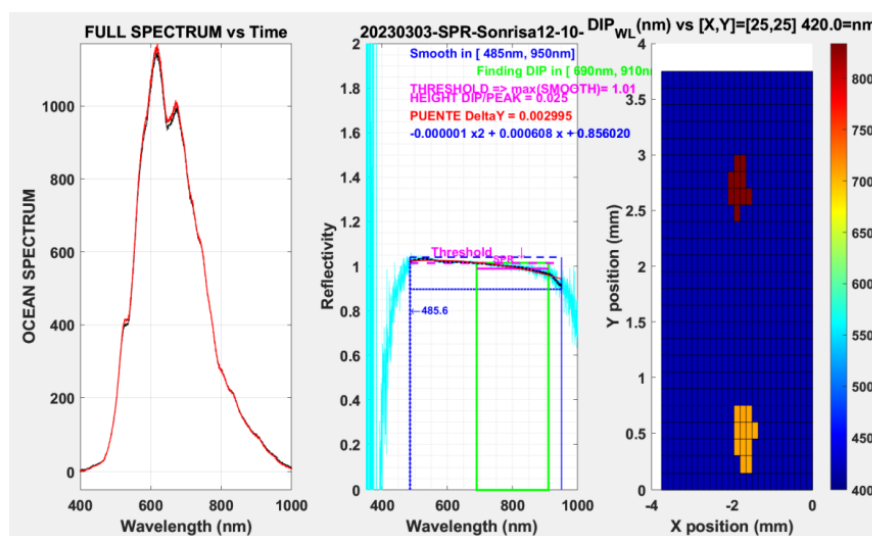
20230228_SPR_Sonrisa34_06_SPEC OBLEA S2103: RIE 24" = 30nm + Ti=3nm + Gold=40nm	Wednesday 28-02-2023	ISOPROPOANOL. Fluidics
POLARIZATION = 0°		
[X <sub>REF</sub> ,Y <sub>REF</sub> ]=[0mm,0mm] [X <sub>0</sub> ,Y <sub>0</sub> ]=[1mm,1mm]		
Δx=	NX=	Lx=
Δy=	NY	Ly=
DARK & REF in FLAT GOLD WITH POLARIZATION = 0°		
<div>- Intentamos medir los dos periodos P1=500nm y P2=600nm</div> <div>- dudas</div>		

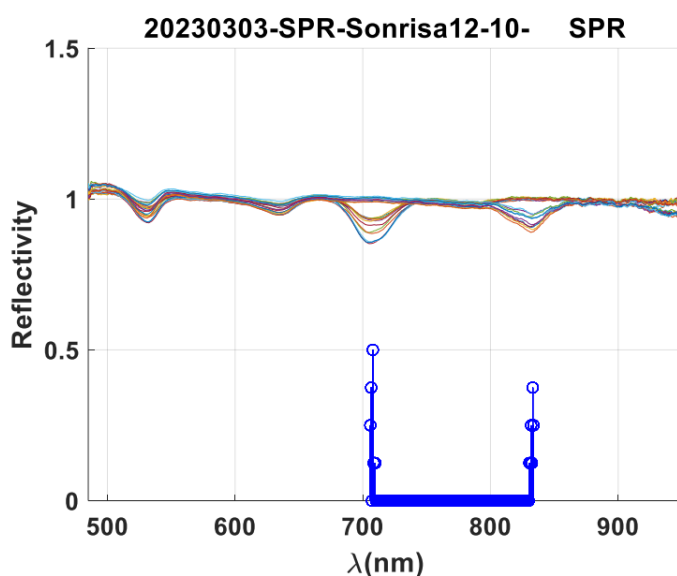
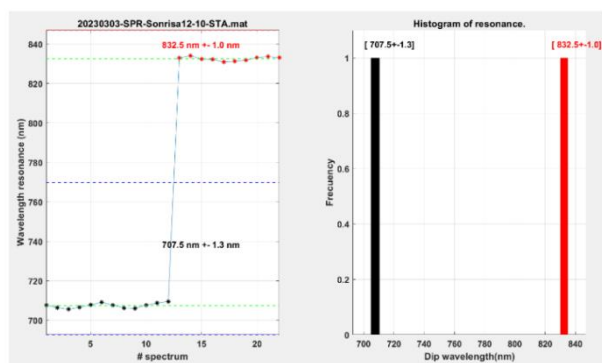
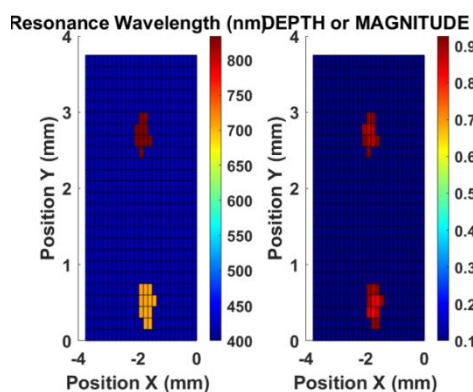




## F) EXPERIMENT FROM THE 3RD OF MARCH WITH METHACRYLATE COVER AND WATER MILLI Q

20230303_SPR_Sonrisa12_10_SPEC OBLEA S2103: RIE 24" = 30nm + Ti=3nm + Gold=40nm	Friday 3-03-2023	SWEEP WATER Methacrylate COVER
POLARIZATION = 0°		
[X <sub>REF</sub> , Y <sub>REF</sub> ]= [X <sub>0</sub> , Y <sub>0</sub> ]=		
DARK & REF in FLAT GOLD WITH POLARIZATION = 0°		
- CAMBIAMOS AL CHIP 12 PARA REALIZAR SWEEP EN AGUA Y ETANOL Y CALCULAR SENSIBILIDAD		
- ESTA MEDIDA ES EN WATER		





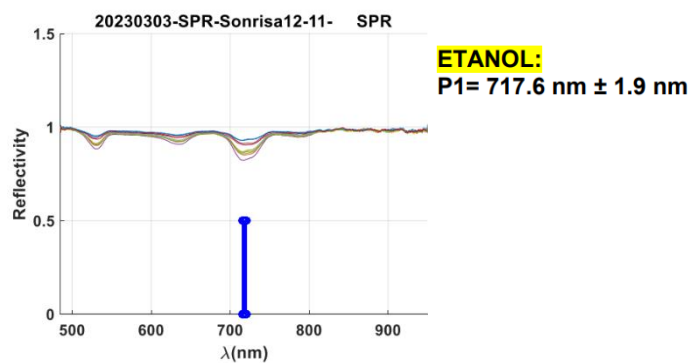
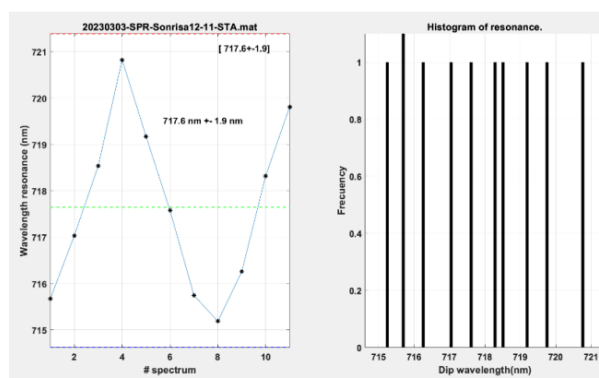
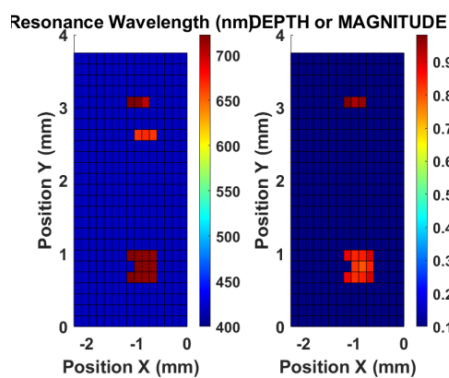
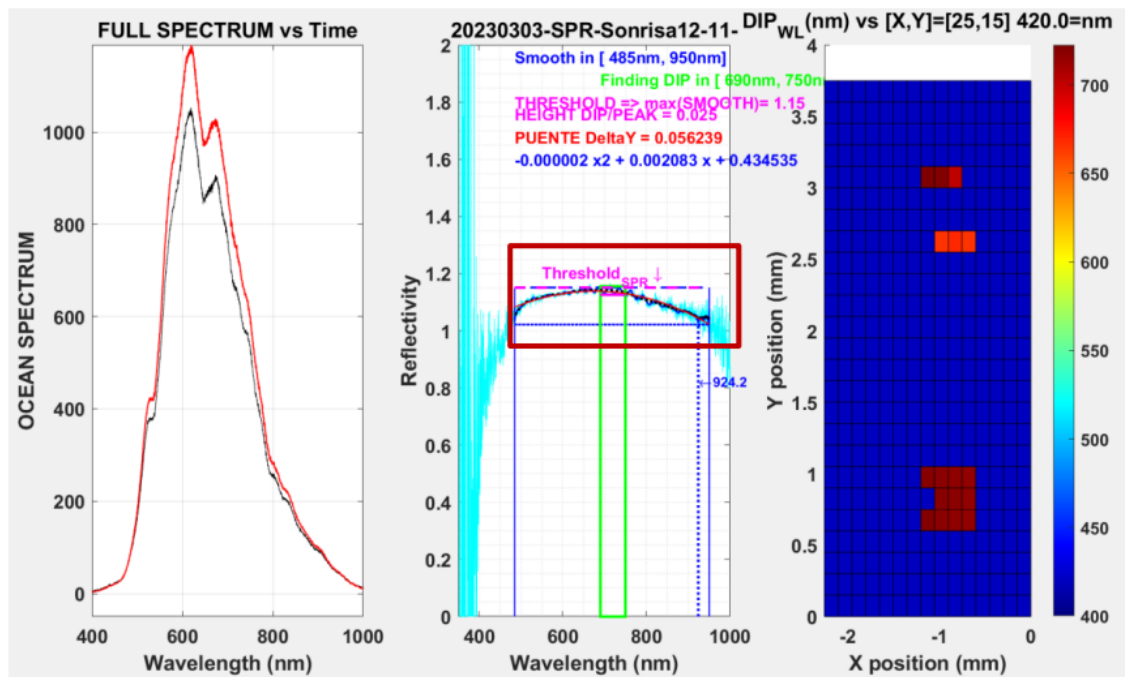
**WATER:**

**P1= 707.5 nm ± 1.3 nm**

**P2= 832.5 nm ± 1.0 nm**

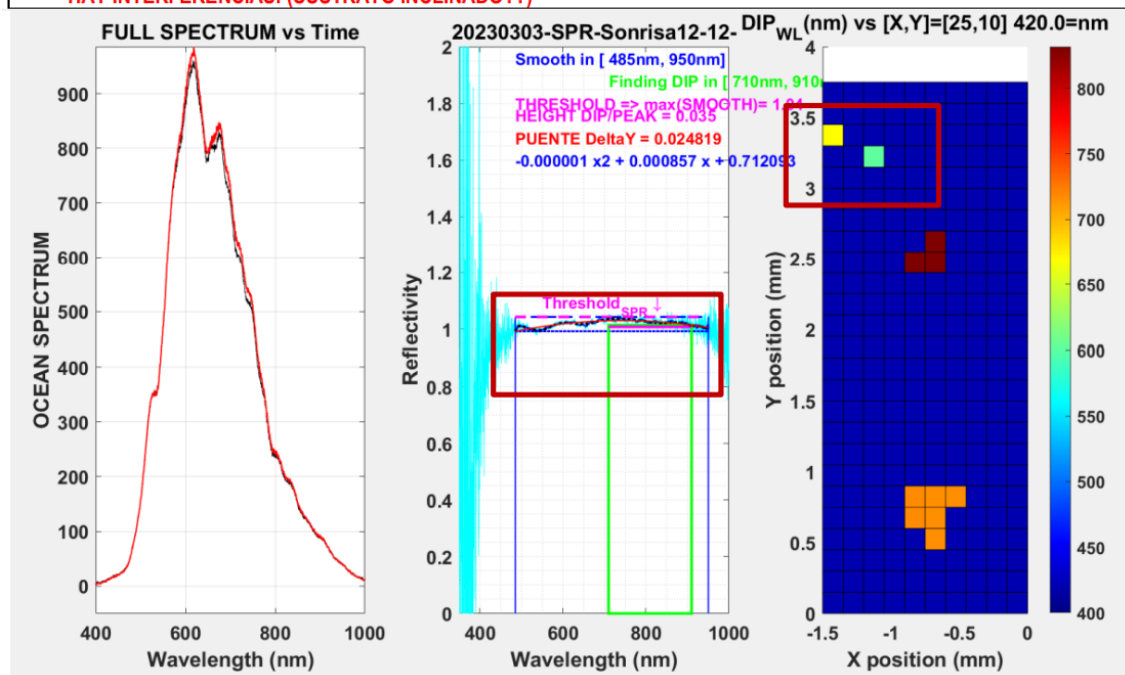
## G) EXPERIMENT FROM THE 3RD OF MARCH WITH METHACRYLATE COVER AND ETHANOL

20230303_SPR_Sonrisa12_11_STA	Friday	SWEEP - ETANOL
OBLEA S2103: RIE 24" = 30nm + Ti=3nm + Gold=40nm	3-03-2023	Methacrylate COVER
POLARIZATION = 0°		
[X <sub>REF</sub> , Y <sub>REF</sub> ]=		
[X <sub>0</sub> , Y <sub>0</sub> ]=		
DARK & REF in FLAT GOLD WITH POLARIZATION = 0°		
<ul style="list-style-type: none"> <li>- CHIP 12 SWEEP EN ETANOL</li> <li>- SOLO SE MIDE P1=500 nm, EL ETANOL SE EVAPORA ANTES DE LLEGAR A MEDIR P2=600 nm</li> <li>- HAY INTERFERENCIAS! (SUSTRATO INCLINADO??)</li> </ul>		

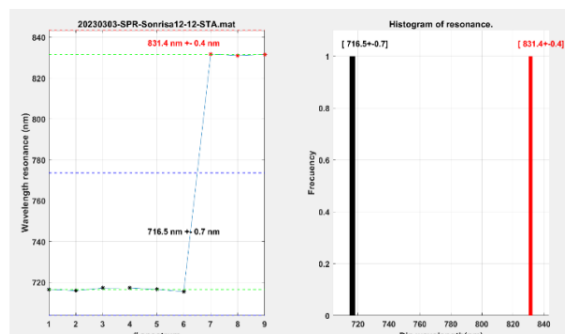
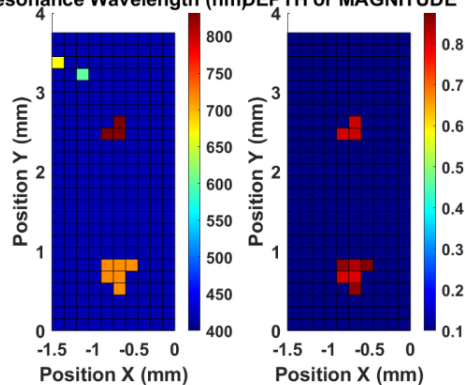


H) EXPERIMENT FROM THE 3RD OF MARCH WITH METHACRYLATE COVER AND ETHANOL

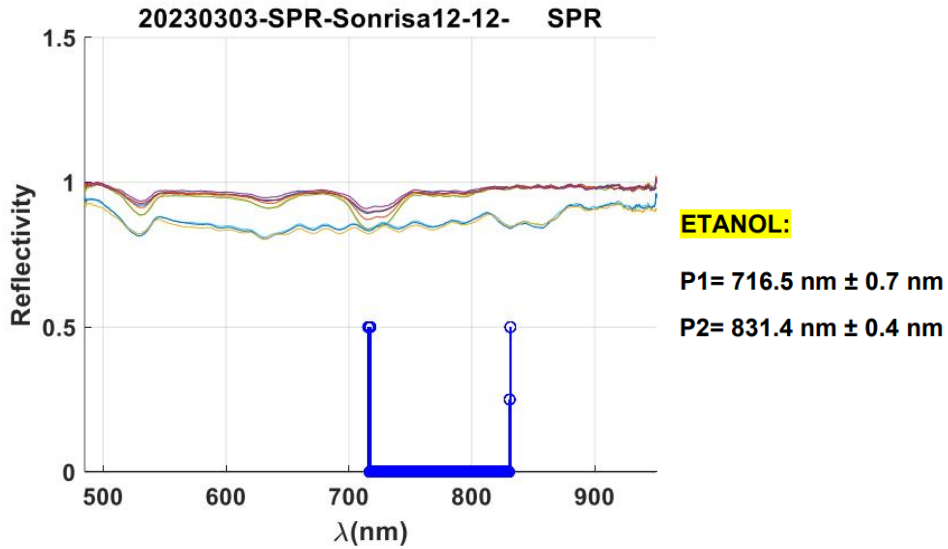
20230303_SPR_Sonrisa12_12_SPEC	Friday	SWEEP - ETANOL
OBLEA S2103: RIE 24" = 30nm + Ti=3nm + Gold=40nm	3-03-2023	Methacrylate COVER
POLARIZATION = 0°		
[X <sub>REF</sub> ,Y <sub>REF</sub> ]=[1.5, 1.5]		
[X <sub>0</sub> ,Y <sub>0</sub> ]=[1.5, 1.5]		
Δx= 0.25	NX= 10	Lx= 2.5
Δy= 0.25	NY= 25	Ly= 6.25
DARK & REF in FLAT GOLD WITH POLARIZATION = 0°		
<ul style="list-style-type: none"> <li>- CHIP 12 SWEEP EN ETANOL</li> <li>- HAY INTERFERENCIAS! (SUSTRATO INCLINADO??)</li> </ul>		



Resonance Wavelength (nm)DEPTH or MAGNITUDE

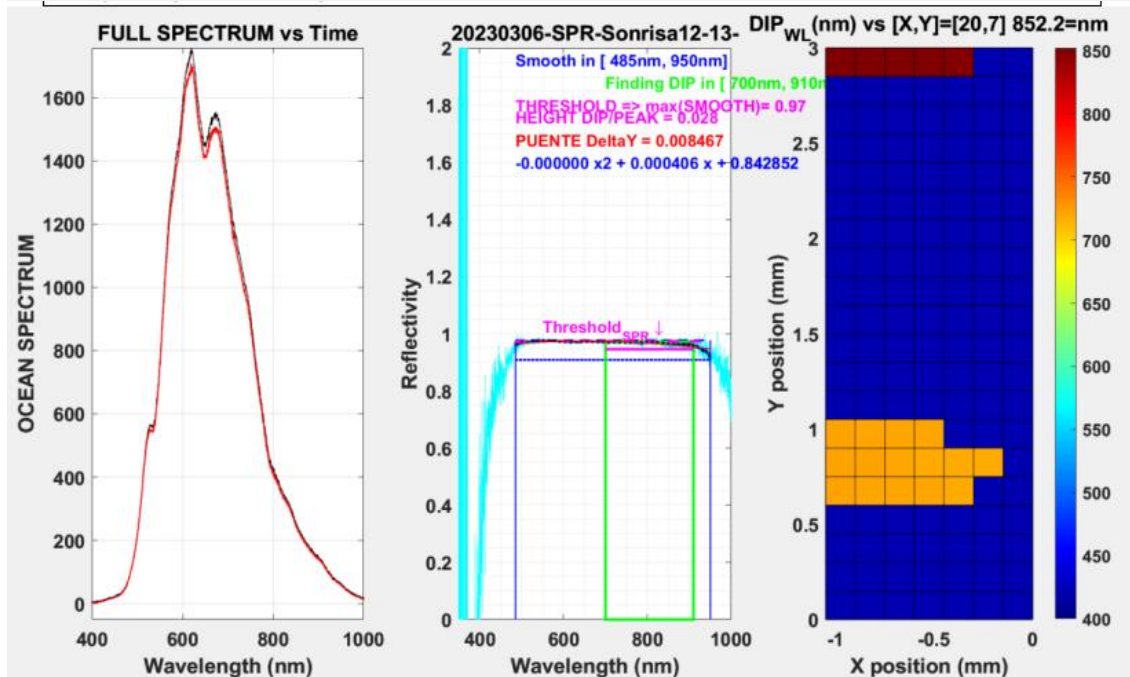


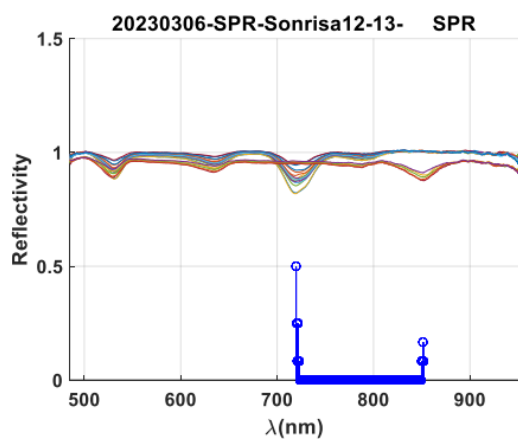
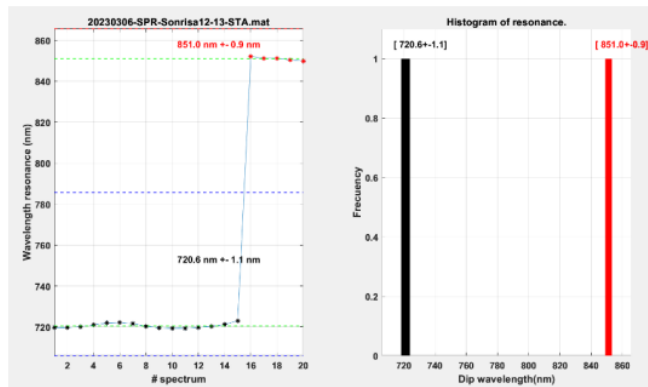
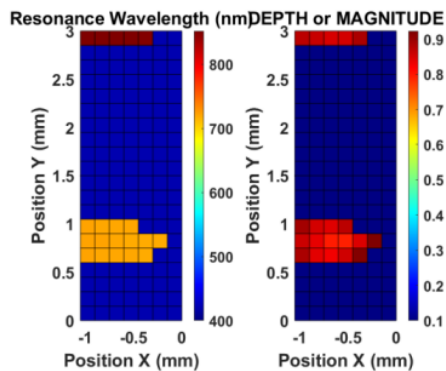




I) EXPERIMENT FROM THE 6TH OF MARCH WITH QUARTZ COVER AND ETHANOL

20230306_SPR_Sonrisa12_13_SPEC	Monday	SWEEP - ETANOL
OBLEA S2103: RIE 24" = 30nm + Ti=3nm + Gold=40nm	06-03-2023	Quartz COVER
POLARIZATION = 0°		
[X <sub>REF</sub> , Y <sub>REF</sub> ] = [1, 1.8]		
[X <sub>0</sub> , Y <sub>0</sub> ] = [1, 1.8]		
$\Delta x = 0.15$	NX= 7	Lx= 1.05
$\Delta y = 0.20$	NY= 20	Ly= 4
DARK & REF in FLAT GOLD WITH POLARIZATION = 0°		
- CHIP 12 SWEEP EN ETANOL		





**ETANOL:**

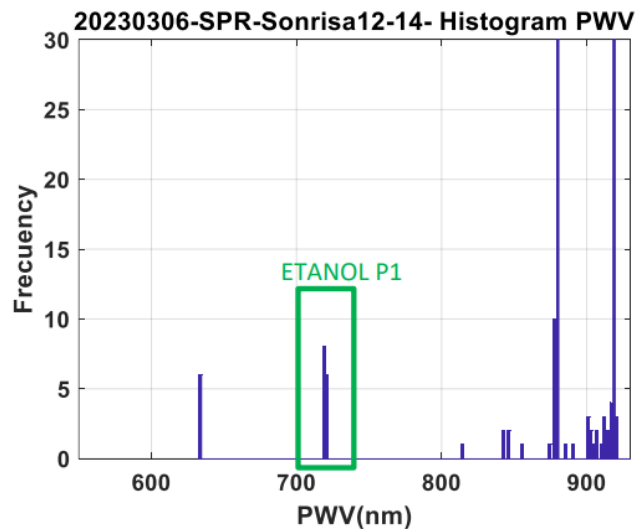
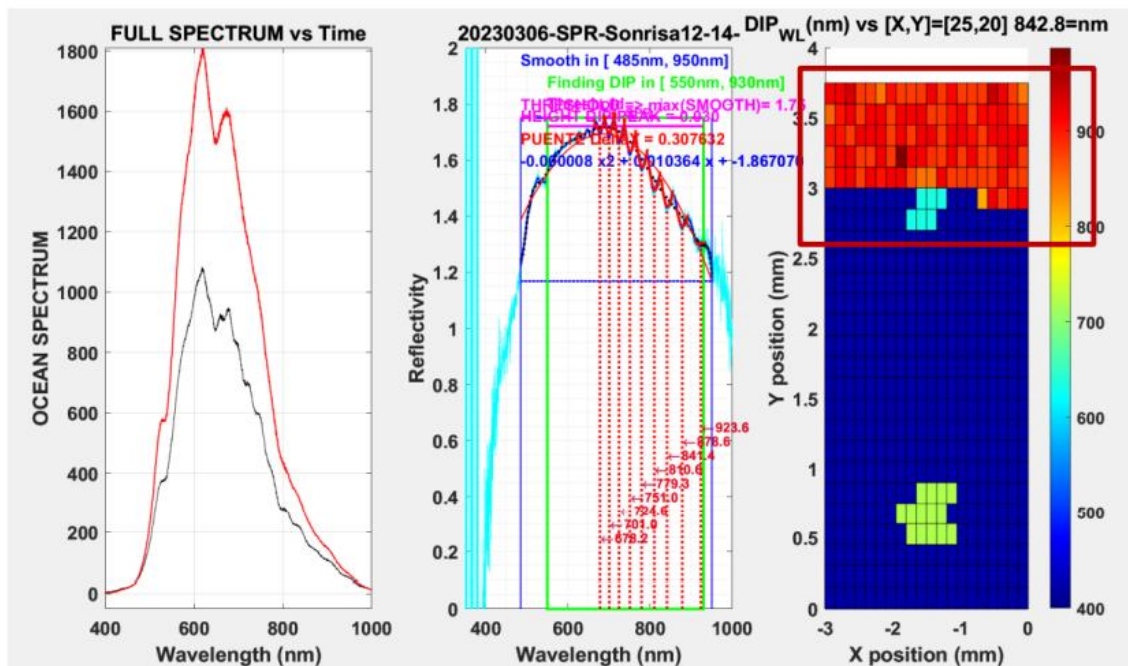
**P1= 720.6 nm ± 1.1 nm**

**P2= 851.0 nm ± 0.9 nm**

## J) EXPERIMENT FROM THE 6TH OF MARCH WITH QUARTZ COVER AND ETHANOL

Due to interference only the measurements for period 500 nm are valid.

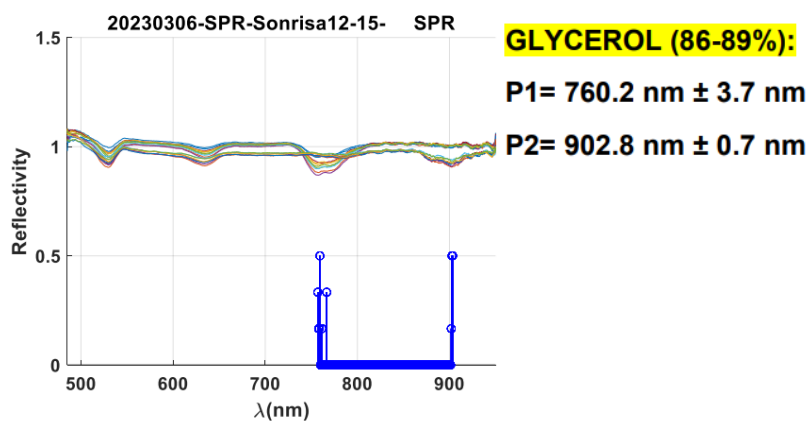
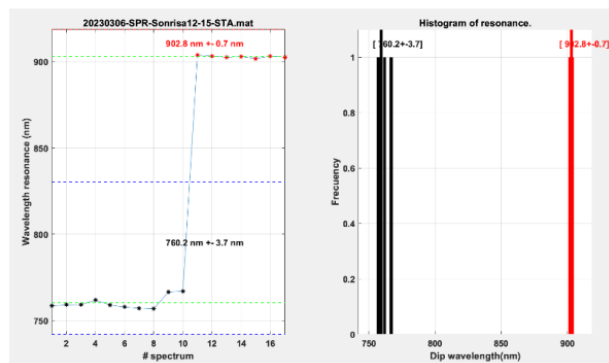
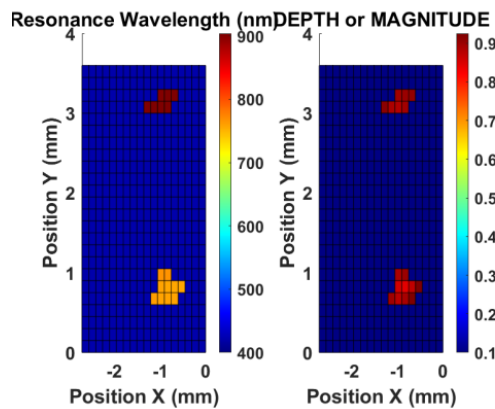
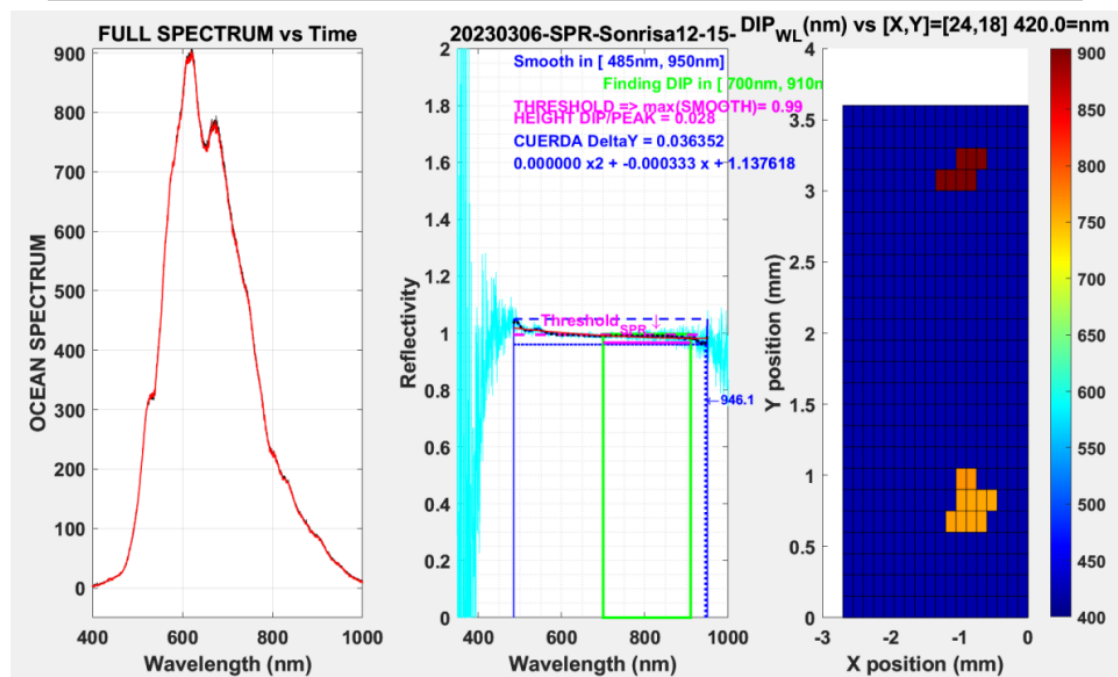
20230306_SPR_Sonrisa12_14_SPEC		Monday	SWEEP – ETANOL
OBLEA S2103: RIE 24" = 30nm + Ti=3nm + Gold=40nm		06-03-2023	Quartz COVER
POLARIZATION = 0°			
[X <sub>REF</sub> ,Y <sub>REF</sub> ]=			
[X <sub>0</sub> ,Y <sub>0</sub> ]=			
Δx=		NX=	Lx=
Δy=		NY=	Ly=
DARK & REF in FLAT GOLD WITH POLARIZATION = 0°			
- CHIP 12 SWEEP EN ETANOL			
- HI HA INTERFERENCIAS!! NOMES ES VALID EL P1=500 nm			



**ETANOL: P1=719nm P2= --- nm**

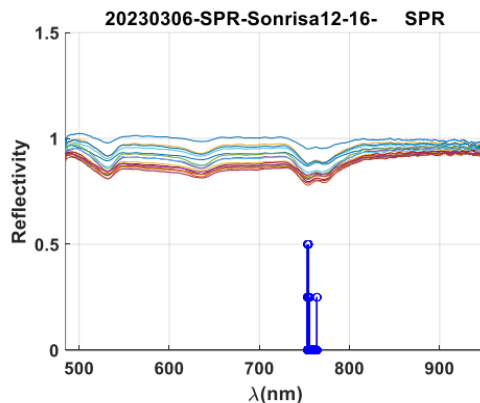
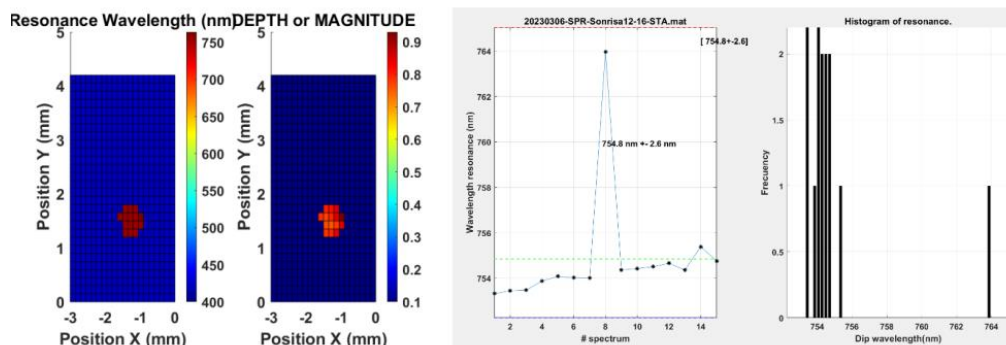
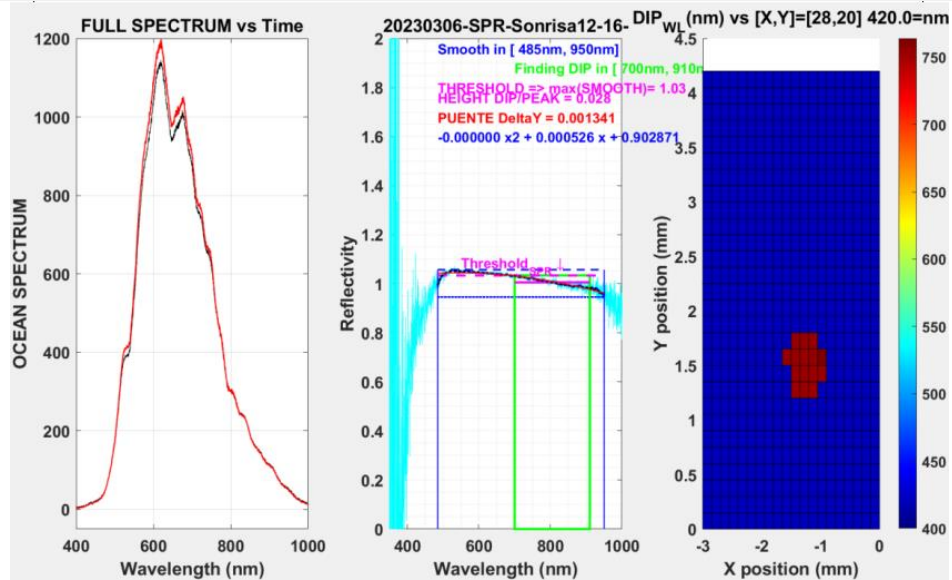
K) EXPERIMENT FROM THE 6TH OF MARCH WITH QUARTZ COVER AND GLYCEROL 86-89%)

20230306_SPR_Sonrisa12_15_SPEC OBLEA S2103: RIE 24" = 30nm + Ti=3nm + Gold=40nm	Monday 06-03-2023	SWEEP – Glycerol (86-89%) Quartz COVER
POLARIZATION = 0°		
[X <sub>REF</sub> , Y <sub>REF</sub> ] = [0.5, 2.3]		
[X <sub>0</sub> , Y <sub>0</sub> ] = [0.5, 2.3]		
Δx= 0.15	NX= 18	Lx= 2.7
Δy= 0.20	NY= 24	Ly= 4.8
DARK & REF in FLAT GOLD WITH POLARIZATION = 0°		
- CHIP 12 SWEEP EN GLYCEROL (86-89%)		
- HI HA INTERFERENCIAS!!		



L) EXPERIMENT FROM THE 6TH OF MARCH WITH QUARTZ COVER AND GLYCEROL 86-89%

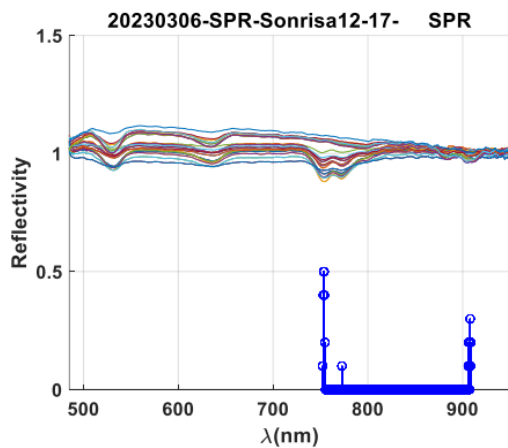
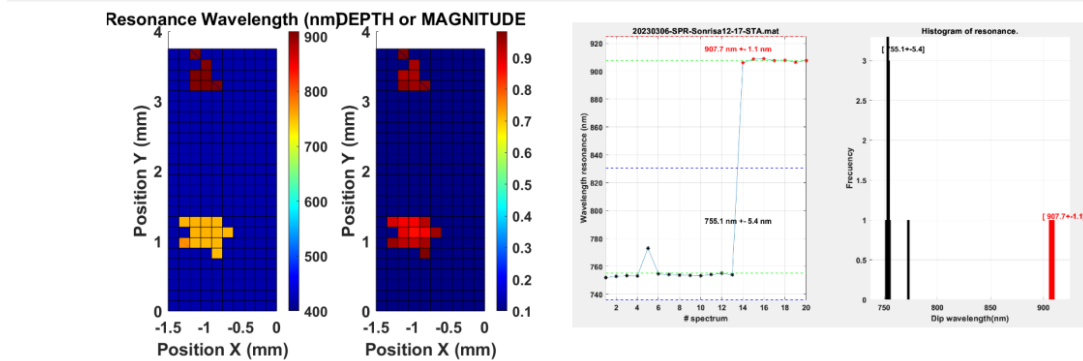
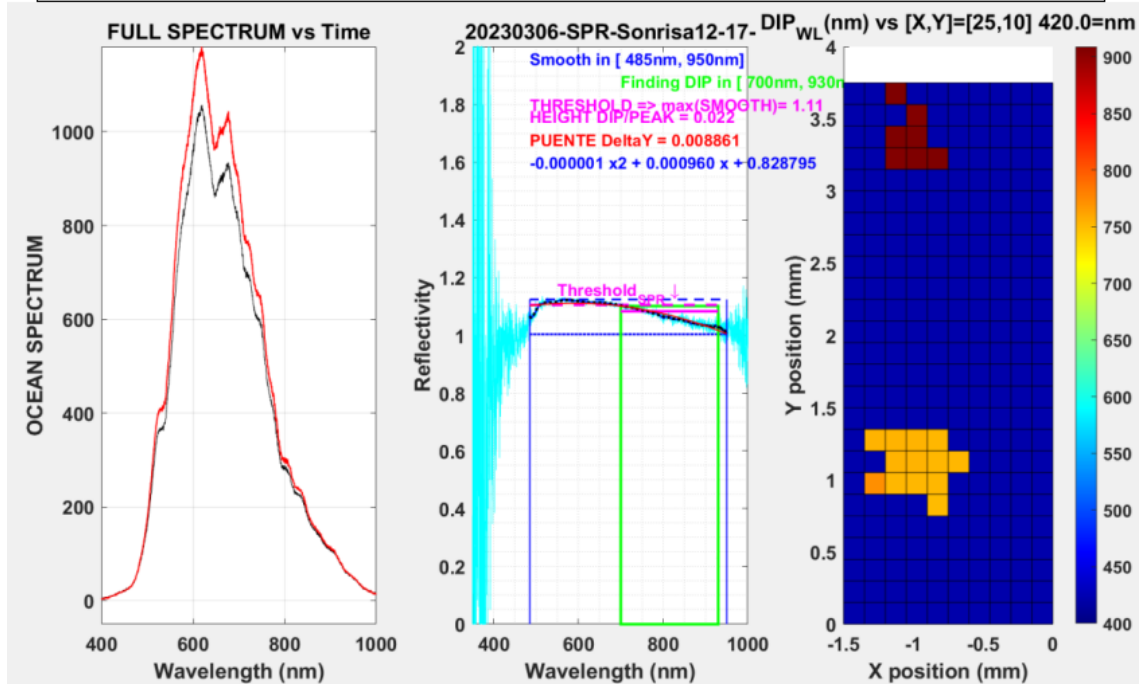
20230306_SPR_Sonrisa12_16_SPEC OBLEA S2103: RIE 24" = 30nm + Ti=3nm + Gold=40nm	Monday 06-03-2023	SWEEP – Glycerol (86-89%) Quartz COVER
POLARIZATION = 0°		
[X <sub>REF</sub> , Y <sub>REF</sub> ] = [1.2, 2] [X <sub>0</sub> , Y <sub>0</sub> ] = [1.2, 2]		
Δx = 0.15	NX = 20	Lx = 3
Δy = 0.15	NY = 28	Ly = 4.2
DARK & REF in FLAT GOLD WITH POLARIZATION = 0°		
<ul style="list-style-type: none"> <li>- CHIP 12 SWEEP EN GLYCEROL (86-89%)</li> <li>- HI HA INTERFERENCIES!!</li> </ul>		



**GLYCEROL (86-89%):**  
**P1 = 754.8 nm ± 2.6 nm**

M) EXPERIMENT FROM THE 6TH OF MARCH WITH QUARTZ COVER AND GLYCEROL 86-89%

20230306_SPR_Sonrisa12_17_SPEC OBLEA S2103: RIE 24" = 30nm + Ti=3nm + Gold=40nm	Monday 06-03-2023	SWEEP – Glycerol (86-89%) Quartz COVER
POLARIZATION = 0°		
[X <sub>REF</sub> , Y <sub>REF</sub> ] = [1.2, 2] [X <sub>0</sub> , Y <sub>0</sub> ] = [1.2, 2]		
Δx = 0.15	NX = 20	Lx = 3
Δy = 0.15	NY = 28	Ly = 4.2
DARK & REF in FLAT GOLD WITH POLARIZATION = 0°		
<ul style="list-style-type: none"> <li>- CHIP 12 SWEEP EN GLYCEROL (86-89%)</li> <li>- HI HA INTERFERENCIAS!!</li> </ul>		



**GLYCEROL (86-89%):**

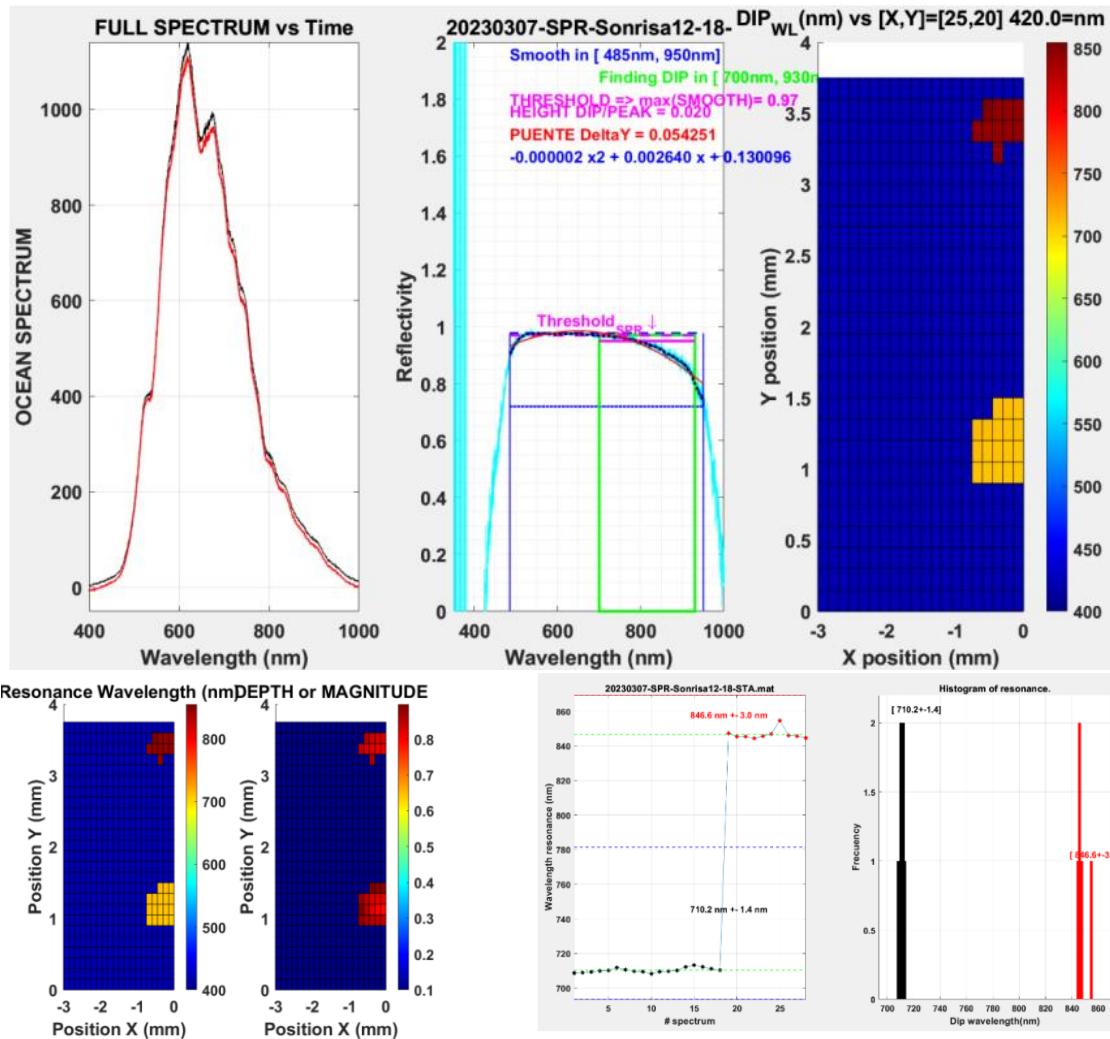
**P1= 755.1 nm ± 5.4 nm**

**P2= 907.7 nm ± 1.1 nm**

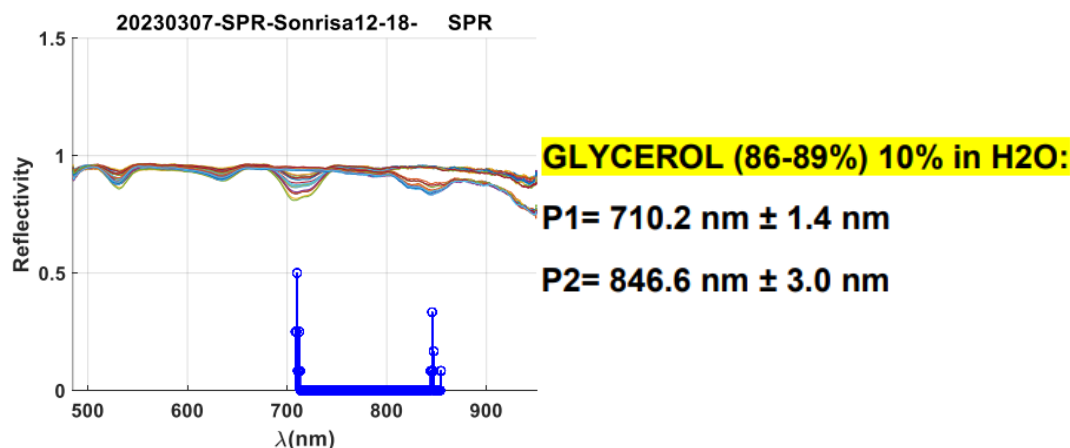


N) EXPERIMENT FROM THE 7TH OF MARCH WITH QUARTZ COVER AND GLYCEROL (86-89%) 10% IN WATER MILLI Q

20230307_SPR_Sonrisa12_18_SPEC OBLEA S2103: RIE 24" = 30nm + Ti=3nm + Gold=40nm	Monday 07-03-2023	SWEEP – Glycerol (86-89%) 10% in H2O Quartz COVER
POLARIZATION = 0°		
[X <sub>REF</sub> , Y <sub>REF</sub> ] = [2, 2] [X <sub>0</sub> , Y <sub>0</sub> ] = [2, 2]		
Δx = 0.1	NX = 20	Lx = 2
Δy = 0.2	NY = 25	Ly = 5
DARK & REF in FLAT GOLD WITH POLARIZATION = 0°		
- CHIP 12 SWEEP EN GLYCEROL (86-89%) 10% in H2O		

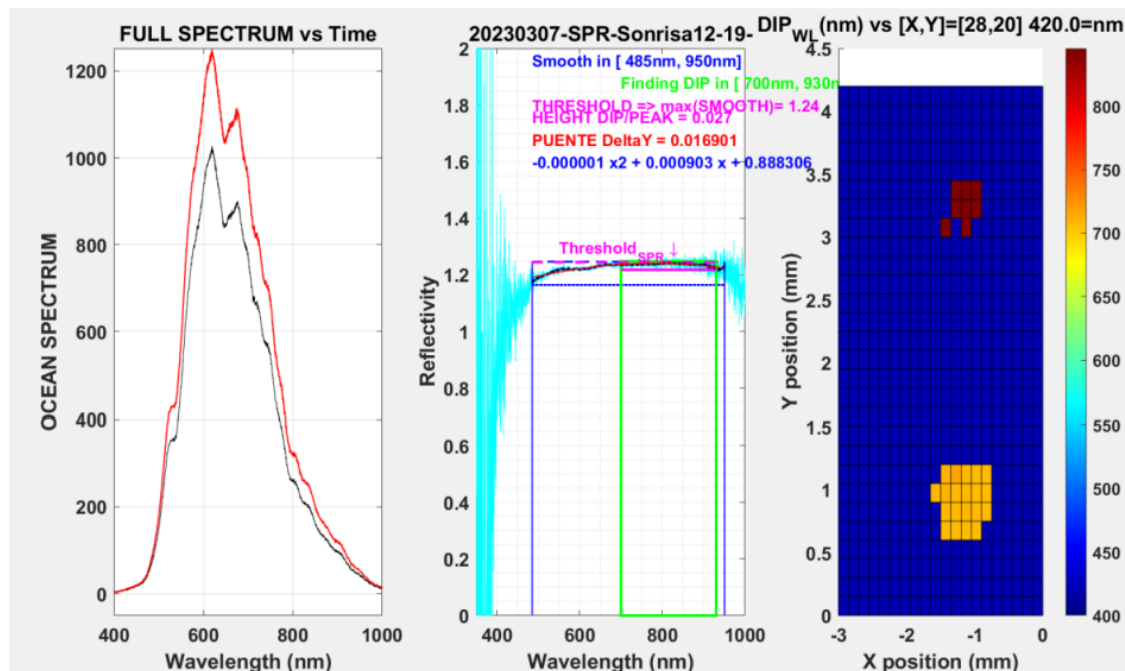


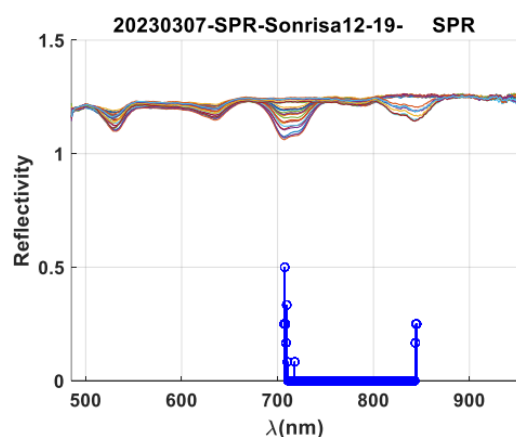
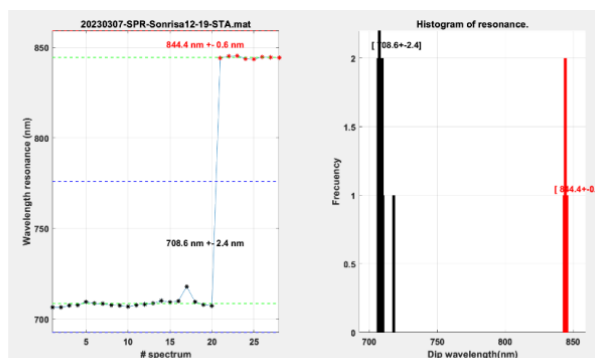
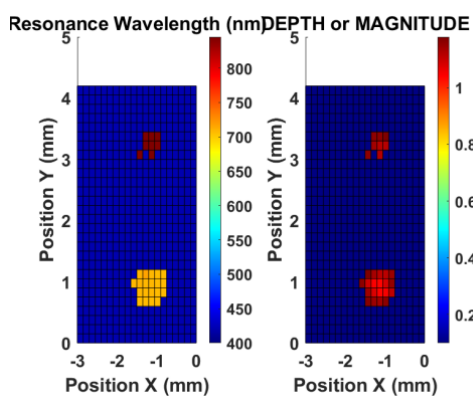




O) EXPERIMENT FROM THE 7TH OF MARCH WITH QUARTZ COVER AND GLYCEROL (86-89%) 10% IN WATER MILLI Q

20230307_SPR_Sonrisa12_19_SPEC OBLEA S2103: RIE 24" = 30nm + Ti=3nm + Gold=40nm	Monday 07-03-2023	SWEEP – Glycerol (86-89%) 10% in H2O Quartz COVER
<b>POLARIZATION = 0°</b>		
[X <sub>REF</sub> , Y <sub>REF</sub> ] = [2, 2] [X <sub>0</sub> , Y <sub>0</sub> ] = [2, 2]		
Δx= 0.1	NX= 20	Lx= 2
Δy= 0.2	NY= 25	Ly= 5
DARK & REF in FLAT GOLD WITH POLARIZATION = 0°		
- CHIP 12 SWEEP EN GLYCEROL (86-89%) 10% in H2O		





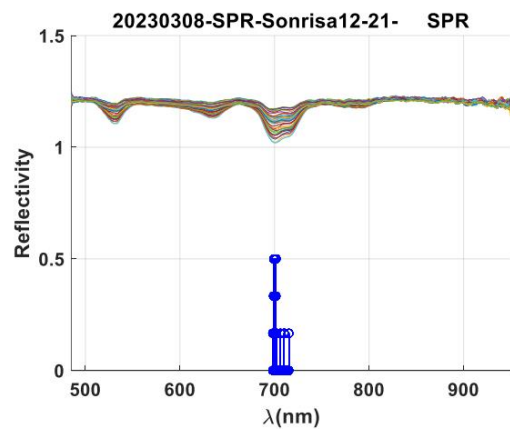
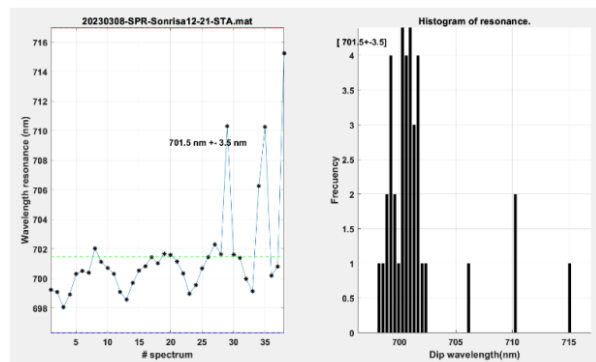
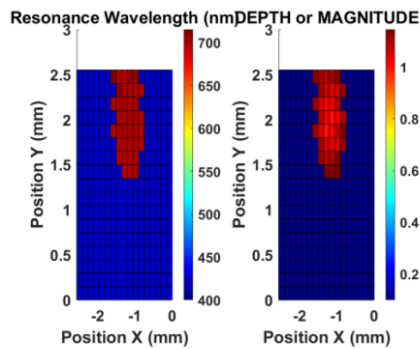
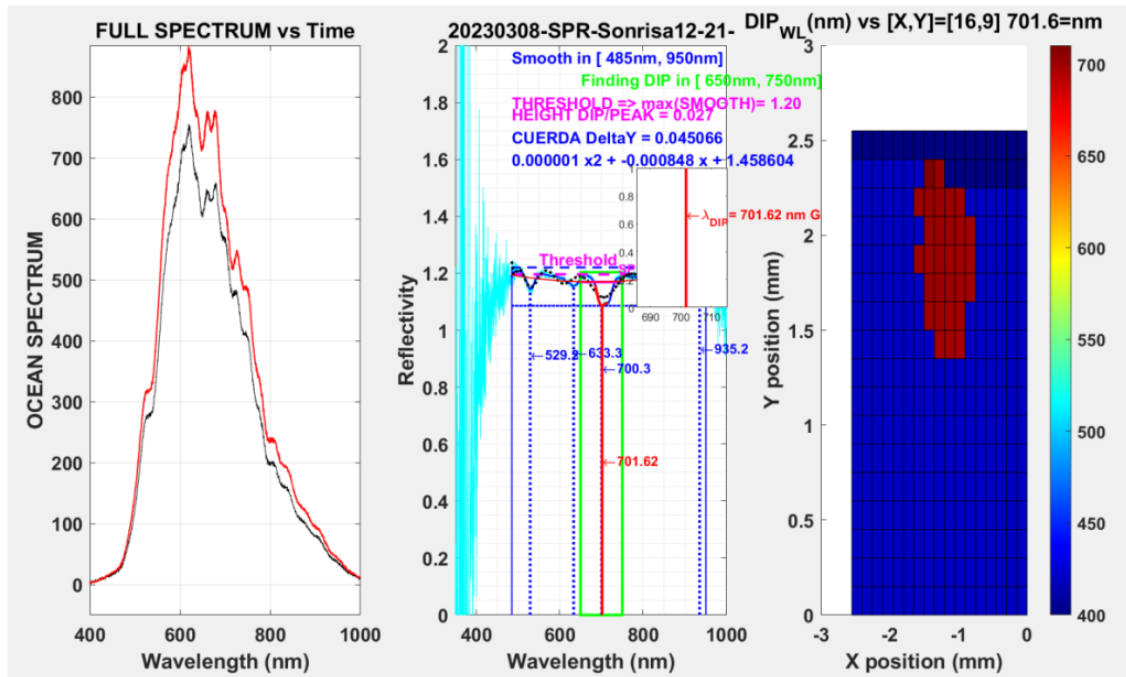
**GLYCEROL (86-89%) 10% in H2O:**

**P1= 708.6 nm ± 2.4 nm**

**P1= 844.4nm ± 0.6 nm**

P) EXPERIMENT FROM THE 8TH OF MARCH WITH QUARTZ COVER AND WATER MILLI Q

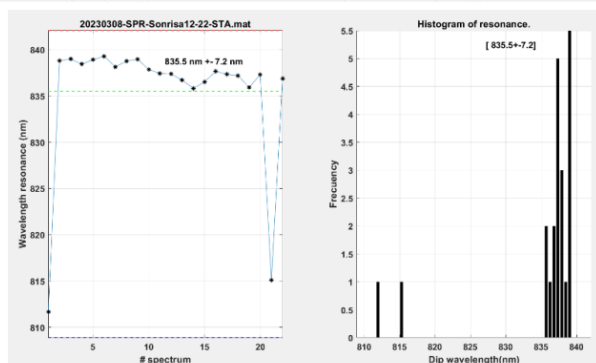
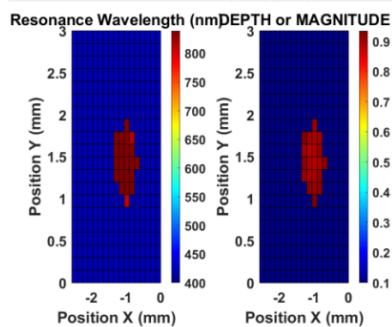
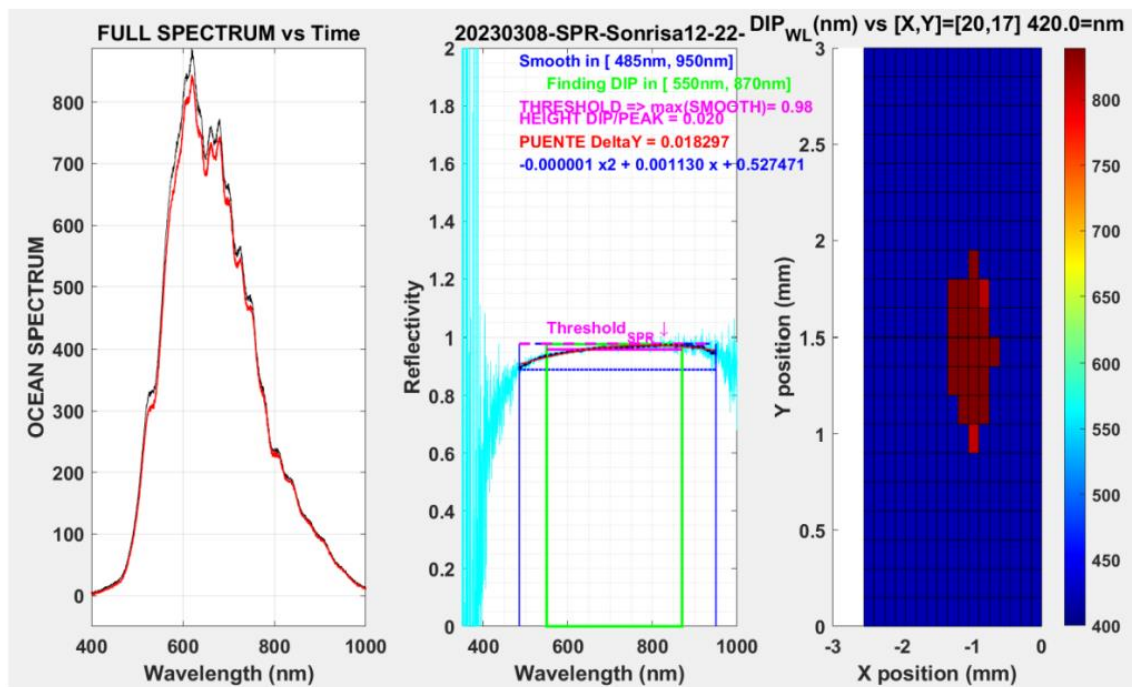
20230308_SPR_Sonrisa12_21_SPEC	Monday	SWEEP – WATER
OBLEA S2103: RIE 24" = 30nm + Ti=3nm + Gold=40nm	08-03-2023	Quartz COVER
POLARIZATION = 0°		
[X <sub>REF</sub> , Y <sub>REF</sub> ] = [0.5, 3.3]		
[X <sub>0</sub> , Y <sub>0</sub> ] = [0.5, 3.3]		
Δx= 0.15	NX= 17	Lx= 2.55
Δy= 0.15	NY= 17	Ly= 2.55
DARK & REF in FLAT GOLD WITH POLARIZATION = 0°		
- CHIP 12 SWEEP EN WATER		
- RASTREO EN P1=500 nm		

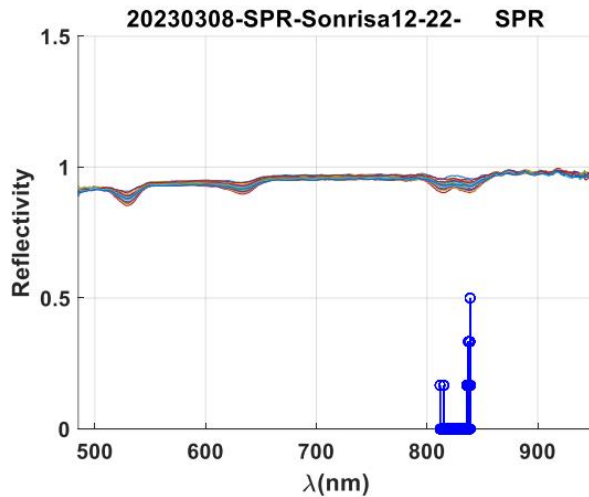


**WATER:** P1= 701.5 nm  $\pm$  3.5 nm

Q) EXPERIMENT FROM THE 8TH OF MARCH WITH QUARTZ COVER AND WATER MILLI Q

20230308_SPR_Sonrisa12_22_SPEC OBLEA S2103: RIE 24'' = 30nm + Ti=3nm + Gold=40nm		Monday 08-03-2023	SWEEP – WATER Quartz COVER
POLARIZATION = 0°			
[X <sub>REF</sub> ,Y <sub>REF</sub> ]=[0.5 , 3.3] [X <sub>0</sub> ,Y <sub>0</sub> ]=[0.5 , 6.5]			
Δx= 0.15		NX= 17	Lx= 2.55
Δy= 0.1		NY= 20	Ly= 2.55
DARK & REF in FLAT GOLD WITH POLARIZATION = 0°			
<div>- CHIP 12 SWEEP EN WATER</div> <div>- RASTREO EN P2=600 nm</div> <div>- Los picos de rojo claro son el primer pico del “doble pico”. Los del rojo oscuro son el segundo pico del “doble pico”.</div>			

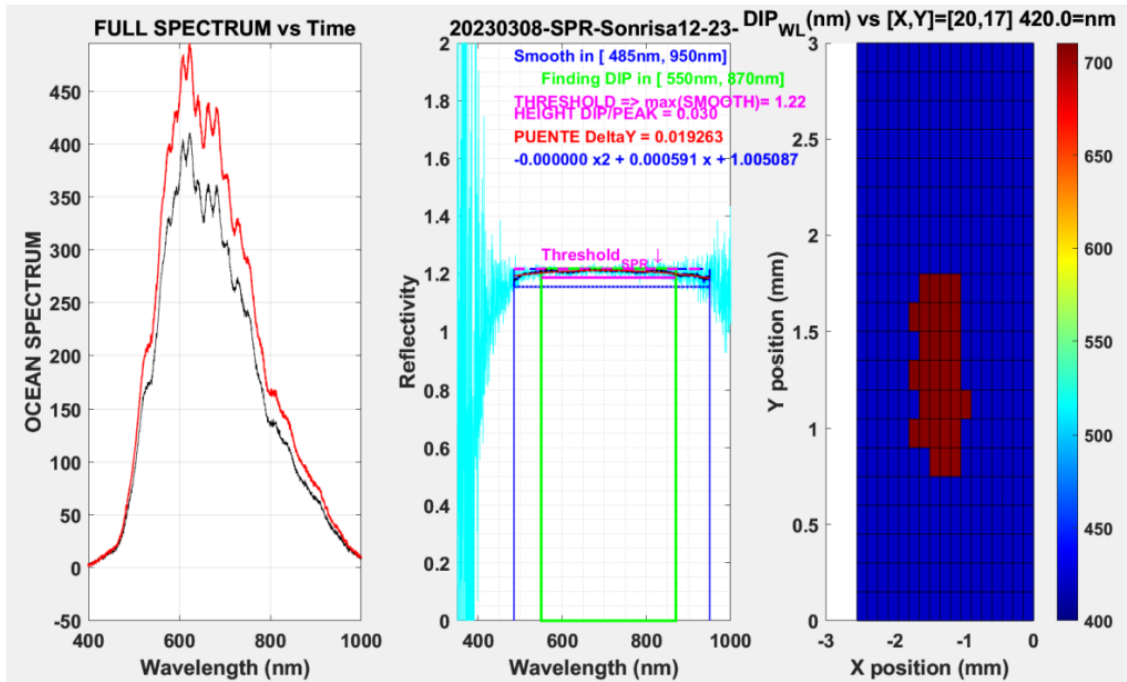


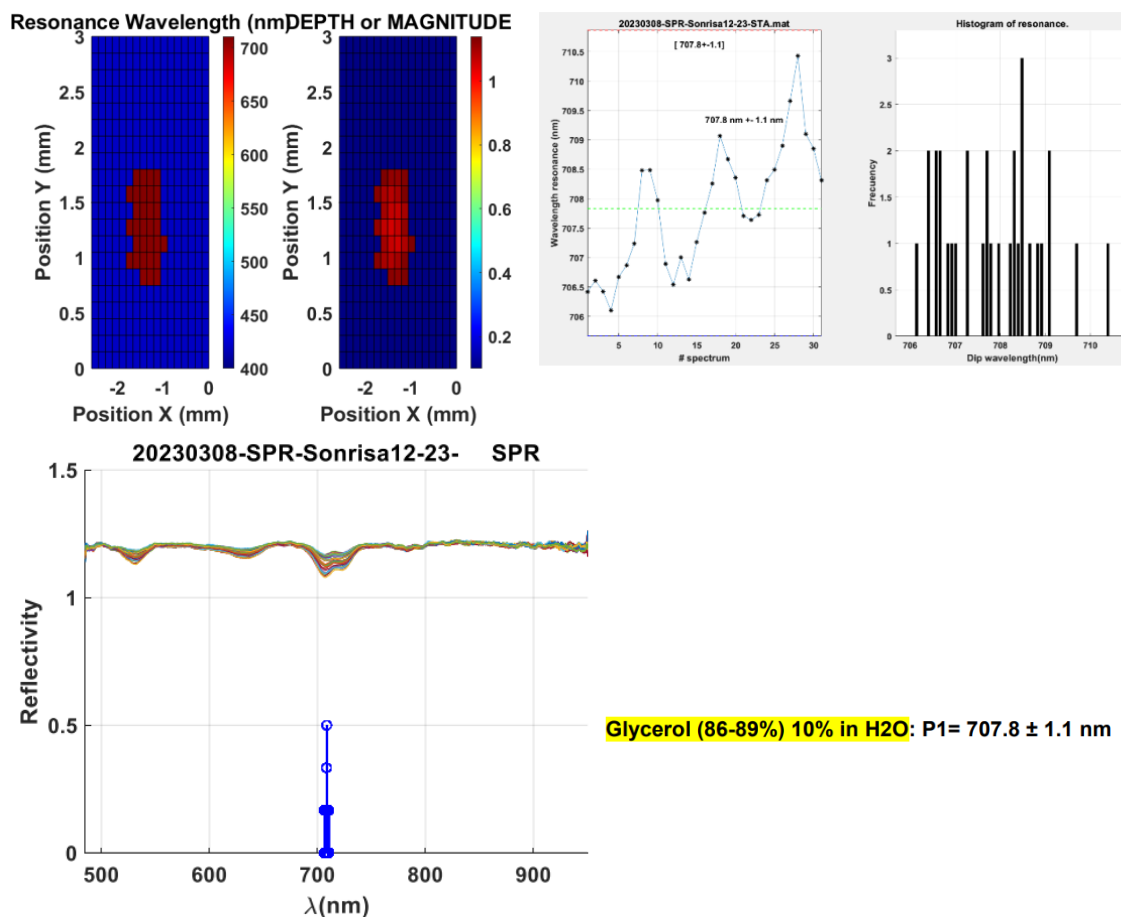


**WATER:** P2= 835.5 nm  $\pm$  7.2 nm

R) EXPERIMENT FROM THE 8TH OF MARCH WITH QUARTZ COVER AND GLYCEROL (86-89%) 10% IN WATER MILLI Q

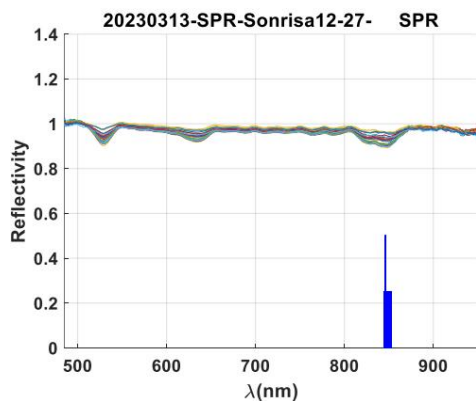
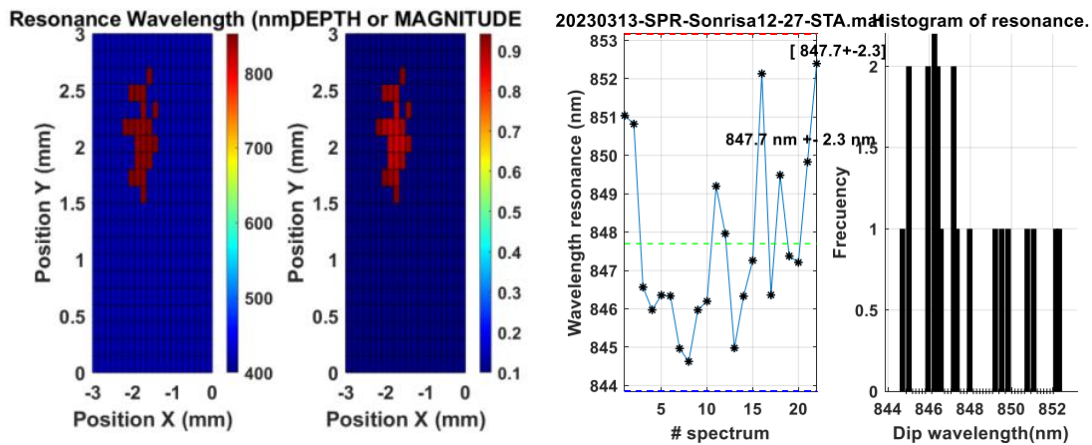
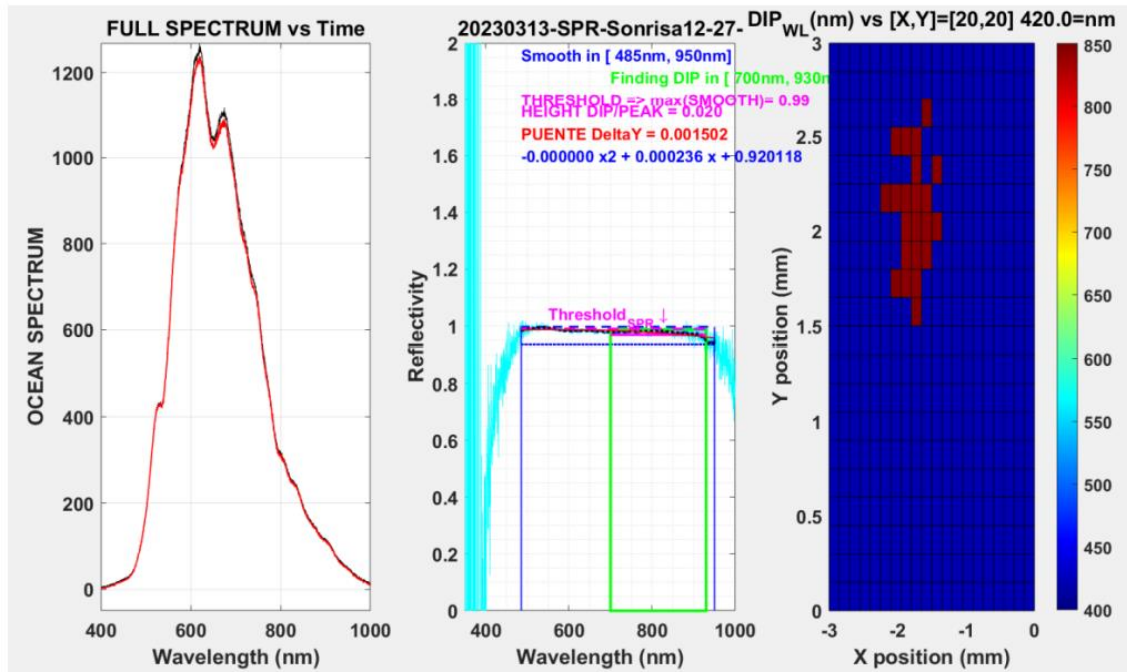
20230308_SPR_Sonrisa12_23_SPEC OBLEA S2103: RIE 24" = 30nm + Ti=3nm + Gold=40nm	Monday 08-03-2023	SWEEP - Glycerol (86-89%) 10% in H2O Quartz COVER
<b>POLARIZATION = 0°</b>		
[X <sub>REF</sub> , Y <sub>REF</sub> ] = [1, 4] [X <sub>0</sub> , Y <sub>0</sub> ] = [1, 4]		
$\Delta x = 0.15$	NX= 17	Lx= 2.55
$\Delta y = 0.1$	NY= 20	Ly= 2.55
<b>DARK &amp; REF in FLAT GOLD WITH POLARIZATION = 0°</b>		
<ul style="list-style-type: none"> <li>- CHIP 12 SWEEP EN WATER</li> <li>- RASTREO EN P1=500 nm</li> </ul>		





S) EXPERIMENT FROM THE 13TH OF MARCH WITH QUARTZ COVER AND GLYCEROL (86-89%) 10% IN WATER MILLI Q

20230313_SPR_Sonrisa12_27_SPEC OBLEA S2103: RIE 24" = 30nm + Ti=3nm + Gold=40nm	Monday 13-03-2023	SWEEP – Glycerol (86-89%) 10% in H <sub>2</sub> O Quartz COVER
<b>POLARIZATION = 0°</b>		
[X <sub>REF</sub> , Y <sub>REF</sub> ] = [0, 4] [X <sub>0</sub> , Y <sub>0</sub> ] = [1, 4.5]		
Δx= 0.15	NX= 20	Lx= 3
Δy= 0.1	NY= 20	Ly= 2
<b>DARK &amp; REF in FLAT GOLD WITH POLARIZATION = 0°</b>		
<b>- CHIP 12 SWEEP EN GLYCEROL (86-89%) 10% in H<sub>2</sub>O</b>		

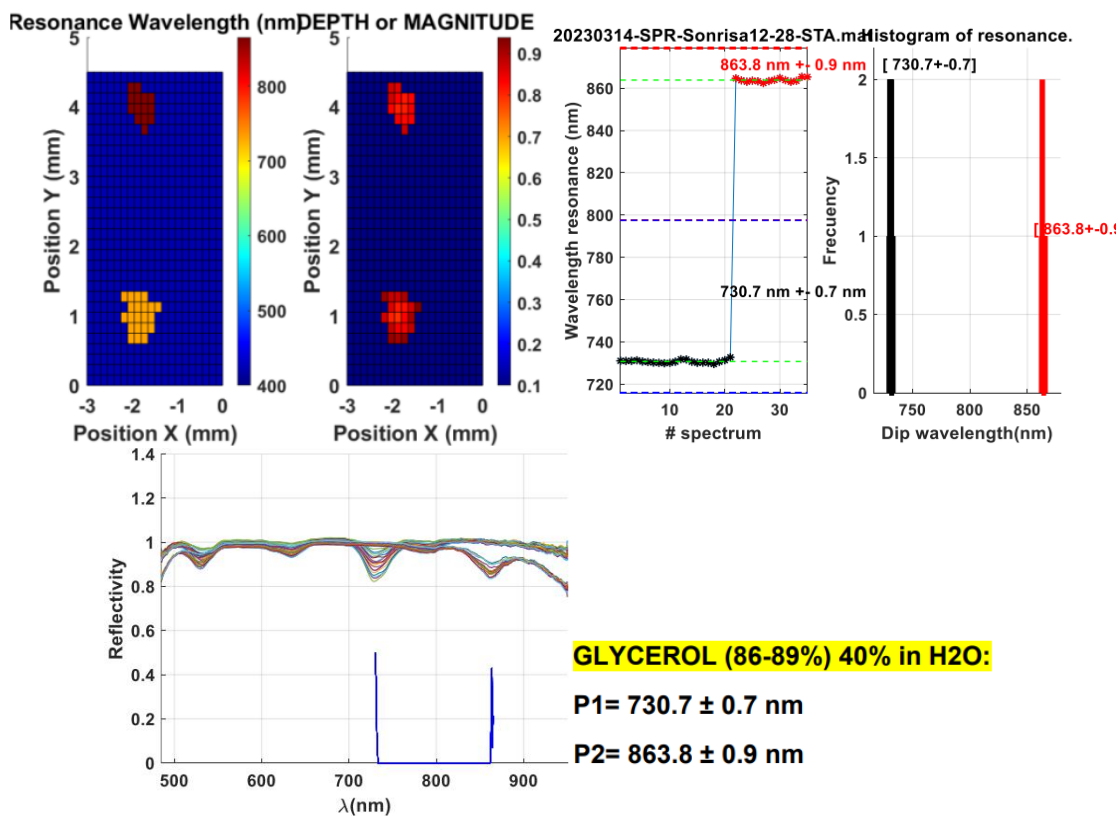
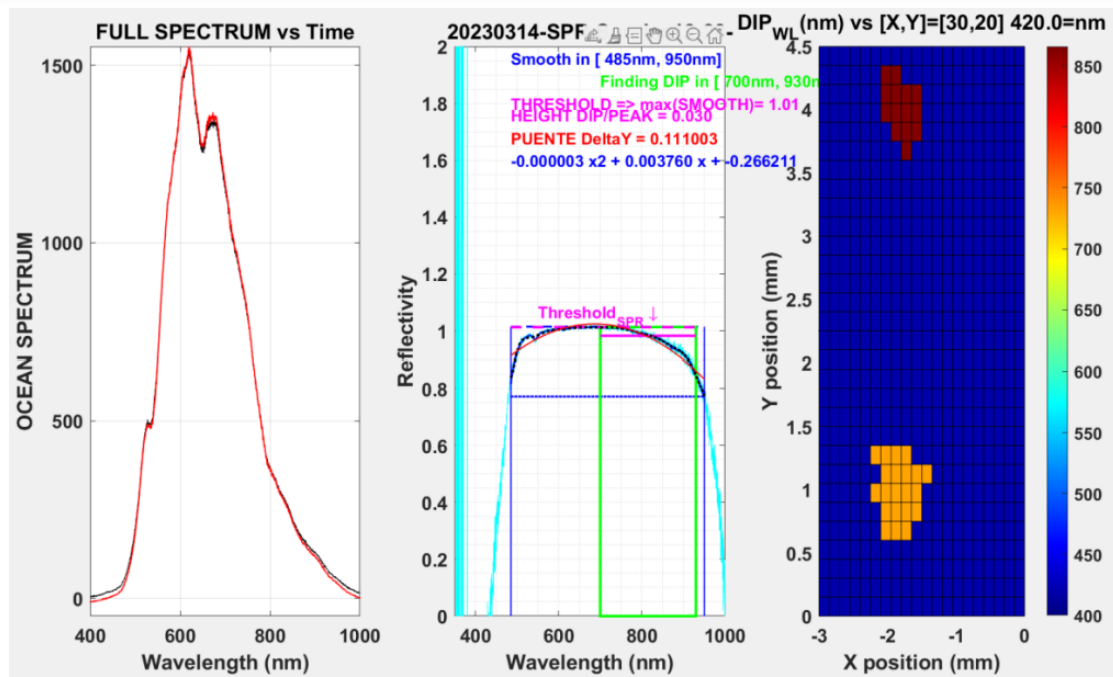


**GLYCEROL (86-89%) 10% in H2O:**  
**P2= 847.7  $\pm$  2.3 nm**

T) EXPERIMENT FROM THE 14TH OF MARCH WITH QUARTZ COVER AND GLYCEROL (86-89%) 40% IN WATER MILLI Q

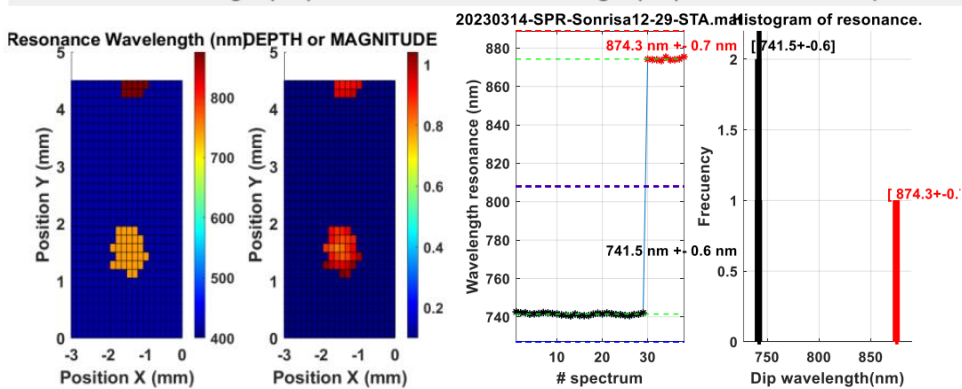
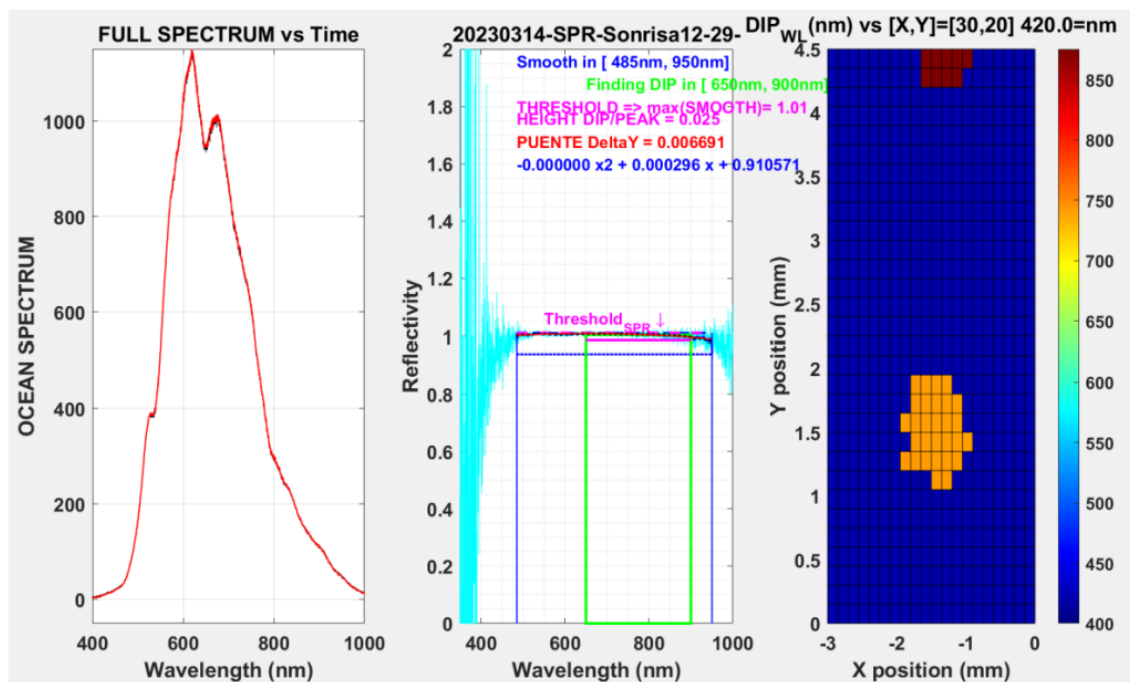


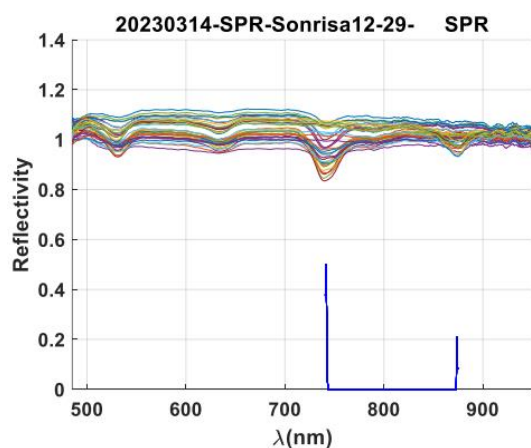
20230314_SPR_Sonrisa12_28_SPEC OBLEA S2103: RIE 24'' = 30nm + Ti=3nm + Gold=40nm	Monday 14-03-2023	SWEEP – Glycerol (86-89%) 40% in H2O Quartz COVER
POLARIZATION = 0°		
[X <sub>REF</sub> ,Y <sub>REF</sub> ]= [1 , 2] [X <sub>0</sub> ,Y <sub>0</sub> ]= [1 , 2]		
Δx= 0.15	NX= 20	Lx= 3
Δy= 0.15	NY= 30	Ly= 4.5
DARK & REF in FLAT GOLD WITH POLARIZATION = 0°		
- CHIP 12 SWEEP EN GLYCEROL (86-89%) 40% in H2O		



U) EXPERIMENT FROM THE 14TH OF MARCH WITH QUARTZ COVER AND GLYCEROL (86-89%) 60% IN WATER MILLI Q

20230314_SPR_Sonrisa12_29_SPEC OBLEA S2103: RIE 24" = 30nm + Ti=3nm + Gold=40nm	Monday 14-03-2023	SWEEP – Glycerol (86-89%) 60% in H2O Quartz COVER
POLARIZATION = 0°		
[X <sub>REF</sub> , Y <sub>REF</sub> ] = [1, 2] [X <sub>0</sub> , Y <sub>0</sub> ] = [1, 2]		
Δx = 0.15	NX = 20	Lx = 3
Δy = 0.15	NY = 30	Ly = 4.5
DARK & REF in FLAT GOLD WITH POLARIZATION = 0°		
- CHIP 12 SWEEP EN GLYCEROL (86-89%) 60% in H2O		





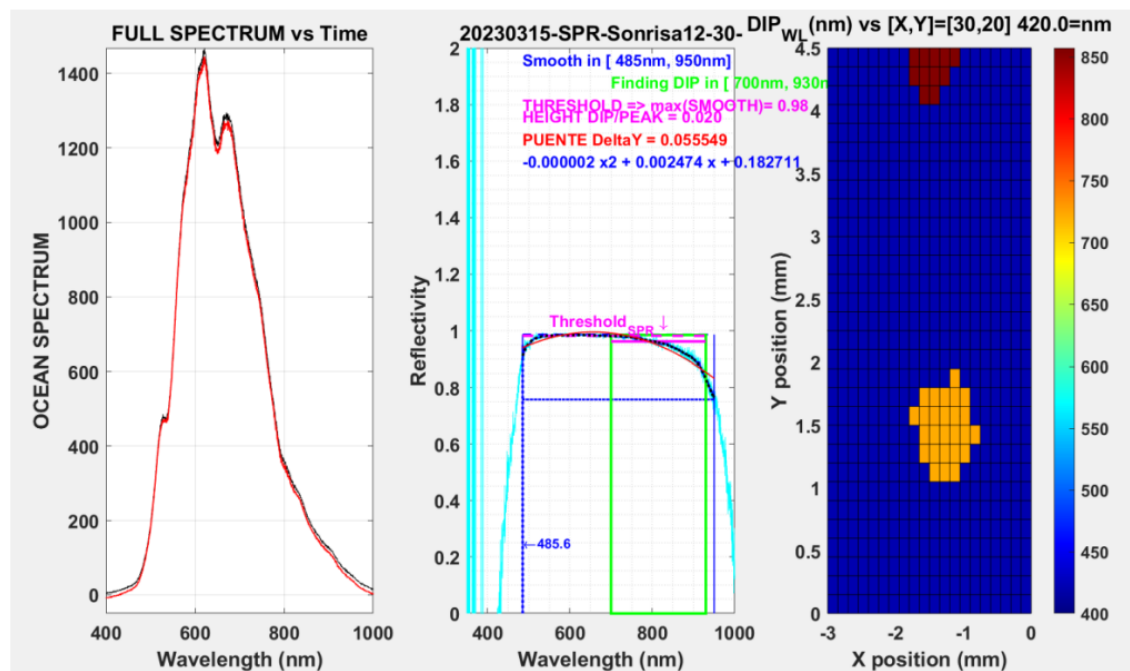
**GLYCEROL (86-89%) 60% in H2O:**

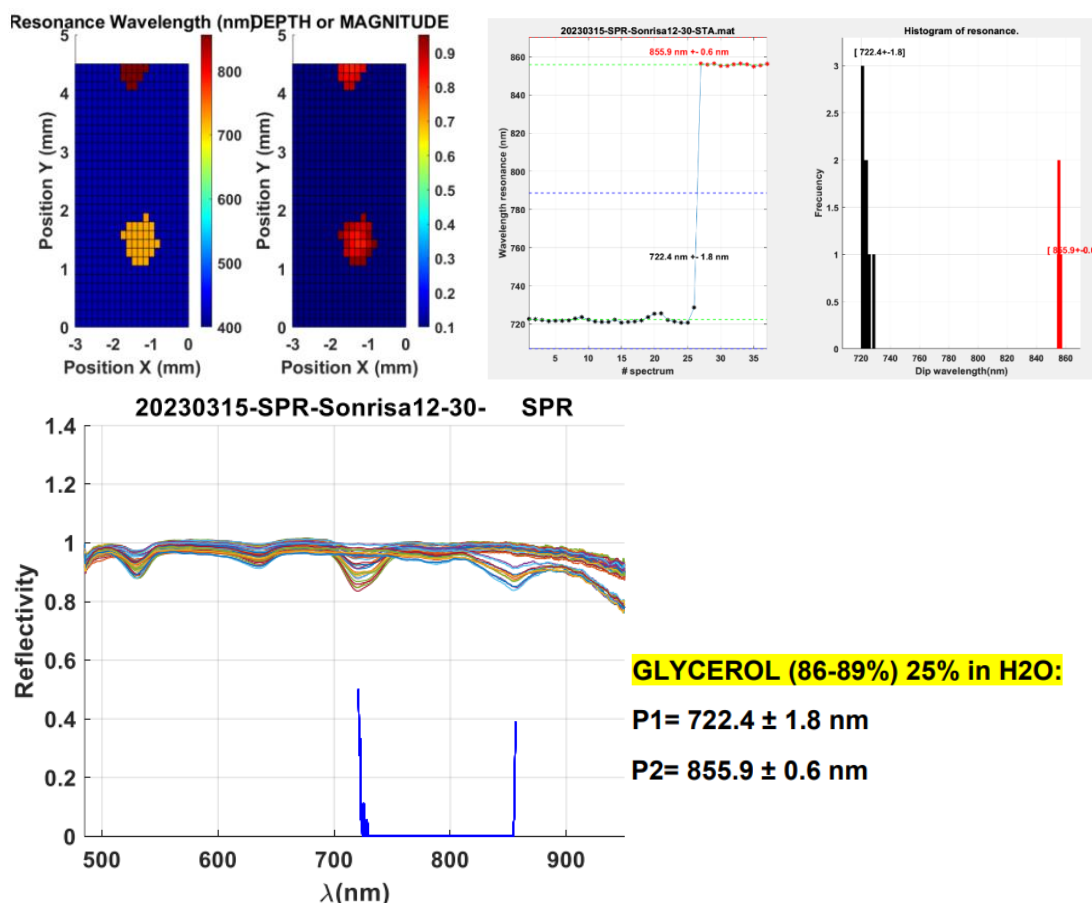
$P1 = 741.5 \pm 0.6 \text{ nm}$

$P2 = 874.3 \pm 0.7 \text{ nm}$

V) EXPERIMENT FROM THE 15TH OF MARCH WITH QUARTZ COVER AND GLYCEROL (86-89%) 25% IN WATER MILLI Q

20230315_SPR_Sonrisa12_30_SPEC OBLEA S2103: RIE 24" = 30nm + Ti=3nm + Gold=40nm	Monday 15-03-2023	SWEEP - Glycerol (86-89%) 25% in H2O Quartz COVER
POLARIZATION = 0°		
$[X_{\text{REF}}, Y_{\text{REF}}] = [1, 2]$ $[X_0, Y_0] = [1, 2]$		
$\Delta x = 0.15$	$NX = 20$	$Lx = 3$
$\Delta y = 0.15$	$NY = 30$	$Ly = 4.5$
DARK & REF in FLAT GOLD WITH POLARIZATION = 0°		
- CHIP 12 SWEEP EN GLYCEROL (86-89%) 25% in H2O		





### ANNEX 3: FLOW PUMP RATE STUDY

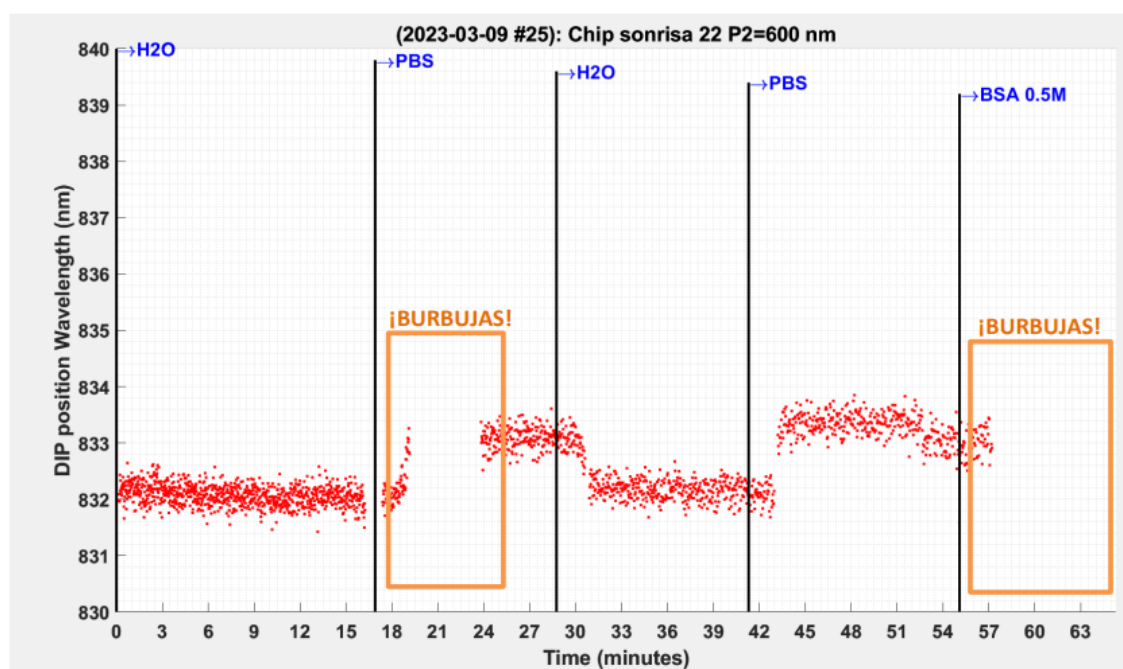
The analysis of the flow pump rate is important because in some experiments there are low volumes of substances, and they must be infused at low velocities without producing air bubbles. This is the reason why the minimum flow rate that doesn't lead to the high presence of bubbles must be found.

The flow pump used is called NE-300 Just Infusion™ Syringe Pump. The diameter of the syringe, which is connected through a thin tube to the inlet of the microchip, is 4.78 mm, and this value must be introduced in the machine. The flow pump units are rpm however the equivalence to ml/min is found experimentally, 2.5 rpm are 0.1 ml/min. The experiment to study the flow pump rate was performed the 9th of March with CHIP 22 at the period of 600 nm. It starts by adding H<sub>2</sub>O and PBS at 0.05 ml/min. This rate is too low and leads to a high formation of bubbles, as seen in figure K. The same cycle of H<sub>2</sub>O and PBS is repeated but the velocity of infusion is doubled to 0.1 ml/min and bubbles are not formed. However, BSA of 0.5 M is introduced right after at a very low rate, 0.03 ml/min, and a huge air bubble is formed again. Other flow rates (seen in Table K) are tried, and it is concluded that for flow rates smaller than 0.1 ml/min the presence of bubbles is highly probable.

Compound	Time (min)	Volume (ml)	Velocity (ml/min)
H <sub>2</sub> O	10 min	0,5 ml	0,05 ml/min
PBS	10 min	0,5 ml	0,05 ml/min
H <sub>2</sub> O	10 min	1 ml	0,1 ml/min
PBS	10 min	1 ml	0,1 ml/min

BSA 0.5M	30 min	1 ml	0,03 ml/ min
PBS	15 min	1 ml	0,067 ml/min
BSA 1M	30 min	1 ml	0,03 ml/ min
PBS	15 min	1 ml	0,067 ml/min
BSA 1,5 M	30 min	1 ml	0,03 ml/ min
PBS	15 min	1 ml	0,067 ml/min

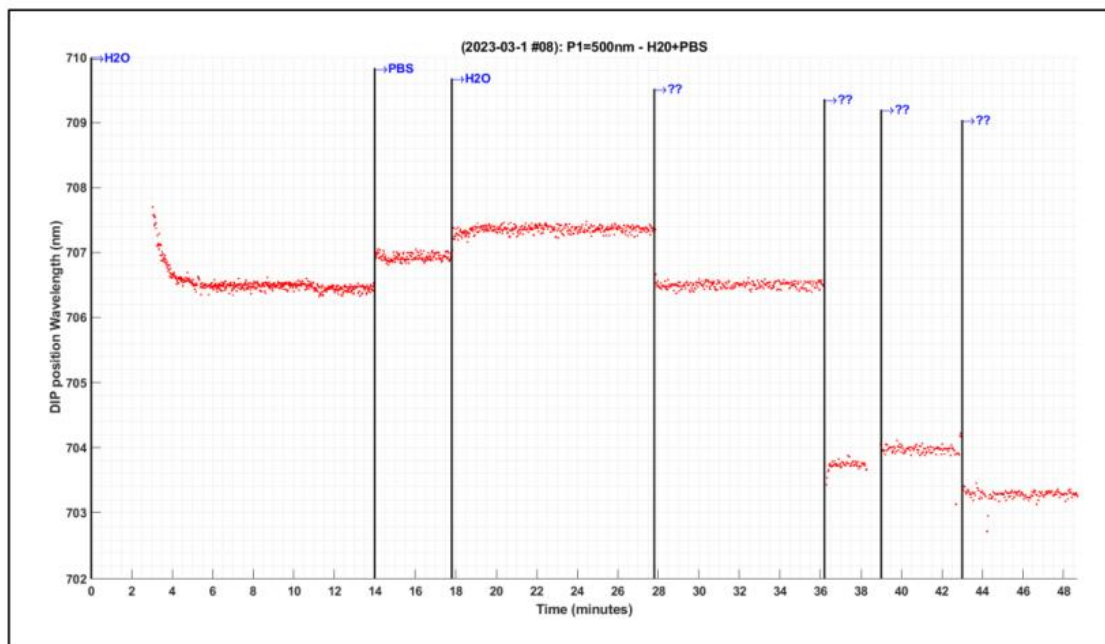
20230309_SPR_Sonrisa22_25_TIME	Thursday 09-03-2023	TIME CHIP 22 CON FLUIDICA
OBLEA S2103: RIE 24" = 30nm + Ti=3nm + Gold=40nm		
POLARIZATION = 0°		
[X <sub>REF</sub> , Y <sub>REF</sub> ] = [1, 2] in H2O		
P2= 600 nm [X <sub>0</sub> , Y <sub>0</sub> ] = [3.65, 3.35]		
DARK & REF in FLAT GOLD WITH POLARIZATION = 0°		
<ul style="list-style-type: none"> <li>- CHIP 22</li> <li>- INLET conectado a SYRINGEPUMP (φ = 4,78mm)</li> </ul>		



## ANNEX 4: INITIAL EXPERIMENTS

### A) EXPERIMENT FROM THE 2ND OF MARCH WITH CYCLES OF H2O AND PBS

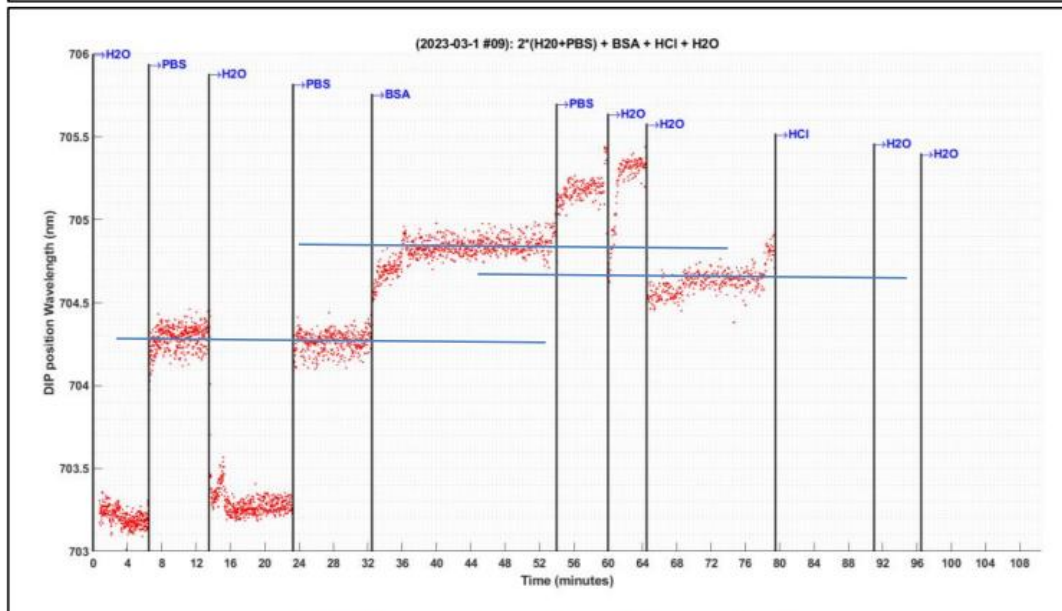
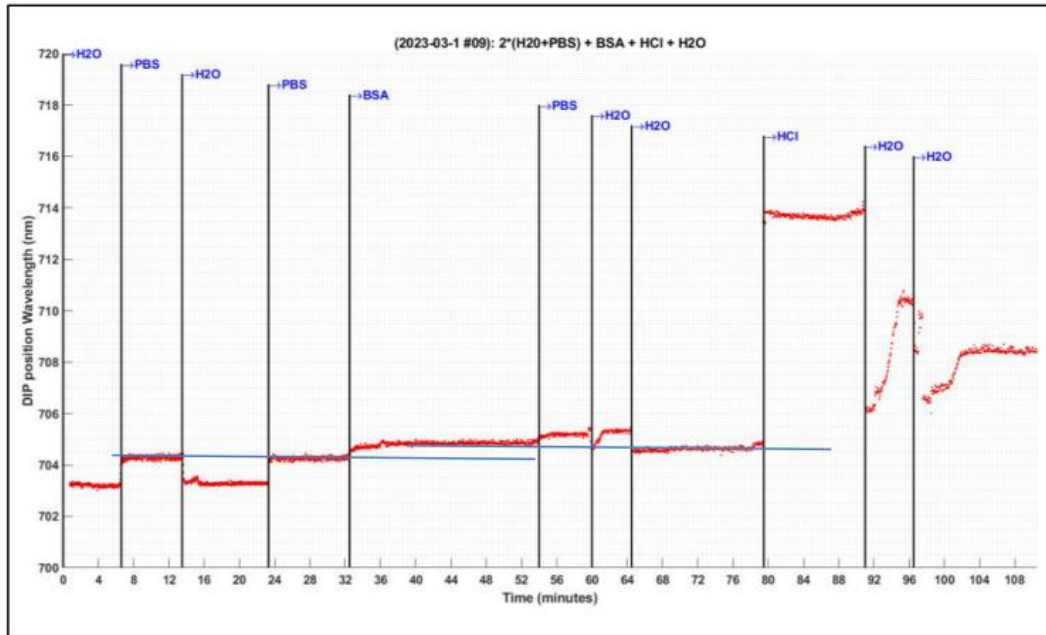
20230302_SPR_Sonrisa34_08_TIME	Wednesday 2-03-2023	H2O+PBS Fluidics
OBLEA S2103: RIE 24" = 30nm + Ti=3nm + Gold=40nm		
POLARIZATION = 0°		
[X <sub>REF</sub> , Y <sub>REF</sub> ] = [0mm, 0mm]		
[X <sub>0</sub> , Y <sub>0</sub> ] = [1mm, 1mm]		
DARK & REF in FLAT GOLD WITH POLARIZATION = 0°		
<ul style="list-style-type: none"> <li>- La medida dinámica se realiza con la red de difracción de P1=500nm.</li> </ul>		



B) EXPERIMENT FROM THE 1ST OF MARCH WITH CYCLES OF H2O AND PBS AND BSA. REGENERATION WITH HCL.

20230302_SPR_Sonrisa34_09_TIME OBLEA S2103: RIE 24" = 30nm + Ti=3nm + Gold=40nm	Thursday 1-03-2023	H2O+PBS+BSA+HCl. Fluidics
POLARIZATION = 0°		
[X <sub>REF</sub> , Y <sub>REF</sub> ] = [0mm, 0mm] [X <sub>0</sub> , Y <sub>0</sub> ] = [1mm, 1mm]		
DARK & REF in FLAT GOLD WITH POLARIZATION = 0° La medida dinámica se realiza con la red de difracción de P1=500nm.		
<ul style="list-style-type: none"> <li>- t=32min. Se inyecta BSA. Hay un incremento en el índice de refracción y una cierta dinámica más lenta que en la inyección de los líquidos.</li> <li>- REALIZAR LOS EXPERIMENTOS CON LA BOMBA A VELOCIDAD CONSTANTE. ASÍ PODRIAMOS CONTROLAR MEJOR EL VACIADO Y RENOVACION DE LO LIQUIDOS EN LA MICROCAMARA.</li> <li>- t=54min. Se inyecta PBS 50%/50% y la señal se incrementa en lugar de disminuir ligeramente. ¿Esto es resultado de que el BSA se adherido a la superficie de oro?</li> <li>- t=60min. 1ª limpieza con H2O. Hay una fuerte disminución inicial y un nuevo incremento.</li> <li>- t=64min. 2ª limpieza con H2O. Parece que la señal si disminuye.</li> <li>- t=80min. Inyectamos HCl pensando que se podría REGENERAR LA SUPERFICE DE ORO. Hay un fuerte incremento debido al índice de refracción del HCl.</li> <li>- t=91min. 1ª limpieza con H2O y disminución del índice de refracción. NOS SORPRENDE LA DINÁMICA Y EL INCREMENTO DEL ÍNDICE DE REFRACCIÓN.</li> <li>- t=96min. 2ª limpieza don H2O. Rápida disminución, dinámica y estabilización.</li> <li>- REPETIR CON BOMBA PARA TENER MAS CONTROLADA LA INYECCIÓN DE LOS DIFERENTES LÍQUIDOS.</li> </ul>		





**ZOOM. El rango de esta gráfica es de 3nm**

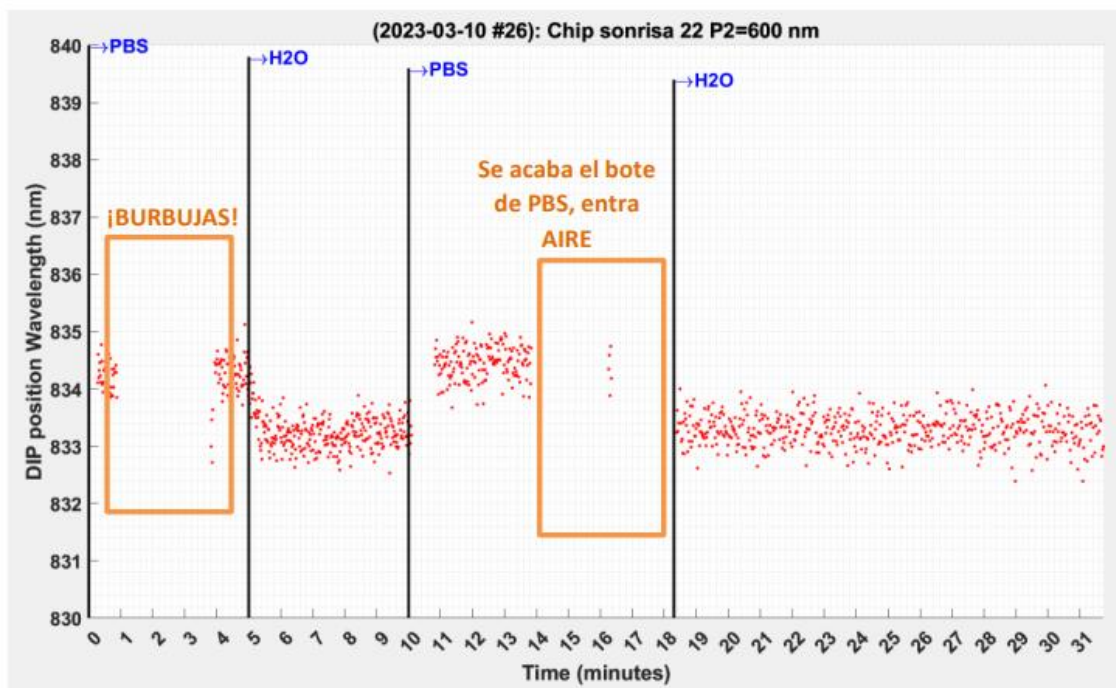
**H<sub>2</sub>O n=1.33 ⇒λ=703.25nm**

**PBS n=1.339 ⇒λ=704.25nm**

### C) EXPERIMENT FROM THE 10TH OF MARCH WITH CYCLES OF H<sub>2</sub>O AND PBS

20230310_SPR_Sonrisa12_26_TIME	Friday	TIME
OBLEA S2103: RIE 24" = 30nm + Ti=3nm + Gold=40nm	10-03-2023	CHIP 22 CON FLUIDICA
POLARIZATION = 0°		
[X <sub>REF</sub> , Y <sub>REF</sub> ] = [...] in PBS		
P2= 600 nm [X <sub>0</sub> , Y <sub>0</sub> ] = [... , ...]		
DARK & REF in FLAT GOLD WITH POLARIZATION = 0°		
- CHIP 22		
- INLET conectado a GILSON MINIPULS 3 "empujando"		

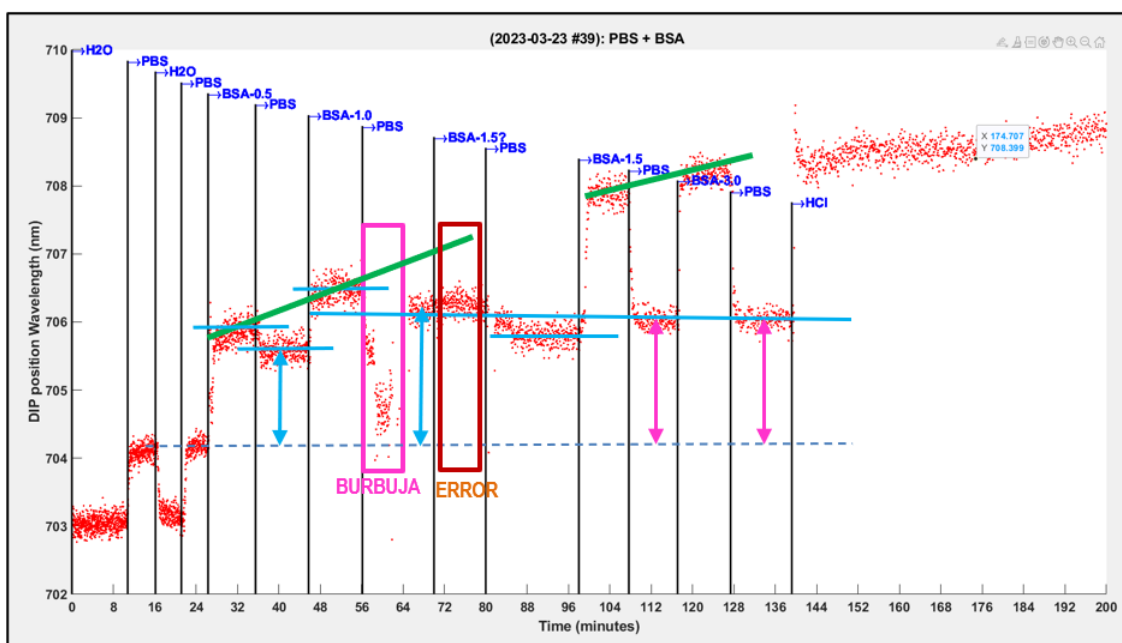




## ANNEX 5: EXPERIMENTS WITH DIFFERENT CONCENTRATIONS OF BSA

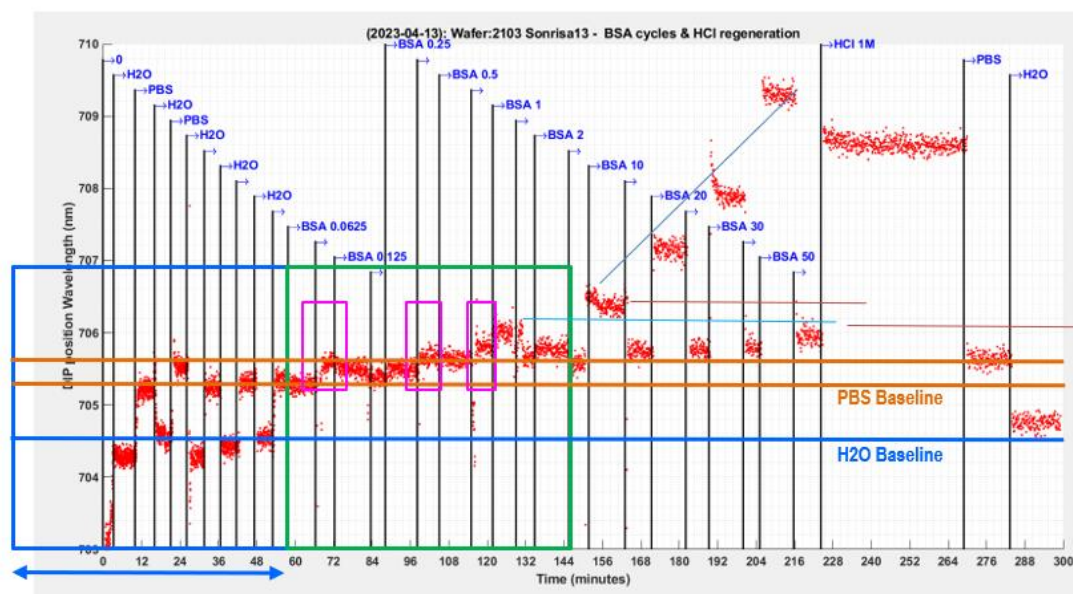
### A) EXPERIMENT FROM THE 23RD OF MARCH

20230323_SPR_Sonrisa23_39_TIME OBLEA S2103: RIE 24" = 30nm + Ti=3nm + Gold=40nm POLARIZATION = 0°	Thursday 23-03-2023	H2O+PBS+n*(BSA+PBS)+HCl. Fluidics
[X <sub>REF</sub> ,Y <sub>REF</sub> ]=[0mm,0mm] [X <sub>0</sub> ,Y <sub>0</sub> ]=[1mm,1mm]		
DARK & REF in FLAT GOLD WITH POLARIZATION = 0° La medida dinámica se realiza con la red de difracción de P1=500nm.		
instante = [0,10.8, 16.16, 21.16, 26.33, 35.5, 45.75,56.16,70, 80, 98, 107.66,117.08, 127.33, 139.16] ; liquido = {'H2O','PBS','H2O','PBS','BSA-0.5','PBS','BSA-1.0','PBS','BSA-1.5?','PBS','BSA-1.5','PBS','BSA-3.0','PBS','HCl'} ;		
<ul style="list-style-type: none"> <li>- t=0. Se parte con agua.</li> <li>- t=10.8min. 1ª inyección de PBS. Hay un incremento en el índice de refracción.</li> <li>- t=16.16min. Se inyecta H2O.</li> <li>- t=21.16min. 2ª inyección de PBS. Hay un incremento en el índice de refracción.</li> <li>- t=26.33min. 1ª inyección de BSA. C=0.5. Hay un SHIFT debido al incremento del índice de refracción. La dinámica puede quedar enmascarada con la dinámica de la bomba peristáltica.</li> <li>- t=35.5min. 1ª LIMPIEZA con PBS. Hay un decremento de la resonancia, <b>PERO POR ENCIMA DEL INICIAL. ¿Ha quedado adherido BSA en la superficie de oro?</b></li> <li>- t=45.75min. 2ª inyección de BSA. C=1.0. Nuevo SHIFT y mayor, posiblemente a un mayor índice de refracción con la concentración. ¿VEMOS un EFECTO VOLUMEN?</li> <li>- t=56.16min. 2ª LIMPIEZA con PBS. Al principio aparece una burbuja y al final parece recuperarse la señal. <b>Por debajo del nivel de BSA y por encima del nivel de PBS anterior.</b></li> <li>- t=70min. 3ª inyección de BSA. C=1.5. La respuesta no es correcta. <b>SE DUDA SI LA CONCENTRACIÓN SE HA PREPARADO CORRECTAMENTE. Se prepara una nueva muestra con esta concentración.</b></li> <li>- t=80min. 3ª LIMPIEZA con PBS. Parece que se alcanza un nivel por debajo del PBS anterior. <b>ESTO ES MALO!!</b></li> <li>- t=98min. 4ª inyección de BSA. C=1.5. La inyección parece correcta. El SHIFT es mayor</li> <li>- t=107.6min. 4ª LIMPIEZA con PBS. La señal se recupera al mismo nivel similar al PBS anterior.</li> <li>- t=117.08min. 5ª inyección de BSA. C=3.0. Aunque la concentración es el doble que la anterior, sólo se tiene un ligero SHIFT de la resonancia.</li> <li>- t=127.33. 5ª LIMPIEZA con PBS. La señal se recupera al nivel de PBS anterior.</li> <li>- t=139.16. Inyección de HCl para regenerar la superficie de oro. Aparece alguna burbuja.</li> </ul> <p>➤ Al introducir el BSA parece que vemos sobre todo el efecto de columna (BULK). Si hay cinética puede que esté enmascarada con la velocidad de inyección de la bomba.</p> <p>➤ Concentraciones mayores de BSA producen SHIFTS mayores.</p> <p>➤ En los dos últimos ciclos, es posible que hayamos alcanzado la saturación. Después de la limpieza con BSA el nivel base no se incrementa.</p>		
- Las concentraciones son mg/mL		



## B) EXPERIMENT FROM THE 14<sup>TH</sup> OF APRIL

20230413_SPR_Sonrisa13_44_TIME		Thursday	H2O+PBS+n*(BSA+PBS)+HCl.
OBLEA S2103: RIE 24" = 30nm + Ti=3nm + Gold=40nm		14-04-2023	Fluidics
POLARIZATION = 10°			
DARK & REF in FLAT GOLD WITH POLARIZATION = 10°			
La medida dinámica se realiza con la red de difracción de P1=500nm.			
instante = [0, 3.33,10,16.11, 21.12,26.12, 31.67, 36.67, 41.67,47.25, 53, 57.8, 66.33, 72.33, 83.63,88.16,98.16, 105,115, 121.7,129, 134.8,145.42,151.7,163 171.3,182,189.2,199.92, 205.08,215.67,224.2,268.8,283.2 ] ;			
liquido = { '0','H2O','PBS','H2O','PBS','H2O','H2O','H2O','BSA 0.0625','BSA 0.125','BSA 0.25','BSA 0.5','BSA 1','BSA 2','BSA 10','BSA 20','BSA 30','BSA 50','HCl 1M','PBS','H2O' }			
t = 0min	- Se parte con agua y se reajusta la posición del sensor		
t = 3.33min	- H2O Baseline		
t = 10.16min	- 3 ciclos PBS + H2O. Los ciclos H2O-PBS no son repetitivos.		
	- Sí parece que el nivel de PBS se mantiene, mejor que el del agua.		
	- PBS baseline		
t = 57.8min	1ª inyección de BSA 0.0625mg/ml. No se aprecia incremento respecto al nivel de PBS		
t = 66.33min	Lavado con PBS. Sorprende que se incrementa el valor de la resonancia.		
-	t=16.16min. Se inyecta H2O.		
-	t=21.16min. 2ª inyección de PBS. Hay un incremento en el índice de refracción.		
-	t=26.3min. 1ª inyección de BSA. C=0.5. Hay un SHIFT debido al incremento del índice de refracción. La dinámica puede quedar enmascarada con la dinámica de la bomba peristáltica.		
-	t=35.5min. 1ª LIMPIEZA con PBS. Hay un decremento de la resonancia, PERO POR ENCIMA DEL INICIAL. ¿Ha quedado adherido BSA en la superficie de oro?		
-	t=45.75min. 2ª inyección de BSA. C=1.0. Nuevo SHIFT y mayor, posiblemente a un mayor índice de refracción con la concentración. ¿VEMOS un EFECTO VOLUMEN?		
-	t=56.16min. 2ª LIMPIEZA con PBS. Al principio aparece una burbuja y al final parece recuperarse la señal. Por debajo del nivel de BSA y por encima del nivel de PBS anterior.		
-	t=70min. 3ª inyección de BSA. C=1.5. La respuesta no es correcta. SE DUDA SI LA CONCENTRACIÓN SE HA PREPARADO CORRECTAMENTE. Se prepara una nueva muestra con esta concentración.		
-	t=80min. 3ª LIMPIEZA con PBS. Parece que se alcanza un nivel por debajo del PBS anterior. ESTO ES MALO!!		
-	t=98min. 4ª inyección de BSA. C=1.5. La inyección parece correcta. El SHIFT es mayor		
-	t=107.6min. 4ª LIMPIEZA con PBS. La señal se recupera al mismo nivel similar al PBS anterior.		
-	t=117.08min. 5ª inyección de BSA. C=3.0. Aunque la concentración es el doble que la anterior, sólo se tiene un ligero SHIFT de la resonancia.		
-	t=127.33. 5ª LIMPIEZA con PBS. La señal se recupera al nivel de PBS anterior.		
-	t=139.16. Inyección de HCl para regenerar la superficie de oro. Aparece alguna burbuja.		
➤	Al introducir el BSA parece que vemos sobre todo el efecto de columna (BULK). Si hay cinética puede que esté enmascarada con la velocidad de inyección de la bomba.		
➤	Concentraciones mayores de BSA producen SHIFTS mayores.		
➤	En los dos últimos ciclos, es posible que hayamos alcanzado la saturación. Después de la limpieza con BSA el nivel base no se incrementa.		
-	Las concentraciones son mg/ml.		

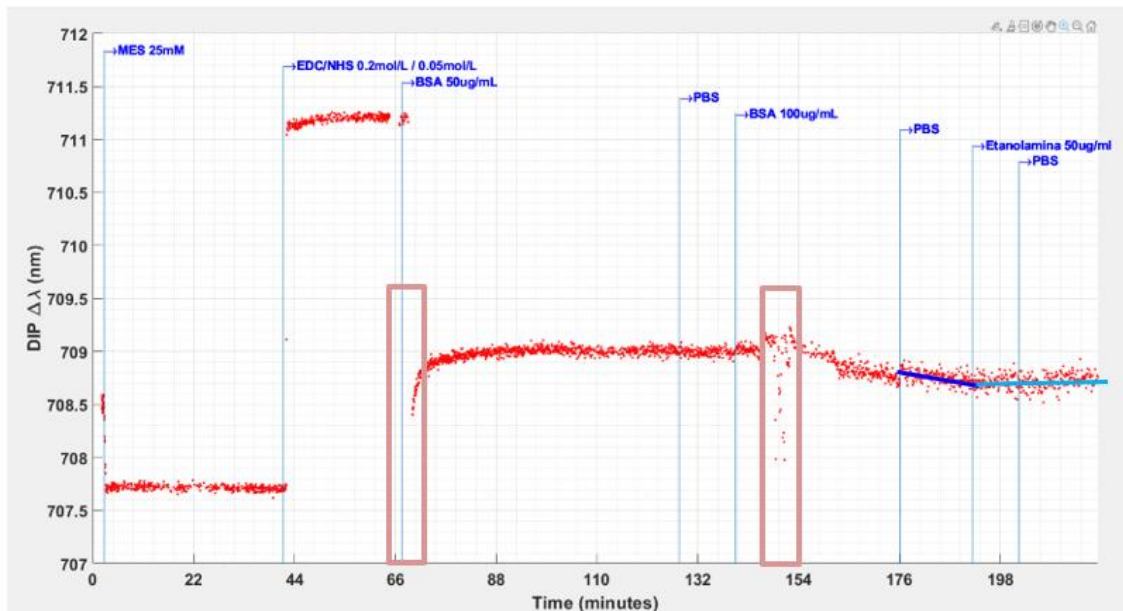


- En el primer bloque, los ciclos H2O-PBS no son repetitivos.
- Si parece que el nivel de PBS se mantiene, mejor que el del agua.

## ANNEX 6: EXPERIMENTS WITH SAM

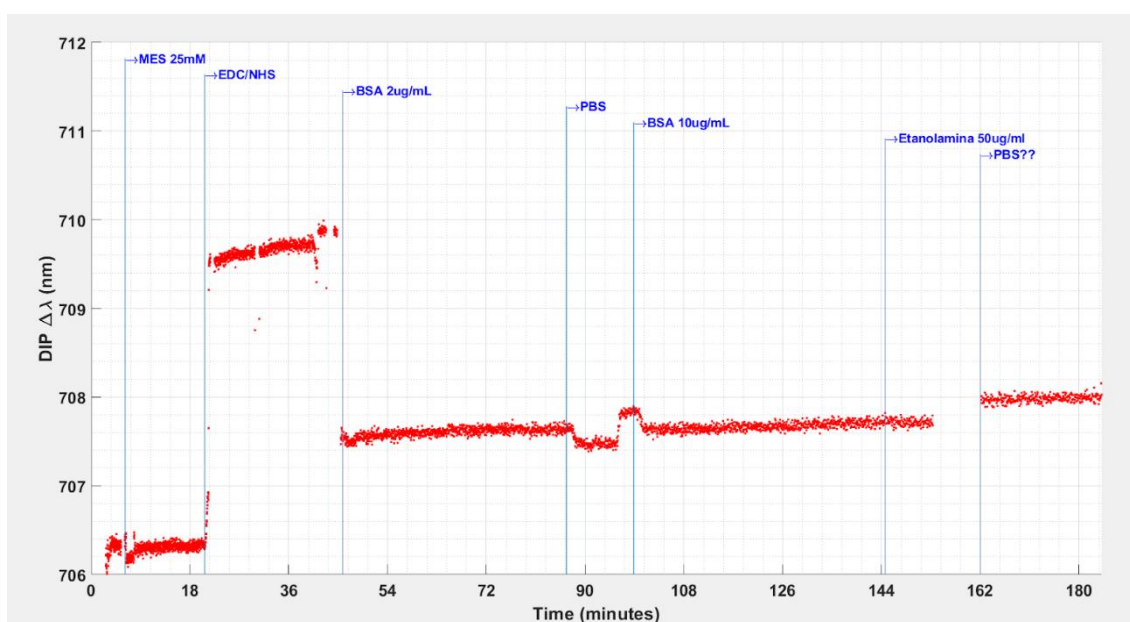
A) EXPERIMENT FROM THE 11TH OF APRIL WITH CONDITION, ACTIVATION OF THE SAM AND COUPLING PROCEDURE WITH TWO CONCENTRATIONS OF BSA, 50 AND 100  $\mu\text{G}/\text{ML}$ .

20230511_SPR_Sonrisa34_47_TIME OBLEA S2103: RIE 24'' = 30nm + Ti=3nm + Gold=40nm CHIP SONRISA1 funcionalizado con MUA		Thursday 11-04-2023	
DARK & REF in FLAT GOLD WITH POLARIZATION = 32° La medida dinámica se realiza con la red de difracción de P1=500nm.			
instante = [2.5, 41.6, 67.5, 128, 140.25, 176.16, 191.9, 202] ; liquido = {'MES 25mM', 'EDC/NHS 0.2mol/L / 0.05mol/L', 'BSA 50ug/mL', 'PBS', 'BSA 100ug/mL', 'PBS', 'Etanolamina 50ug/mL', 'PBS'}			
t = 0min	PBS	➤ El experimento se realiza en flujo. La velocidad de la bomba peristáltica es 2.5rpm	
t = 2.5min	MES	➤ 2-Morpholinoethanesulfonic acid monohydrate	
t = 41.6min	EDC/NHS	➤ ACTIVACIÓN de los grupos funcionales ➤ Liquido con índice de refracción elevado $\Rightarrow$ SHIFT > 3nm	
t = 67.5min	BSA 50ug/ml	➤ Aparece una burbuja junto a la red de difracción. No afecta mucho a la medida. ➤ Liquido con índice de refracción elevado $\Rightarrow$ SHIFT > 3nm ➤ Hay un comportamiento dinámico como es de esperar. Aparece una saturación en DIP=709nm. ➤ Alrededor de t=110min hay una leve disminución de la resonancia. ¿DISOCIACIÓN?	
t = 128min	PBS	➤ No se observa disminución de la señal. ➤ Sería de esperar un cambio brusco debido a la diferencia de índice de refracción antes [PBS+BSA] y después [PBS] ➤ ¿Puede ser que todo el BSA haya quedado adherido al MUA?	
t = 140.25in	BSA 100ug/ml	➤ En los primeros minutos no hay variación del DIP. ➤ Es posible que con C=50ug/ml ya esté saturado. ➤ Aparece una burbuja y la señal decrece, posiblemente por que el espectro se odifica por el aire.	
t = 176.25in	PBS	➤ Se observa una ligera disminución de la señal. ➤ Sería de esperar un cambio brusco debido a la diferencia de índice de refracción antes [PBS+BSA] y después [PBS]	



B) EXPERIMENT FROM THE 18TH OF MAY WITH CONDITION, ACTIVATION OF THE SAM AND COUPLING PROCEDURE WITH TWO CONCENTRATIONS OF BSA FITC, 2 AND 50  $\mu\text{G/ML}$ .

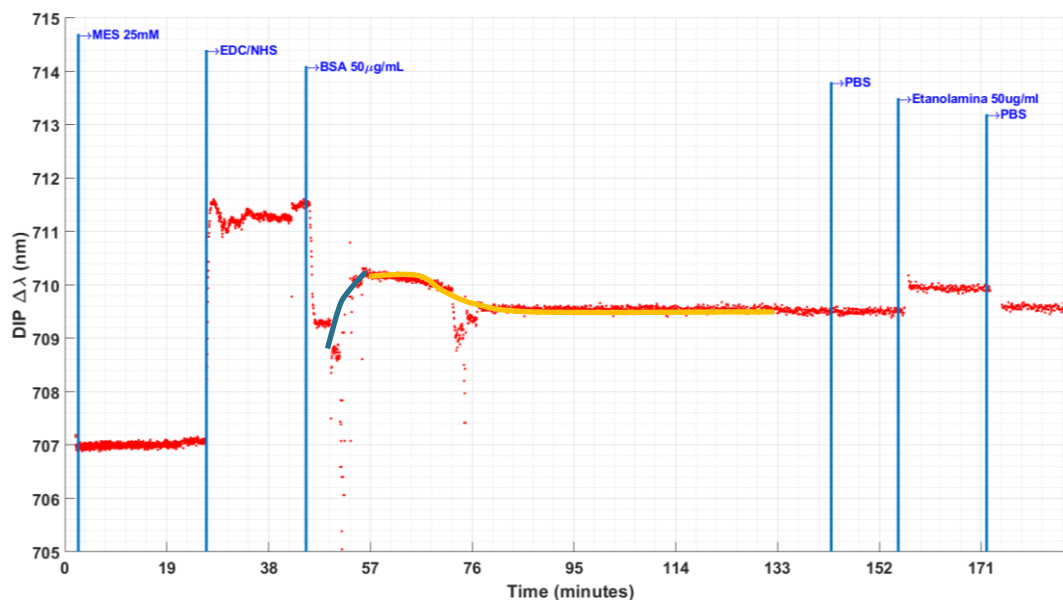
Chemical substance	Concentration	Time of addition (sec)	Estimated Duration (min)	Flow rate	Observations
MES	25mM	370s	20 min	0,1 ml/min	
EDC/NHS	EDC 0.2 mol/L and NHS 0.05 mol/L en 2 ml MES	1240 s	20 min	0,1 ml/min	
BSA	2 $\mu\text{g/ml}$	2750 s	45 min	0,1 ml/min	Air bubble
PBS	1x	5195 s	10 min	0,1 ml/min	
BSA	10 $\mu\text{g/ml}$	5930 s	45 min	0,1 ml/min	Air bubble in the introduction moment
Ethanolamine	50 $\mu\text{g/ml}$	8680 s	15 min	0,1 ml/min	
PBS	1x	9580s	10 min	0,1 ml/min	





Chemical substance	Concentration	Time of addition (sec)	Estimated Duration (min)	Flow rate	Observations
MES	25mM	150	15 min	0,1 ml/ min	
EDC/NHS	EDC 0.2 mol/L and NHS 0.05 mol/L in 5 ml MES	1586	20 min	0,1 ml/ min	
BSA	50 $\mu$ g/ml	2700	90 min	0,1 ml/ min	
PBS	1x	8600	10 min	0,1 ml/ min	
Ethanolamine	50 $\mu$ g/ml	9330	15 min	0,1 ml/ min	bubble at 9400
PBS	1x	10300	10 min	0,1 ml/ min	bubble at 10500 aprox

C) EXPERIMENT FROM THE 31ST OF MAY WITH CONDITION, ACTIVATION OF THE SAM AND COUPLING PROCEDURE WITH BSA FITC 50  $\mu$ G/ML.

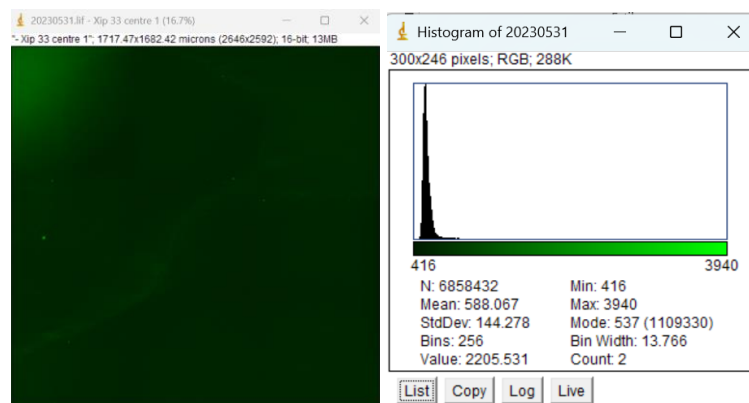


## ANNEX 7: FLUORESCENT MICROSCOPY RESULTS

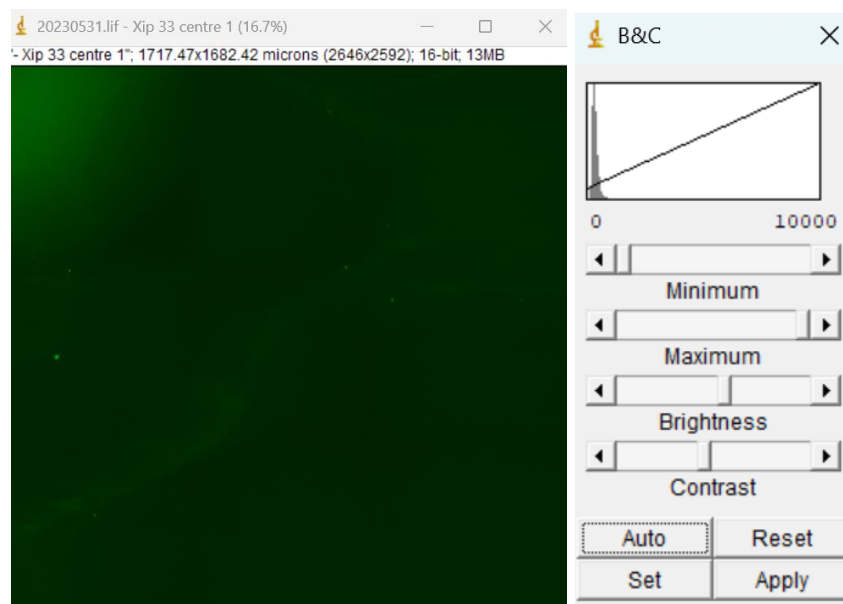
To process images with image J a homogenous criterion must be established so the images can be compared. To do so, first, the images will be imported for that the package Bio formats has to be

downloaded to read .lif files. The procedure will be shown with an example of an image corresponding to CHIP 33.

1. The image is imported, and the Histogram is plotted to visualize the color distribution.

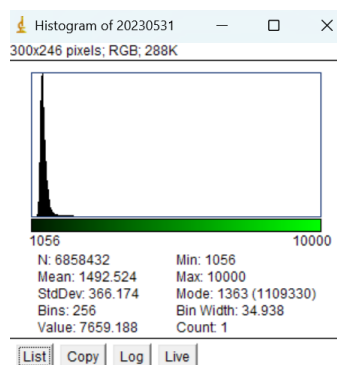


2. The intensity of the pixels will be change by the option Image> Adjust> brightness and contrast. They are changed to a minimum of zero and a maximum of 10000, this will be the homogenous criteria for all the imported images. The maximum value of the histogram is chosen because of the higher range values of the border images. The border image have higher fluorescence and therefore have many values near the 10000, so a smaller maximum limit would erase valuable information.



3. To apply this to the Histogram Process > Math > Divide or multiply by a factor. This factor is the needed value to divide or multiply the old pixel intensity value to obtain the new, 10000. In this case, the factor is 2,538 which is the result of  $10.000/3940$ .
4. Then the histogram is plotted, and it is seen that the color scale and the x-axis changes.





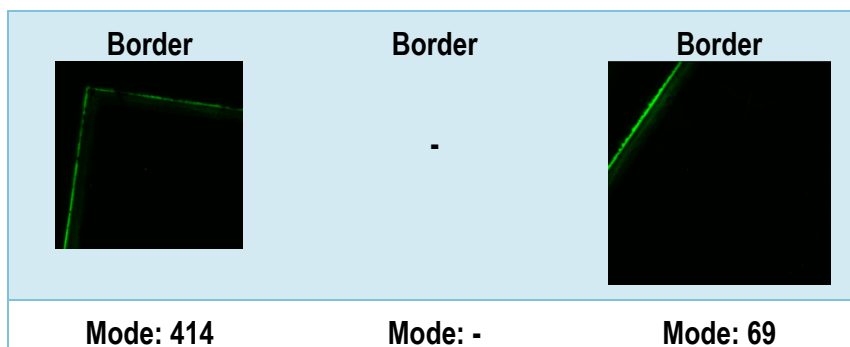
In conclusion, by normalizing the pixel intensities to a common scale for all images, their overall brightness levels are equalized, providing a similar baseline intensity, allowing comparison. The contrast is not going to be enhanced for quantification since it alters the values. However, it is going to be used to visualize the images.

#### A) SUMMARY 1OF FLUORESCENT MICROSCOPY IMAGES FROM THE 16TH OF MAY PROCESSED BY IMAGEJ OF THE TWO GOLD WAFERS CONDITIONED DRY OR IN ETHANOL

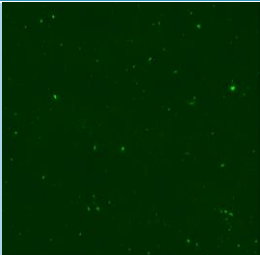
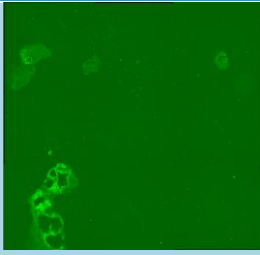
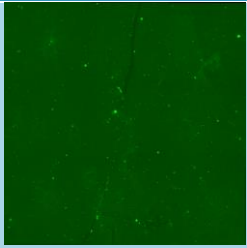
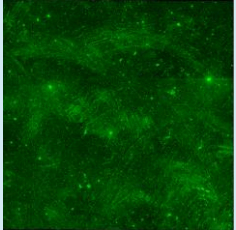
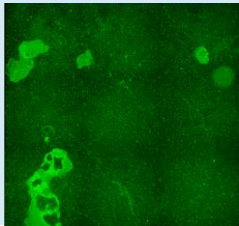
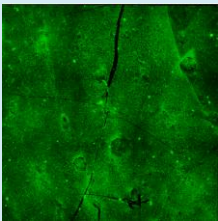
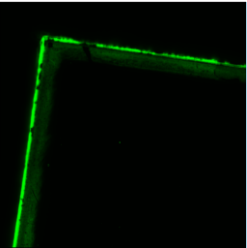
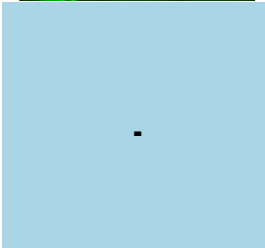
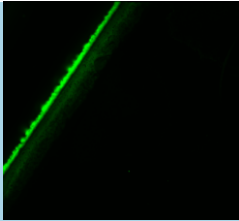
- Dry conditioned wafer gold surface: Functionalized gold wafer that was conserved in dry conditions. Images from the Gold surface.
- Dry conditioned wafer no-gold surface: Functionalized gold wafer that was conserved in dry conditions. Images from the non-gold surface.
- Ethanol conditioned wafer gold surface: Functionalized gold wafer that was conserved in Ethanol. Images from the Gold surface.

For quantification, each image with a pixel intensity range between 0 and 10000, the maximum value is this one because the border has many values around this intensity. The mode is computed for each to quantify the level of fluorescence per image:

DRY CONDITONED WAFER GOLD SURFACE	DRY CONDITIONED WAFER NO GOLD SURFACE	ETHANOL CONDITONED WAFER GOLD SURFACE
Center	Center	Center
Mode: 66	Mode: 95	Mode: 101



For visualization the contrast is enhanced, and the range of intensities is not changed. This is not useful for comparison.

	Image J parameters	Dry conditioned wafer gold wafer surface	Dry conditioned wafer no-gold surface	Ethanol conditioned surface
Center	Normalized, enhanced contrast of 20%			
	Equalized histogram, enhanced contrast of 20%			
Border	Normalized, enhanced contrast of 20%			

Note that the equalized histogram option is only for a more detailed visualization of the images.



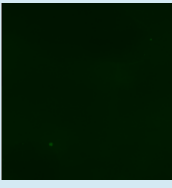
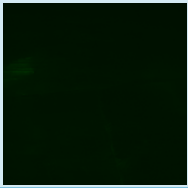

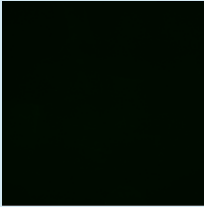
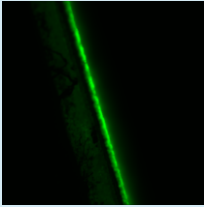
## B) SUMMARY OF FLUORESCENT MICROSCOPY IMAGES FROM THE 31ST OF MAY PROCESSED BY IMAGEJ

- CHIP 33: Functionalized with all the steps by microfluidics. It is not possible with the fluorescent microscope to determine if the image is from the inside or the outside of the microfluidics. However, it can be deduced since the areas with more fluorescent should be inside the microfluidics where the BSA FITC is flowed over.
- CONTROL WAFER: Only MUA formed.


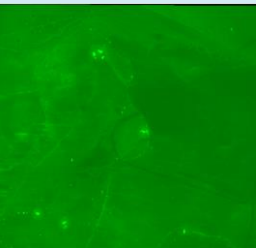
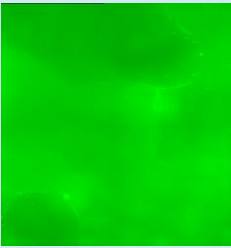
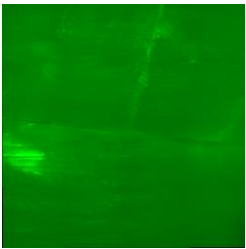
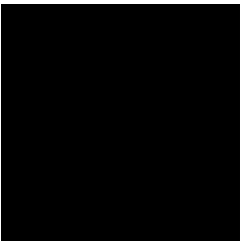
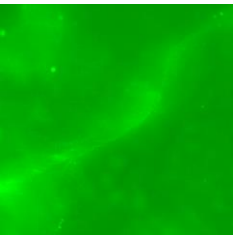
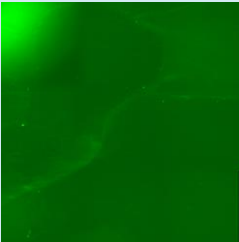
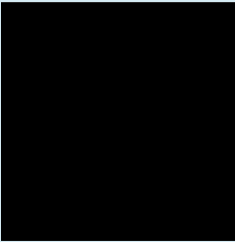
- NON-ACTIVATED WAFER: MUA and BSA FITC coated but without the activation step.

For the quantification, each image with pixel intensity range between 0 and 10000 and the mode is computed:

Note that the border and second center images of the control wafer could not be uploaded because of an image acquisition problem.

CHIP 33	CONTROL WAFER	NON-ACTIVATED WAFER
Center 	Center 	Center 
Mode: 1363	Mode: 0	Mode: 901
Center 	-	Center 
Mode: 645		Mode: 1034
Center 	-	Border 
Mode: 394		Mode: 68

For visualization, enhances contrast of 20% is applied without changing the range of intensities.

CHIP 33	CONTROL WAFER	NON-ACTIVATED WAFER
Center 	Center 	Center 
Center 	Center 	Center 
Center 	Border 	Border 